Czech Technical University In Prage

České Vysoké Učení Technické v Praze

Carlos III University of Madrid

Universidad Carlos III de Madrid

Power supply using Wireless Transmission

Author: Ester Mandrisi Puig

Czech supervisor: Miloš Mazánek

Spanish supervisor: Daniel Segovia-Vargas

Advisor: Jan Kraček

Master Thesis

Telecommunication Engineering

October 2009-September 2010

A mis padres, a Claudia y Giovanni,

a Juan

Acknowledgments

With these lines I would like to thank all the people that have contributed to the realization of the present thesis and to my whole education.

En primer lugar quisiera dar las gracias a Daniel Segovia. Gracias por haber confiado en mí, por animarme para la realización de este proyecto y por haberme facilitado la estancia en Praga este año.

Děkuju moc Miloš Mazánek for the oportunity to work in collaboration with the Department of Electromagnetic Field in the CVUT during this year. Despite all the incidents it has been a pleasure working with you and learning from you. Taky děkuju moc Jan Kraček. Thank you for all the advices, help and patience. I really enjoyed all the time spent together. Thank also to all the other members of the Department that have helped me, especially to Petr Piksa. Těší mě ☺

Muchísimas gracias a todos los que habéis hecho de estos años de universidad una aventura maravillosa.

De la universidad, mención especial merecéis todos aquellos que me habéis soportado antes de cualquier examen y con los que he compartido muy buenos momentos: Guille, Iñaki, Quique, Fran, Carolina, Olalla y muchos más. Gracias a mis compañeros de prácticas, en la mayoría de los casos, ha sido un honor. Muy especialmente gracias a mis dos ángeles de la guarda en Leganés: Gracias a Javi por estar a mi lado desde el primer día, por tanto como me ha ayudado y apoyado siempre, también por tanto como ha soportado y siempre con paciencia. Gracias a Juan (Morcillo) por compartir tanto conmigo. Gracias por darme la oportunidad, por estar a mi lado en tan variopintas situaciones. Los dos sois los "culpables" de que haya sido un placer pasar tantas horas, y días (incluso cientos de ellos) en el tren para poder vivir un día mas de regalo a vuestro lado.

Gracias a mis checo-compañeros: Loira, Gerar, Iván, Pablo, Ramona, Marysia, Bozena (Dzięki!), Javi y todos los demás. ¡Viva ese bloque 5! Especialmente gracias a Jesús, gracias por tanto. Sin vosotros este año no hubiera sido lo mismo.

Muchas gracias a Carolina y a Cris, las *amigaas*. Por tanto como me ayudáis a desconectar, por creer en mí siempre, por animarme en los días de bajón y saber siempre escucharme. Gracias por reír y compartir conmigo. Formar parte de vuestras vidas es un regalo por el que vale la pena darlo todo. Siempre en Él. Gracias también a María Jesús y a Mónica, que a pesar de las distancias siempre están ahí.

Moltes gràcies també a tota la familia. Grazie a tutti. Als avis i als tiets, que m'han ensenyat molt, potser no de telecos, però sense els quals no hauria arribat mai fins aquí. Gràcies a la Claudia i al Giovanni que sempre em cuiden i em mimen tant. Gràcies per ensenyar-me a jugar de nou, a viure amb il·lusió. Sou una llum molt gran a la meva vida, un regal que mai no m'hagués esperat. Gràcies perquè feu de cada dia una aventura màgica. Grazie a papá per avermi accolto sempre, per come ai avuto cura di me. Grazie per insegnarmi tanto della vita, per i tuoi consigli, e per avermi incoraggiato nei miei progetti anche quando ho

deciso di farli in modo mio. Gracies a la mama per l'educació que m'ha donat i per tant mes... Gràcies per haver-me regalat la confiança amb mi mateixa, el saber estimar als altres, la humilitat de no saber-me millor que ningú, per fer una inversió amb mi a fons perdut. Gràcies per haver confiat sempre en mi, perquè sense tu mai hauria arribat tant lluny.

Y por último, gracias a Juan. Contigo emprendo la mejor, la mayor de las aventuras. Voy con la garantía de que en ti he encontrado lo que me hace más feliz en este mundo, y además he encontrado contigo a Quien me hace más feliz. Gracias por estar siempre a mi lado, por cuidarme tanto, por tener tanta paciencia. Gracias por estos casi 80 meses. Que sean muchos, muchísimos más (al menos toda la vida, y dos eternidades), pero a tu lado.

Contents

Figure index

Table index

Astract (Resumen)

En el presente proyecto se trata estudiar y construir una solución efectiva para el problema de la alimentación de los dispositivos sin cables cuyo uso ha ido creciendo en los últimos años. La principal motivación, pues, viene de la dependencia real que existe de toda clase de baterías y cargadores que requiere el uso de dichos dispositivos. Para conseguir un entorno realmente sin cables, resulta necesario un sistema que no solo sea inalámbrico en cuanto a transmisión de datos, sino también en cuanto a la alimentación de los dispositivos.

En el **segundo capítulo**, tras la introducción se presentan las diferentes tecnologías existentes hoy en día que permiten transmitir potencia son cables. La transmisión de potencia inalámbrica es la técnica que distribuye la energía eléctrica sin la necesidad de utilizar una onda guiada. Cualquier sistema que implemente esta técnica tendrá que cubrir necesariamente tres pasos:

1. Conversión de la energía eléctrica DC en potencia RF
2. Transmisión de la potencia RF
3. Recepción de la potencia RF y su posterior reconversión a DC.

Se consideran tres tecnologías distintas que cumplen el propósito anunciado. En primer lugar el acoplo reactivo, que consiste en el uso de bobinas y sus propiedades de acoplamiento mutuo para proveer energía desde el transmisor hasta el receptor. Esta solución estará aplicada en su mayoría a soluciones pertenecientes al campo cercano, donde trabaja en un entorno de transmisión inductiva. La acción de un transformador eléctrico es el ejemplo más simple de transferencia de energía inalámbrica. Al igual que en este ejemplo, el circuito primario y el secundario no están directamente conectados; es por esto que el sistema puede ser considerado inalámbrico. A pesar de que en un principio esta tecnología estaba restringida a aplicaciones de corto alcance, en los últimos años se han diseñado sistemas con un alcance entre el receptor y el transmisor de hasta 5 metros [18].

También es posible construir una estructura especial que permita la transmisión tanto de potencia como de datos a través de una fina lámina a frecuencias de microondas.

En las aplicaciones propias para campo lejano será importante considerar que la distancia existente entre los dispositivos susceptibles de ser alimentados y el transmisor debe ser mucho mayor que el diámetro de los receptores construidos. En la mayoría de los casos tendremos unas grandes pérdidas debidas a la propagación en el espacio libre (dependiendo en todo caso de la frecuencia de operación, de la distancia y del entorno). Es en este supuesto donde situamos la solución basada en la transmisión con la ayuda de ondas electromagnéticas a través del espacio libre. Esta solución será la utilizada en el Para estos sistemas, además del transmisor, se considerará una combinación formada por una antena en recepción y un rectificador en una estructura conjunta conocida como rectena que actuará como el receptor que cumple la misión del tercer paso necesario para la transmisión inalámbrica de potencia

descrita anteriormente. Esta parte del sistema será la clave para el desarrollo de un sistema eficiente que de buenos resultados, debido a que el receptor va a determinar la eficiencia del sistema completo ya que será la parte más restrictiva. Ya que las propiedades de las comunicaciones por microondas han sido ampliamente estudiadas y probadas, el principal objetivo será encontrar el mejor modo de integrar estos dos elementos para aumentar la eficiencia lo máximo posible. El uso de altas frecuencias nos permitirá tener dispositivos de tamaño muy reducido. Sin embargo, por otro lado, nos forzará a realizar unos diseños de muy alta precisión para compensar en la mayor medida posible las grandes pérdidas ocasionadas por la transmisión por el espacio libre.

En un breve repaso de las historia de las tres tecnologías, se hace especial hincapié en algunos artículos entre los cuales se destacan [1] y [2] que detallan el inicio de las investigaciones para la transmisión de potencia inalámbrica llevados a cabo por Nikola Tesla y por un instituto alemán. En lo referente a la transmisión de potencia inalámbrica basada en inducción, cabe señalar que los primeros experimentos fueron llevados a cabo en los años 60 y se detallan en [5]. Estos primeros experimentos estaban mayormente basados en la investigación de sistemas relacionados con aplicaciones médicas. Se repasan los principales avances hasta hoy.

En la historia de la transmisión de potencia inalámbrica basada en la emisión de ondas electromagnéticas se destaca a William C. Brown como el pionero de los estudios relacionados con la materia [3]. Se repasa la aparición de las distintas frecuencias de trabajo desde los 2.45GHz iniciales, viendo como se han indo incorporando distintas frecuencias en [26], [27], [28] y [31] hasta la gran variedad de frecuencias que se usan hoy en día para la construcción de los sistemas. Se deben destacar las importantes aportaciones de Kai Chang cuyas publicaciones han servido de base para el diseño presentado en el presente proyecto [29]-[33].

En [33] se presenta un proyecto que sirve como clara referencia al desarrollado para este Proyecto Fin de Carrera. Utilizando el diodo MA4E 1317 de MACOM Technologies se construye una rectena. Mediante un condensador de bloqueo de DC se construye un filtro paso DC que no solo desacopla la reactancia del diodo, sino que además minimiza el nivel de potencia de los armónicos. La distancia óptima entre el filtro paso DC y el diodo se optimiza de tal modo que se consigue una conversión máxima RF a DC del 85%. Esta eficiencia de conversión establece la máxima eficiencia que se conseguirá con la rectena. Se utilizan un tipo especial de líneas de transmisión, llamadas Coplanar Stripline (CPS) por su simplicidad y pequeño tamaño. Las dimensiones de la CPS tienen que aportar el tamaño suficiente para el soldado del diodo y el condensador y para satisfacer el criterio de impedancia de línea deseada. Además, la impedancia característica correspondiente a la CPS es mayor que la que ofrece una línea microstrip y adapta mejor a la parte real de la impedancia del diodo. Con este tipo de líneas, se construye un filtro rechaza banda que solo permite el paso de la frecuencia de 5.8GHz desde la antena al diodo y bloquea el segundo y el tercer armónicos (que son los que tienen mayor nivel en el espectro). Se ha diseñado una geometría especial de tal modo que se mejora el rechazo de las bandas superiores añadiendo stubs. Como antena para la estructura se utiliza una de las llamadas antenas DRLA (Dual-Rhombic-Loop Antenna) en configuración de array. Cada uno de los DRLA se construye con una terminación en dos orificios. Estos orificios causan la polarización circular deseada para el sistema. Se coloca un plano reflectante detrás del

substrato de la rectenna de tal modo que se aumenta la ganancia del array DRLA al estrechar el haz del diagrama de radiación de la antena aumentando su directividad en una dirección. La máxima eficiencia conseguida con el sistema completo es del 82% con una densidad de potencia de 2mW/cm^2 El filtro construido con las líneas CPS rechaza el primer armónico hasta aproximadamente unos 14dB por debajo de la ganancia a la frecuencia fundamental.

En el **tercer capítulo** se estudia la normativa de seguridad que regula la emisión de potencia en el espacio libre y en base a dicho estudio se calcula el valor máximo de la potencia que es posible emitir para el diseño del sistema. En las Figuras 3.1 y 3.2 se pueden observar los umbrales máximos para los campos eléctrico y magnético en función de la frecuencia dependiendo de la gente potencial que estará expuesta a la radiación. A la frecuencia de trabajo del sistema a desarrollar, 2.45GHz, consideramos para el cálculo el valor más restrictivo del campo eléctrico, al ser este directamente proporcional a la potencia que debemos calcular. Para dicho cálculo se supone que la antena transmisora radia uniformemente en un ángulo solido de $\pi/2$ radianes (con lo que la antena tendría una directividad de unos 9dB). Usando este dato se calcula el diámetro estimado con la expresión mostrada en la ecuación (3.2). Utilizando las ecuaciones básicas de propagación en el espacio libre en las ecuaciones (3.4)-(3.10) se calcula la potencia máxima radiada que es de 25.7876dBm.

En el **cuarto capítulo** se estudia y diseña la antena adecuada para el sistema. El tipo de antena elegido para dicho desarrollo es el de las antenas de parche. Estas antenas, también llamadas antenas de microstrip, se basan en las líneas de transmisión o resonadores en substratos dieléctricos. Las dimensiones de estas líneas o resonadores se eligen de forma que la potencia se disipa de un modo radiante. Las formas que pueden adoptar las antenas de parche son muy variadas a pesar de que la forma más básica y más utilizada es el rectángulo o cuadrado.

Las antenas de parche se pueden alimentar de múltiples formas, de las cuales solo se detallan las principales. En primer lugar, mediante una línea de transmisión convencional, de modo que el tramo de línea se conecta directamente al parche, como se puede ver en la Figura 4.3. Otro modo posible consiste en el uso de una sonda coaxial. De esta manera, el conductor interno del cable coaxial que incide en el parche se conecta al parche, mientras que el conductor externo se conecta al plano de masa; como se puede apreciar en la Figura 4.4. También es posible alimentar mediante el acoplo por medio de una apertura realizada en un plano de masa que separa dos substratos. Este es el modo de alimentación cuya construcción es más complicada, como se puede comprobar en las Figuras 4.5 y 4.6. El método utilizado para la construcción de la antena buscada es la alimentación mediante una sonda coaxial. El modo fundamental de radiación de las antenas de parche es el TEM_{100} o el TEM_{010} en función de la relación de aspecto de la antena. La frecuencia de resonancia para este modo esta expresada en la ecuación (4.1) y de ella se deduce que la longitud del parche para resonar en una frecuencia determinada deberá ser cercana a $\lambda/2$. Existe un compromiso entre dos

parámetros de diseño del parche que deberá ser estudiado cuidadosamente: es la relación existente entre la permitividad y el espesor del dieléctrico y el factor de calidad y el ancho de banda. Cuando la permitividad del dieléctrico crece y disminuye su espesor el factor de calidad disminuye. Por otro lado, cuando el factor de calidad disminuye el ancho de banda aumenta. Por tanto será necesario estudiar las características del dieléctrico a utilizar para conseguir los resultados que se ajusten mejor a lo deseado.

En el caso que nos ocupa, el parche utilizado deberá tener polarización circular. Esta es la mejor opción para la polarización tanto de la antena transmisora como de la receptora. Las antenas emiten ondas circularmente polarizadas cuando dos componentes ortogonales del campo con igual amplitud y en cuadratura de fase se emiten. Este requerimiento hace que la alimentación del parche o su forman deban variar de la alimentación y/o la forma común. Asimismo, también es posible diseñar un array de parches que conseguiría la polarización circular. Utilizando un solo parche, se puede conseguir polarización circular con doble alimentación o alterando la forma básica rectangular de la forma conveniente. Como se muestra en la Figura 4.17, en el caso que nos ocupa se alterará la forma rectangular cortando dos de las esquinas del rectángulo y posicionando la alimentación en uno de los dos ejes en función de la polarización deseada (a derechas o a izquierdas). En las ecuaciones (4.3)-(4.17) se desarrolla la relación entre la relación de aspecto del parche truncado y su factor de calidad.

Como se ha señalado anteriormente, la polarización deseada es circular, por lo que en todo momento se intentará que la Razón Axial del parche sea igual a 1. Para ello, se ha llevado a cabo un estudio de la influencia de la variación de los parámetros susceptibles de cambio del parche. Estos parámetros son: la longitud del lado del parche, que es cuadrado, (llamado parámetro *a*); la longitud de la parte truncada del parche (llamada parámetro *c*) y por último, la posición de la alimentación del parche (llamado F=(*feed_x*, *feed_y*)). Para conseguir la polarización circular con el parche truncado uno de los dos últimos parámetros deberá ser igual a cero para que la alimentación se encuentre situada sobre uno de los dos ejes (mostrados en la Figura 4.17).

Debido a la falta de referencias donde se señalen los valores adecuados de los diferentes parámetros citados para conseguir los resultados deseados, se ha procedido a llevar a cabo un detallado estudio paramétrico de cada uno de los diferentes parámetros.

En el caso del lado del parche, parámetro *a*, se ha tomado como valor inicial la longitud calculada en la ecuación (4.18), correspondiente a la longitud que tendría el parche en el caso de tratarse de un modelo básico con el que se obtiene polarización lineal. Este valor se ha aumentado y disminuido razonablemente viendo en todo momento como variaba la polarización y la frecuencia de resonancia. Para la longitud del truncamiento, al no disponer de ningún valor inicial se ha hecho en primer lugar un muestreo muy espaciado desde la menor (0cm) hasta la mayor posición (25cm aprox.). Una vez se ha visto el comportamiento general de la variación del parámetro, se ha estudiado con más detalle aquella zona más próxima a los resultados deseados. Para estudiar la posición de alimentación se ha procedido de igual modo que en el caso de la longitud del truncamiento.

Este estudio se ha llevado a cabo en dos ocasiones. En primer lugar, como se puede ver en las páginas 30-33, se ha realizado un primer diseño con un punto de alimentación ideal que no

considera el modo concreto de alimentación sino solo la excitación teórica en un punto determinado del parche. Los valores de los parámetros para el modelo final para esta primera versión ideal del parche se pueden ver en la Tabla 4.2. Los resultados obtenidos con estos valores se presentan en las Figuras 4.33 a la 4.38.

En segundo lugar, se ha realizado el modelo para la alimentación con coaxial agregando al esquema inicial el substrato que se añade en la parte posterior de la antena y la sonda coaxial conectada como se ha explicado anteriormente. En la Figura 4.39 se puede ver un corte del parche en el que se aprecia cómo se han añadido estos elementos. Los valores iniciales de los diferentes parámetros son los detallados en la Tabla 4.2, los valores finales del estudio para el caso idea. El estudio paramétrico para este caso se encuentra en las páginas 37-41. Los valores definitivos son los que se muestran en la Tabla 4.3 y de nuevo son los que, tras el estudio paramétrico y considerando la precisión máxima para la construcción, resultan los valores más cercanos a los deseados. Los resultados obtenidos con los valores definitivos se muestran en las Figuras 4.52 a la 4.58. Como se puede observar la frecuencia de resonancia de la antena es muy próxima a la deseada y la polarización es circular. La polarización obtenida es circular a izquierdas.

Una vez obtenidos los resultados deseados para la antena, esta ha sido construida y medida. Los resultados de la medición de la antena construida se ven en la Figura 4.59. En la Figura 4.60 podemos observar la gráfica comparativa entre los resultados simulados y los resultados de las medidas a la antena construida.

En el **quinto capítulo** se estudia y diseña un rectificador adecuado para el sistema planteado. Para el diseño del rectificador en primer lugar se estudian las características principales del diodo. La curva característica del diodo se presenta en la ecuación (5.1). Se hace necesario tener un modelo del diodo para poder diseñar un circuito aceptable con un simulador. Algunos modelos en gran señal están disponibles, como el modelo del diodo en microondas, el modelo PIN o el modelo SPICE. El diodo usado para el presente proyecto será un diodo Schottky y el más sencillo y mejor modelo a escoger para su modelado es el SPICE. El modelo en gran señal del diodo se muestra en la Figura 5.1. Asimismo, en la Tabla 5.1 están detallados los parámetros que caracterizan al modelo SPICE de un diodo. En la gran mayoría de los casos, la capacitancia del diodo se modela como un condensador dependiente del voltaje, que se conecta en paralelo con una fuente de corriente no lineal para representar los efectos del almacenamiento de carga en la unión. Existen dos componentes que modelan esta carga y que generan dos portadoras que fluyen a través del diodo. Por un lado tenemos el efecto capacitivo de voltaje inverso de la región de deplexión y por el otro, la carga correspondiente a la corriente directa representada por portadores móviles en la unión del diodo. Los diodos de barrera Schottky difieren con los diodos de unión en que la corriente que fluye solo implica una portadora en lugar de las dos. La acción del diodo resulta del potencial de contacto establecido entre el metal y el semiconductor. El diodo, por tanto, trabaja cuando se aplica un voltaje positivo al metal. Basándose en las ecuaciones (5.2)-(5.6) se explican los principales parámetros del diodo, como la resistencia serie, la corriente de saturación, etc.

En base a este desarrollo del diodo, se plantea y diseña el esquema general del rectificador. Su diagrama de bloques se puede ver en la Figura 5.2 y esta extraído de las referencias indicadas del capítulo dos. En primer lugar, conectando la antena receptora y el circuito de rectificación se encuentra un condensador de bloqueo. El rectificador se compone de cuatro grandes bloques. En primer lugar debemos construir un circuito que rechace los armónicos de orden superior generados en el diodo y que debe tener bajas perdidas de inserción a la frecuencia de operación. En algunos casos, un circuito de adaptación será necesario debido a que no se pueda alcanzar la impedancia deseada directamente de la antena cambiando solamente el punto de alimentación. Situado a una distancia adecuada, separado por una línea de transmisión, estará el diodo conectado. De nuevo mediante una línea de transmisión se construirá un filtro paso DC que rechazará toda componente distinta a la corriente continua. En último lugar, se situará una carga para finalizar el circuito.

Cada bloque ha sido diseñado en función de las necesidades del circuito. El primer bloque en ser diseñado ha sido el filtro paso DC. En segundo lugar, se planeo el diseño de la adaptación y el filtrado a la entrada para conseguir un valor optimo de la impedancia de entrada del circuito.

Acerca del bloque del diodo, solo se ha tomado la decisión de si colocar el diodo en serie o en paralelo. Debido al uso como rectificador que se le da al diodo, éste trabaja en gran señal. Si se sitúa en paralelo trabajará como un recortador y el circuito actuará como un detector. Por lo tanto, el diodo se colocará en serie.

El filtro paso DC se basa en un solo condensador cuyo valor se calcula en las ecuaciones (5.7)-(5.9). Las simulaciones para obtener un buen resultado para poder construir el circuito se han realizado con el software AWR Design Environment 2003 from Applied Wave Research, Inc.

Para un desarrollo óptimo del sistema se han estudiado tres diferentes diodos, viendo su comportamiento y respuesta para elegir el mejor. Tanto los diodos como sus parámetros del modelado SPICE se pueden encontrar en la tabla 5.2.

Una decisión importante que fue necesario tomar es la potencia de entrada que se considera en las simulaciones. Como se detallo en el capitulo tres, la potencia recibida estaba alrededor de los 25dBm. Tomando una distancia media de tres metros entre el emisor y el receptor, se hace el balance de enlace mediante la ecuación de Friis como se puede ver en las ecuaciones (5.10) y (5.11). Tomando los datos adquiridos de la antena diseñada en el capitulo anterior, la ganancia de la antena es de 9.87dBm. Con todos estos datos, es posible crear un primer modelo con el software para ver los primeros resultados.

En el caso del primer diodo estudiado, el HSMS 2820, se diseña un circuito presentado en la Figura 5.3. Como se puede apreciar en dicha figura, se han conectado los diferentes bloques con líneas de transmisión cuyas longitudes han sido optimizadas. La tendencia general es que para los tramos en los que la señal está en RF (antes de rectificar la señal) se han utilizado líneas “largas” (respecto a la longitud de onda), mientras que en las partes DC del circuito (tras la rectificación), las líneas utilizadas han sido cortas. La impedancia de entrada del circuito se ha tomado de las mediciones realizadas a la antena diseñada en el capítulo anterior. Se ha

añadido el efecto de las vías cilíndricas que conectan los elementos del circuito con el plano de masa. Durante el diseño se puso de manifiesto la necesidad de una segunda etapa en el filtrado DC. Sin esta segunda etapa, la componente en RF presenta en la carga era demasiado alta. El principal objetivo consistía en eliminar por completo la componente senoidal en la tensión de salida. Las simulaciones se han llevado a cabo a la frecuencia central con una potencia de entrada de -5dBm como se calculó en (5.11). Los resultados se presentan en la Figura 5.4. En dicha figura, es posible apreciar dos formas de onda. La forma de onda representada en rosa corresponde al voltaje aplicado a la entrada del circuito y la forma de onda de color marrón corresponde al voltaje obtenido a la salida. Como se puede ver en la figura, los resultados son bastante malos ya que el nivel obtenido DC es muy bajo y además la componente senoidal se puede apreciar con facilidad en la forma de onda de salida debido a que es muy grande. Para explicar los resultados obtenidos es importante tener en cuenta dos factores que resultarán ser muy esclarecedores. En primer lugar, la frecuencia de operación es bastante alta teniendo en cuenta las frecuencias para las que está recomendado el uso del presente diodo. De hecho, en el datasheet del diodo es posible leer que el diodo es adecuado para construir sistemas de características similares para frecuencias de hasta 1.5GHz. Es posible simular el comportamiento del circuito a frecuencias menores de 2.45GHz, como 900MHz o 1GHz. Los resultados obtenidos con estas frecuencias son a simple vista mejores, como se puede apreciar en la Figura 5.5. A pesar de las mejoras en los niveles de DC, todavía es posible apreciar la componente sinusoidal de la frecuencia central, aunque ha disminuido. A esta consideración sobre la adecuación de la frecuencia de trabajo, le podemos añadir que la potencia recibida en el rectificador es demasiado baja para poder tener el diodo completamente abierto. Esta es la razón por la cual el nivel de DC no es suficientemente bueno, y por el que la eficiencia conseguida no es ni siquiera similar a la conseguida en la mayoría de las referencias. Si simulamos el mismo circuito añadiendo 10 o 15dB a la componente de entrada la eficiencia crece, pudiendo ver como mejora la relación entre el valor máximo de la tensión de entrada y la tensión DC a la salida. En las Figuras 5.6 y 5.7 podemos observar las mejoras obtenidas al aumentar la potencia de entrada al circuito.

Es necesario establecer una medida válida para poder comparar diferentes resultados procedentes de distintos circuitos con distintas características, como pueden ser distintos diodos, distintas potencias a la entrada, etc. Con este fin, en la ecuación (5.12) se deduce un valor p comparativo que cumple los requisitos establecidos. En la Tabla 5.3, podemos observar los porcentajes de voltaje recuperado a la salida. Se aprecia como el valor es muy bajo en el caso de la mínima potencia de entrada estudiada, que es -5dBm, mientras que al aumentar el valor de esta potencia de entrada el porcentaje aumenta considerablemente. Esto pone de manifiesto que las condiciones del circuito han cambiado ya que la medida establecida en (5.12) es relativa y no absoluta, debido a que los valores están normalizados al valor efectivo de la potencia recibida.

Se ha estudiado también la variación del voltaje DC en función de la frecuencia de entrada. En el caso de 2.45GHz los resultados del diodo son peores ya que la potencia a la entrada debe crecer más antes de obtener los mismos resultados a la salida que para otra frecuencia. Esto sugiere que el diodo tarda más en abrirse ya que cuando el diodo está abierto la curva pasa a ser lineal, como se muestra en la Figura 5.9.

En el caso del diodo HSCH 5312 se diseña un circuito presentado en la Figura 5.10. Las consideraciones de diseño son iguales a las del caso anterior. En este caso también ha sido necesario el segundo filtrado DC, se ha introducido también el efecto de las vías cilíndricas y la impedancia de entrada es la misma para todos los rectificadores estudiados, debido a que la antena no varía. La primera simulación se realiza con una frecuencia de 2.45GHz y un nivel de potencia de entrada de -5dBm. El resultado se puede apreciar en la Figura 5.11. Una vez más el nivel DC es muy bajo. Se comprueba si al aumentar el nivel de la potencia de entrada unos 10 o 15dBm la salida mejora, y los resultados se muestran en las Figuras 5.12 y 5.13. Para comparar los resultados con una medida que compense las diferencias entre la potencia de entrada se calcula el valor p para todos los casos y de nuevo se presenta en una tabla, la 5.4. Como se concluyó en los resultados anteriores, cuando la potencia de entrada es demasiado baja el porcentaje de voltaje recuperado es muy bajo también y parece indicar que el diodo está cerrado. Una vez más este porcentaje se encuentra alrededor del 5% para la mínima potencia de entrada y alrededor del 30% para las mayores. A pesar de que los valores son mejores, se debe resaltar que la mejor solución para este diodo no nos da un resultado en la tensión de salida DC tan plano como el conseguido con el diodo anterior, ya que la componente sinusoidal es más fácilmente reconocible. Para completar el análisis de este nuevo diodo, se presenta la curva del voltaje a la salida en función de la potencia de entrada en la Figura 5.14. Se puede apreciar que el resultado es muy similar al obtenido anteriormente con el diodo trabajando a 900MHz.

El último diodo estudiado es el MA4E 1317. El circuito para este diodo es muy similar a los dos anteriores y se puede encontrar en la Figura 5.15. En la Figura 5.16 se presentan los resultados a la simulación del circuito bajo los supuestos iniciales de frecuencia de trabajo y potencia recibida. Asimismo, se han llevado a cabo simulaciones con potencia de entrada mayor, la misma que en los casos anteriores, con el fin de poder comparar los tres diodos en las Figuras 5.17 y 5.18. En la Tabla 5.5 se presentan los valores p para el diodo bajo estudio. En este caso todos los valores porcentuales son mayores los anteriores. De especial interés resulta el que para una potencia recibida de 10dBm el porcentaje de voltaje recuperado llega a ser del 50%. Si se observa la Figura 5.19 donde se representa el voltaje de salida en función de la potencia de entrada, se puede apreciar como el voltaje a la salida crece muy rápidamente, mucho más que en los casos anteriores.

Para comparar los tres diodos y elegir el más adecuado, se comparan los valores del parámetro p definido anteriormente. Como se puede observar en la Tabla 5.6 los mejores resultados son los obtenidos con el diodo de MACOM Technologies.

A pesar de esto, aun con los mejores resultados obtenidos con el tercer diodo, el nivel DC en la carga es demasiado bajo, siendo el porcentaje de voltaje recuperado a la salida aproximadamente del 9%. Se deduce de este resultado y al estudiar la curva que muestra la relación entre la potencia a la entrada y el voltaje a la salida que ninguno de los diodos, ni el que da los mejores resultados, consigue estar completamente abierto cuando la potencia recibida es de -5dBm.

En el **sexto** y último **capítulo** es donde se presentan las conclusiones del trabajo realizado tras el completo estudio llevado a cabo sobre los componentes de un sistema para la transmisión de potencia inalámbrica. El estado del arte ha sido presentado y se ha elegido una tecnología apropiada en función de las características requeridas del sistema. Asimismo se ha diseñado y construido una antena de parche con polarización circular y alimentación simple. Finalmente se han estudiado tres posibles circuitos para el rectificador.

La principal conclusión a la que se llega es que a pesar de que el problema de la transmisión de potencia inalámbrica ha sido aparentemente muy estudiada y discutirá en las últimas décadas, no existe una solución eficiente basada en el uso de la propagación de ondas electromagnéticas cuando se utiliza para dicha solución un diodo. Todos los trabajos publicados hasta hoy demuestran que cuando la potencia recibida es alta, se consiguen buenas eficiencias de conversión. Pero el sistema completo no es factible, al menos no con las tecnologías que conocemos hoy en día.

Los límites del sistema se discuten a lo largo de todo el documento. Es importante ver como las restricciones de seguridad limitan la potencia que es posible emitir. Considerando la frecuencia de operación y el escenario medio estudiado, resulta que la potencia que se alcanza en recepción no es lo suficientemente alta como para que el diodo esté completamente abierto. En cualquier caso no está lo suficientemente abierto como para poder alcanzar una buena eficiencia de conversión. De este modo, las pérdidas son verdaderamente altas y una gran cantidad de energía se desperdicia. Además, la solución basada en ondas electromagnéticas es bastante limitada debido a la dificultad de alcanzar el compromiso existente entre la libertad de posicionamiento del receptor en una habitación (un potencial dispositivo que debe ser “alimentado” por el sistema) y el deseado (o necesario) nivel de potencia en esa posición. La primera condición requiere antenas casi omnidireccionales que suelen tener bajas ganancias. La segunda condición requiere altas ganancias, por lo que se forzará a las antenas a ser mucho más directivas. En este último caso se pierde por completo la condición de libertad en el posicionamiento del receptor. A pesar de que la antena transmisora puede tener un diagrama de radiación más estrecho, la antena receptora se debe poder colocar en cualquier punto de la habitación y con cualquier orientación, lo que eliminaría la necesidad de alineación. En cualquier caso, necesitaríamos un diodo que fuera verdaderamente zero-biased, cuya gráfica tuviera la curvatura comenzando exactamente en 0W o en un lugar muy cercano al cero. Un diodo con estas características no se ha encontrado y parece ideal hoy en día. Un avance realmente importante en la tecnología de los diodos se hace necesario por tanto para conseguir buenos resultados para un sistema de características similares al estudiado en el presente proyecto.

Con esta idea, la decisión tomada ha sido la de no construir ningún circuito rectificador debido a que el sistema no tiene el comportamiento deseado. En el presente documento se prueba ampliamente que sería posible construir un sistema con las características requeridas si se consiguiera recibir una mayor cantidad de energía en la antena.

Si se encontrara un diodo apropiado, el siguiente paso sería la integración del receptor juntando la antena receptora y el circuito rectificador, dando lugar a una antena activa. Posiblemente mejoraría el funcionamiento y los resultados del sistema crear un circuito

rectificador no solo con un solo diodo, sino con varias etapas consistentes en un diodo y un filtro paso DC conectadas en cascada. Esta configuración puede aumentar la eficiencia a valores mucho mejores. Aun así, esta solución de conectar varias etapas rectificadoras en cascada no elimina la necesidad de que el diodo este abierto para conseguir buenos resultados. Por lo tanto, incluso en este caso se requiere el uso un diodo con un voltaje umbral verdaderamente bajo en el circuito.

Chapter 1.

Introduction

The request from all the electronic users around the world the possibility to work wirelessly has grown dramatically during the last years. Therefore the number of wireless devices is growing on and on every day. But, can we say that all this devices are really wireless? There is no doubt that when they are in use, transmitting information, for example, they do not need any wires to work. Nonetheless, they are actually “wire-dependents” since they need integrated batteries in them. So these batteries will need to be charged or replaced. Sometimes the replacement of the batteries is not possible or very expensive; hence a real necessity of a feasible solution exists. If a real wireless system is needed it will be necessary to study, not only the transmission of information, but also the power supply to increase their lifetime.

The present project comes up from this motivation and wants to be a starting point for the development of a whole system which will supply power to a device placed in a small room, as an office. Therefore the distance between the transmitter and the receiver will be short, but with the system dimensioned in such a way that allows us to work in the far field region. It will compromise the frequency and the dimensions of the transmitter antenna. The average distance from the corner of the room (where the antenna will be placed) to the receiver will be 3 meters. The system will be working at 2.45 GHz, an ISM frequency (standing for Industrial, Scientific and Medical frequencies).

In a first place we will have a look to the technologies that exist to wireless power supply. Secondly, we will choose the best and most adequate for our requirements. Then, three different technologies will be presented and briefly explained.

Thirdly, the regulation for the safety will be studied and the maximum level of the radiated power will be calculated.

In fourth place, we will present the principles for an antenna with the desired characteristics found in the previous chapters. An antenna with such characteristics will be designed and built.

Finally, a circuit to prepare the power to be delivered to the receiver will be studied, designed, constructed and the results will be presented with the measurements upon the receiver.

Chapter 2.

Wireless Transmission Concepts

Wireless powering is the technique which allows the distribution of electrical energy without using a guided wave. Contrary to the data transfer, the efficiency is the key parameter. Wireless power transmission needs a system which covers 3 steps:

1. Conversion of DC electrical power into RF power.
2. Transmission of the RF power
3. Collection of the RF power, and convert it into DC electrical power again.

We can consider three ideas for wireless supply: Firstly, reactive coupling which consists in the use of coils and its coupling properties to the supply of energy wirelessly from the source to the receiver. It is also possible to design a special structure that will allow us to transmit both signal and electrical power supply through a thin sheet at microwave frequencies. The last proposal is the transmission with the help of electromagnetic waves through the free space.

Using a rectifier scheme in the receiver is possible to convert the incoming frequency to DC, so we can have the energy available to be used in any charging process. These three ideas will be developed and we will choose the best solution for the problem studied in the present chapter.

We can divide the scenarios of Wireless Power Transmission in two big groups. On one hand, we have the near field scenarios, and on the other the far field scenarios.

For near field applications we will be working in an inductive transfer environment. The major part of the losses will be associated in the coils due to their resistance. The action of an electrical transformer is the simplest example of wireless energy transfer. The primary and secondary circuits of a transformer are not directly connected. The transfer of energy takes place trough electromagnetic coupling in a process known as mutual induction. (An added benefit is the capability to step the primary voltage either up or down.) The battery chargers of a mobile phone or the transformers on the street are examples of how this principle can be used. Induction cookers and many electric toothbrushes are also powered by this technique. The main drawback to induction, however, is the short range. The receiver must be very close to the transmitter or induction unit in order to inductively couple with it. It is also under this principle where the design and fabrication of special structures to supply power wirelessly will rise.

In far field applications, we will have to considerate that the distance of the device(s) to the source will have to be widely bigger than the diameter of the device(s). We will have large free space looses in many of the scenarios (depending on the frequencies, the distance and the environment). It is in this scenario where the electromagnetic solution will be placed. It is also remarkable that some of the implementations of induction, as principle for WPT (wireless

power transmission), are nowadays working in the far field region with acceptable results. For this configuration, in addition to the transmitter, we will consider the combination of a receiving antenna and a rectifier in a joint structure, known as rectenna. Then, for a wireless power transmission system, the last step (collection of the RF power and later conversion into DC electrical power) is the key step for the electromagnetic solution. The design of the receiver will determine the efficiency of the whole system, since it will be the most restrictive part. As the properties of the microwave communications have been widely proofed and the technologies involved are really advanced (antenna and rectifiers), the main goal will be to determine the best way to integrate these two elements in order to increase the efficiency as much as possible. These high frequencies will allow us to have small size of the elements. However, on the other side, it will force us to make as accurate designs as possible because of the high free space losses.

The beginnings of WPT

The first idea for wireless power transmission appeared in the late XIX century with the ideas and experiments of Nikola Tesla [**1**]. Between 1891 and 1893 he patented a system of electric lighting and demonstrated the wireless illumination of phosphorescent lamps. He used a Tesla coil which was connected to a 60 m high mast of with a 90 cm-diameter ball (toroid). A 300kW power was fed to the Tesla coil that resonated at 150 kHz. Nevertheless there are no records about the amount of power that he could really transmit to a distant point. With demonstrative purposes, Tesla tried to keep working some bulbs with the power obtained of the non-collimated energy radiation. Unfortunately, due to economical problems, he was not able to finish the whole project. Definitely, Tesla's researches were large out of time. This is the reason why until 20 years later there were no more attempts to develop Tesla's ideas.

In 1930, much progress in generating high-power microwaves was achieved by invention of the magnetron and the klystron. Though the magnetron was invented by A. W. Hull in 1921, the practical and efficient magnetron tube only gathered the world interest after Kinjiro Okabe proposed the divide anode-type magnetron in 1928. Microwave generation by the klystron was achieved by the Varian brothers in 1937 based on the first idea by the Heil brothers in Germany in 1935[**2**].

A new era for the wireless power transmission (WPT) began in the 50s, with the high power microwave generators. In 1958 a S-band cross-field amplifier tube was invented with a average power of 15KW. It achieved a conversion efficiency of 81% [**3**], [**4**].

Modern history of WPT based on induction

New attempts to continue with the researches in the Wireless Power Transmission appeared in 1960. In this year a research to build artificial hearts powered by induction began [**5**]. The researches were carried out mainly in the field of health. Attention was paid to applications with low separation between the transmitter and the receiver to feed artificial organs. It motivated lots of investigations in that field, because of the reliability of its

applications. This is the reason why many papers about the subject have been published since then.

It is worthy to mention the paper published in 1965, where improvements in the efficiency of energy transportation are achieved by using a suitable ferrite core for the implanted coil. A detailed theoretical analysis is undertaken, with particular emphasis upon hollow spherical and oblate spheroidal cores indicates the way in which the improvement is related to the geometry of the core and the electrical and magnetic parameters of the ferrite.[**6**]

In 1977, Wen H. Ko Sheau, P. Liang Cliff and D. F. Fung wrote a paper where a seven step design procedure for the transmitting and receiving coils was described based on R.F. [**7**]. Experimental results were within the desired total system efficiency ranges of 18% and 23%, respectively. A transcutaneous signal transmission system for an auditory prosthesis has been designed in a study wrote on 1984 by Erwin S. Hochmair. The main goal of this work was to optimize the coil geometries and prevent the RF output amplifier from saturating [**8**].

A series resonant converter was introduced as a part of a WPT achieving the transmission for a 1-2cm distance between the transmitter and the receiver. The efficiency for this scheme was 72% [**9**]. The generalized and optimal topologies of zero-voltage-switching and zero-current-switching resonant DC/DC power converters are presented in paper by Marian K. Kazimierczuk and Jacek Jozwik. It was shown that many equivalent topologies of the converters can be derived from each of the generalized topologies. Furthermore, the generalized topologies of the converters clearly show which of the parasitic capacitances and inductances can be absorbed into the *LC* resonant circuit[**10**].

The Class-E concept was introduced to the field in 1992, with a system based on the single ended class-E power amplification scheme. It is shown that a self oscillating class-E tuned power amplifier involving an inductive link permits high-efficiency coupling-insensitive power transmission. The oscillation frequency is not fixed but influenced by the coupling of the coils [**11**]. One year later, it was brought in the Class-C concept, in a system where the oscillating condition of the circuit matches the condition of the transformer, and the output voltage is always sinusoidal, the noise of the circuit and the core loss of the transformer due to the harmonics are small. The oscillating condition in a class C converter is automatically adjusted by a simple bias circuit which is made with a diode and a resistor [**12**].

The induction as base to wireless power transmission was not only studied to be used in medical applications, but also in many other applications. A study initiated in the late 90s aimed to transfer contactless power energy to add new functions to a tool (drill machine for example). A bi-directional communication was also needed, so it was used an ironless high frequency transformer for both power and information transmission. Different coil geometries have been studied to reduce mutual inductance between power and information coils. This new solution enabled to build low cost and smart energy transfer systems including communication [**13**].

For a case of an automatic inductive charging application, a tank circuit was proposed for a converter which consisted of leakage inductance, magnetizing inductance and two capacitors

with an inductive output filter. This converter allowed the transfer of power without over-sizing the inverter and a witching mode of the transistors. The switching mode and the sensitivity to the load variation, the coupling factor and the air gap (6-8 mm) were studied using the first harmonic method. Theoretical results were experimentally validated with a 3 kW prototype, with satisfactory results [**14**]. Even for compact electronic devices, as mobile phones, a technique enabling the implementation of high-efficiency, high-power-density, fully regulated contactless electrical energy transmission system suitable for applications with a wide input and load range was proposed. The high efficiency of the system is achieved by recovering the energy stored in the leakage inductances of the transformer. It incorporates them in the operation of the circuit and employs a high-frequency-inverter and a controlled-rectifier. These topologies allow a controlled bidirectional power to flow through the transformer. In addition, a feed-forward variable-switching-frequency control of the inverter is used to maintain approximately constant power transfer through the transformer with the input voltage changes. Specifically, the described contactless electrical energy transmission system is suitable for use in a universal-input battery charger. This was verified on a 4.5W prototype battery charger for portable telephones [**15**]. Other examples include material handling systems [**16**] and public transport systems [**17**] where the secondary systems are electrically isolated and move along a long track. The advantages of such systems are safety, reliability, low maintenance and long product life.

Frequencies in UHF band were introduced in 2006, with superconducting inductors. The result shows that a superconducting inductor is almost lossless in comparison with an identical spiral inductor made of copper at ultra-high frequencies (> 100 MHz). Furthermore, the superconducting inductor is capable of carrying high currents. It is also verified that for ultra-high frequency power conversion, a superconducting inductor is a viable option in applications where liquid nitrogen cooling can be implemented and the need for shielding at such high frequencies [**18**].

It is also remarkable the contribution from the Swiss company ABB to the field. This company developed a wireless technology called WISA (standing for Wireless Interface to Sensors and Actuators) centered at 2.45GHz. The range is about some meters, so a huge air-gap is considered. Typically “primary” power loops are installed around the application. These are fed by power supplies that set up an alternating current in the loops, producing a magnetic field. The receivers are built as small “secondary” coils that pick up the energy from the magnetic field and convert it to electric power. The power losses in the loops due to skin and eddy-current effects are dependent on their environment, but typically small. An omnidirectional receiver is used to be angular independent. As a unidirectional primary field could be shielded by metal objects, a rotating field had to be used in some applications [**19**].

Modern history of special structures for WPT

The youngest field is the design and construction of new structures that appear as a solution for the application that needs small distance between the transmitter and the receiver. The first work, published in2004 [**20**], proposed a two-dimensional communication device in which signals travel freely between arbitrary points in flexible two-dimensional space using two-dimensionally-spread electromagnetic field. It also has advantages over other

mechanisms of wireless communication. It consumes less energy for signal transmission, it can provide energy for the connected elements, and the communication capacity is larger because multiple ID signal chains transmit signals simultaneously. This technology consists of two principles. On one side the principle of two dimensional communications. It is a communication in which electromagnetic energy is located in a two dimensional medium and any element connected to the medium can communicate with each other without individual wires. Using this method, we can easily allocate a lot of sensors on the two dimensional sheet, and gather data from each node with high throughput. The configuration for a two dimensional communication sheet consists of three layers. Two conductive layers are set to sandwich the dielectric layer. The sheet has the connection apertures on the surface of it for receiving signals. When an alternate voltage between the conductive layers is impressed through the aperture, there exists a propagation mode of the electromagnetic wave signal within the dielectric layer. This electromagnetic wave is used for signal transmission between each communication node attached to the aperture. Any materials with high conductivity are available as the conductive layers like conductive fabrics and conductive rubbers. This technology was examined successfully using a prototype system, which realized stable communications through the sheet using the IEEE 802.1 protocol [**21**]. On the other hand, we have the transmission of power using an electrode as a resonant proximity connector. When voltage is applied between the two terminals of the electrode, the produced electric field is vertical to the layer and it is proved that the impedance between the terminals becomes zero ideally even though there is no electrical contact between them. There is little dependence on the gap between the connector and the sheet. It was confirmed that electrical power could be received by rectifying the alternate voltages. In the prototype, 20mW was received through the sheet when the microwave signal of 110mW at 2.4 GHz was entered.[**22**].

Another application of this technology is in the field of health. The main use is to do a 2D myoelectric pattern measurement. The myoelectric signal is the signal that can be measured when the muscle contraction occurs [**23**].

Modern history of WPT based on electromagnetic waves

In the earliest 60s William C. Brown, employee at the Raytheon Company, started working on electromagnetic propagation through free space as a solution for Wireless Power Transmission. He developed the first device for an efficient microwave reception and later power rectifying. It consisted of a dipole with a balanced bridge or a semiconductor diode in its reference plane. A frequency of 2.45GHz was chosen because the advanced technology is based and centered in one of the ISM bands (industrial, scientific and medical). In addition, this band has low attenuation in the atmosphere, even with strong storms or other severe weather conditions [**3**]. In 1964 Brown demonstrated how it worked on a model helicopter that received all the power needed for flight from a microwave beam. The first proposal wirelessly transferring solar energy captured in space using "Powerbeaming" technology was done by Peter Glaser in 1968.

Until 1970 the unique used frequency was 2.45 GHz. In 1977 Brown achieved a 90.6% efficiency. The system consisted of a barrier GaAs-Pt Schottky diode, with a microwave power

incident level of 8W. Aluminum bars were used to build the antenna and the transmission lines that formed the overall rectenna [**24**]. Also in the 70s, at Los-Alamos National Lab, the first passive RFID system was designed, built and proved successfully [**25**]. This experiment brought new interest in the field, since its commercial possibilities were really broad.

In 1987, the NASA published the research results about rectennas as they first started exploring a new operating frequency in 20GHZ [**26**]. The main goal of this report was to integrate this new technology to the satellite program, in order to change or complete the powering systems for the satellites. Nevertheless nowadays the company seems no longer interested in wireless power transmission based on rectifying concept since the last collaborations to investigate in this field were some years ago.

Until that moment, the major part of the built systems for wireless power transmission was centered at 2.45GHz. However, this frequency does not allow having antennas with a reduced area. In 1991 ARCO Power Technologies developed a rectenna working at 35GHz with a conversion efficiency of 72% to reduce the area of the antennas [**27**]. This second frequency was chosen in the window between the first H_2O and O_2 absorption peaks since the attenuation is lower. Nevertheless, in the early 1990s the components at such high frequencies were not so developed as nowadays, so they used to be very expensive and ineffective components. Therefore, another intermediate frequency was searched, to reduce the size of the antennas, without sacrificing the efficiency of the components. In 1992 the first rectenna in the C band achieved an efficiency of 80% working at 5.87GHz (ISM band) [**28**]. Five years later Kai Chang published his first work about rectennas. They achieved an 82% efficiency working at 5.8GHz [**29**]. In the year 2000, a circularly polarized rectenna at 5.87GHz was built. It did not need a precise alignment between transmitter and receiver, and achieved an efficiency of 60% [**30**].

Introducing a fourth working frequency, a double polarized rectenna working at 8.51GHz was designed [**31**]. In 1992 new frequencies, as 10GHz and 35GHz have also been studied and receivers have been successfully designed at these new frequencies. It is remarkable the labor of Kai Chang and Tae-Whan Yoo who achieved low efficiencies at both frequencies (60% and 39%). It represented a huge advance and, again, a trustful and complete reference. They also added a detailed explanation about the behavior of the diode at high frequencies when it is disposed as rectifier [**32**].

Choice of an appropriate technology and detailed recent publications

As it was introduced in the beginning of the present project, the scenario is placed in an average office. It seems logical that with our parameters we cannot work in near field, so we are forced to use a far field solution. Therefore, the technology used will be the one based on the propagation of electromagnetic waves in free space, built on rectennas.

A great advantage of the chosen configuration is that we can supply power to many devices at the same time, since it is a point to multipoint technology. It will be only necessary to build one receiver so that we can place several receivers working at the same time. This configuration allows the whole system to spread all the RF power in all the room, so that any receiver placed on any point of the room will work (in some points better than in others).

The basic structure for a rectenna is composed of an antenna and a rectifier circuit forming an active antenna. The rectifying circuit consists on a diode followed by a low pass filter to reject all the higher frequencies. In its basic form it is built as a single diode shunted across the transmission line. Another low pass filter is inserted between the antenna and rectifying circuit to reject some of the higher order harmonics generated from the nonlinear rectifying. It may also be necessary a matching circuit to reduce also the insertion losses. The basic principle of the microwave power conversion is analogous to a diode clamping circuit or a large signal mixer at microwave frequencies. The power conversion efficiency is maximized by substantially confining all the higher order harmonics between the low pass filter and the dc pass filter, using an efficient diode and matching the diode input impedance to the antenna one.

A summary of all the investigations carried out until that date can be seen in [**33**]. The diode used in the rectenna circuit is the M/A COM flip-chip detector diode MA4E1317. A 50 VDC C08BLBB1X5UX dc-blocking chip capacitor manufactured by Dielectric Laboratories, Cazenovia, NY, serves as the dc-pass filter to not only tune out this diode reactance, but also to minimize the power at the harmonic frequencies. The capacitor is used to reflect all of the microwave energy to reach the load resistor and returning the RF energy back to the diode. The optimal distance between the dc-pass capacitor and the diode has been determined in such a way that produces the maximum diode RF-to-dc conversion over 85%. This diode conversion efficiency sets the upper limit on the rectenna's RF-to-dc conversion efficiency. Coplanar stripline (CPS) is chosen as the technology for the transmission lines for fabrication simplicity and size reduction. The dimensions of the coplanar stripline have to provide the proper size for diode and capacitor bonding and the desired coplanar stripline characteristic impedance. In addition, the impedance of coplanar stripline is higher than that of microstrip and matches to the real input impedance of the diode better. A coplanar stripline band-reject filter is used to pass 5.8 GHz from the antenna to the diode and block the second harmonic 11.6 GHz from flowing from the diode to the antenna. A special geometry is designed to improve the rejection of upper bands by adding additional stubs. The coplanar stripline band-reject filter uses stubs to block 11.6 GHz. This filter has high harmonic rejection in comparison with other planar CPS geometries of comparable size. The antenna used is a dual-rhombic-loop antenna in an array configuration. Each dual-rhombic-loop antenna is terminated with two gaps. The positioning of the gaps yields to right-hand circular polarization. If the gaps are mirrored to the opposing sides of each antenna, the dual-rhombic-loop antenna array will become left-hand circular polarization. The advantages for using the dual-rhombic-loop antenna array are high CP gain and fabrication simplicity. A reflecting plane is located behind the rectenna substrate in order to increase the gain of the DRLA array by directing its beam broadside in one direction. The maximum efficiency achieved at 5.8GHz was 82% with a power density of $2\,mW/cm^2$. The coplanar stripline band-reject filter suppresses the second harmonic signal to approximately 14 dB below the gain at the fundamental frequency. This results in minimal radiation at the second harmonic frequency.

Another recent work from Kai Chang tries to develop a rectenna for two frequencies. The paper, published in 2007 proposes a novel dual-frequency rectifying antenna operating at 2.45 and 5.8 GHz [**34**]. The rectifying antenna consists of two compact ring slot antennas, a Hairpin lowpass filter, and a rectifying circuit. The annual slot ring antenna uses a meander line

structure to reduce its size to 52% of the regular ring slot antenna. The hairpin filter helps suppress the second order and the third order harmonics of both operation frequencies.

The lowpass filter is designed based on the elliptic function filter. Two hairpin resonator components are cascaded to obtain a sharper cutoff frequency response. The filter is designed to block the harmonics generated by the nonlinear diode from reradiating through the antenna and to avoid the harmonic power dissipation in the load. It is also a compact design to keep the rectenna small. In this case it is especially difficult because the harmonic of second order of the first frequency, 2.45GHz, is 4.9GHz, very close to the second operation frequency 5.8GHz. Despite it, the filter can reject higher order harmonics of both 2.45 and 5.8 GHz. The used rectifying circuit is a half-wave rectifier. A GaAs Schottky diode (MA4E1317 by M/A COM) is used as the rectifying device. The antenna consists of a slot annual ring antenna. It operates at lower frequency (2.45 GHz) and the slot rectangular ring antenna is used to excite the higher frequency (5.8 GHz). The slot rectangular ring is within the meandered slot annual ring. A simple microstrip feed-line is used to excite both antennas. The rectenna has gains of 2.19 and 3.6dBi at 2.45 and 5.8 GHz, respectively. The rectenna has been tested and it can provide a dc voltage of 2.6 V with a conversion efficiency of 65% as the power density is $10\,mW/cm^2$.

In 2008 a new configuration for the rectenna is proposed in order to supply the energy to far elements when very low level of power is available in the receiver(s) [**35**]. The RF to DC power conversion system is designed to operate in UHF frequencies in the ISM band of 902–928MHz. The system is optimized to operate at distances above 10 meters. Given that the power density drops off as a function of the distance (d) at the rate of $1/d^2$ in free space, the propagation RF signal loss through the air at 915 MHz can be calculated to be 51.6 dB with the Friis equation for free space loss. A RF-DC power conversion system is designed to passively amplify the voltage available for rectification by forming a high-Q resonator; this is the key method to improve the efficiency. The passive voltage gain from the high-Q resonator is directly proportional to its load. With an increase in the amplitude of the voltage coming to the input of the rectifier, the output voltage of the rectifier also increases and, therefore, increases the overall power conversion efficiency of the system. The main aim is to maximize the voltage coming into the RF-DC power conversion system so that it can provide a stable DC output voltage at ultra-low receive power. It consists of an antenna to pick up the power radiated by the RF waves, an impedance matching network to ensure maximum power transfer in the system, and a rectifier circuit to convert the RF signal to a DC voltage. The antenna is designed with meander lines on a printed circuit board to reduce the area of the antenna and to provide the desired antenna input impedance to the impedance matching network. The rectifier is build with NMOS and CMOS transistors forming Floating-Gate Voltage Doubler Rectifier. It is demonstrated that the system works with signals as low as 50 mV and has a maximum measured efficiency of 60%. This allows an increase in the working distance between the circuit and the radiation source. The system operates with a received power as low as -22.6dBm (5.5µW), corresponding to 42 meters distance in free-space with a 4 W radiation source.

Most papers on this topic have paid their attention to the receiver.

Chapter 3.

Safety Regulation and Maximum Radiated Power

Microwave radiation comprising the frequency range from 300 MHz to 300 GHz on the electromagnetic spectrum is very widely used in different areas of science and technology. These radiations are categorized as non-ionizing radiation. The radiation in the frequency range from 300 MHz to 10 GHz can be easily absorbed for biological tissues due to the water and protein molecules present in the body. This produces heat due in the corresponding tissues. In order to prevent secondary effects on biological tissues there are some limits that cannot be overcome in the radiated power. . In [**36**] a detailed information about the limits is exposed. The restrictions in the radiated power are differently applied for two groups of people. On the one hand there is a restriction to apply for all people whose work is involved in the radiation and who are exposed to the radiated field. On the other, there is the restriction for the general public who ignore (or it is not supposed to know) the existence of the electromagnetic field. The restrictions are expressed both in electric field and magnetic field. In each case, there are two recommendations available: the average value and the peak value.

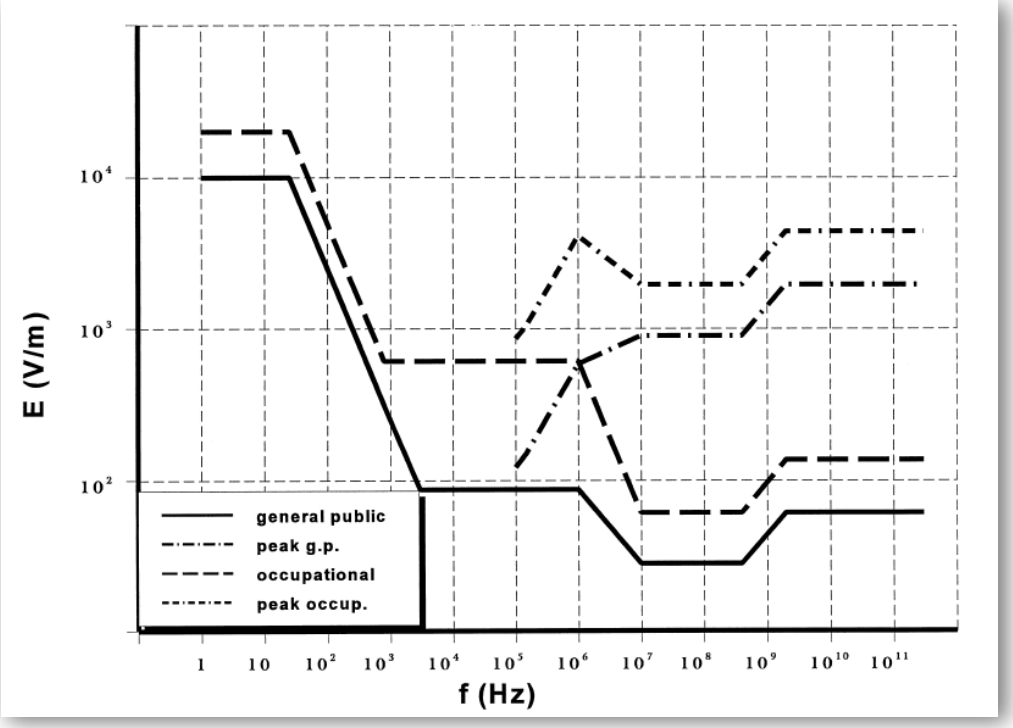

Figure 3.1 Electric Field restriction as function of the frequency [36]

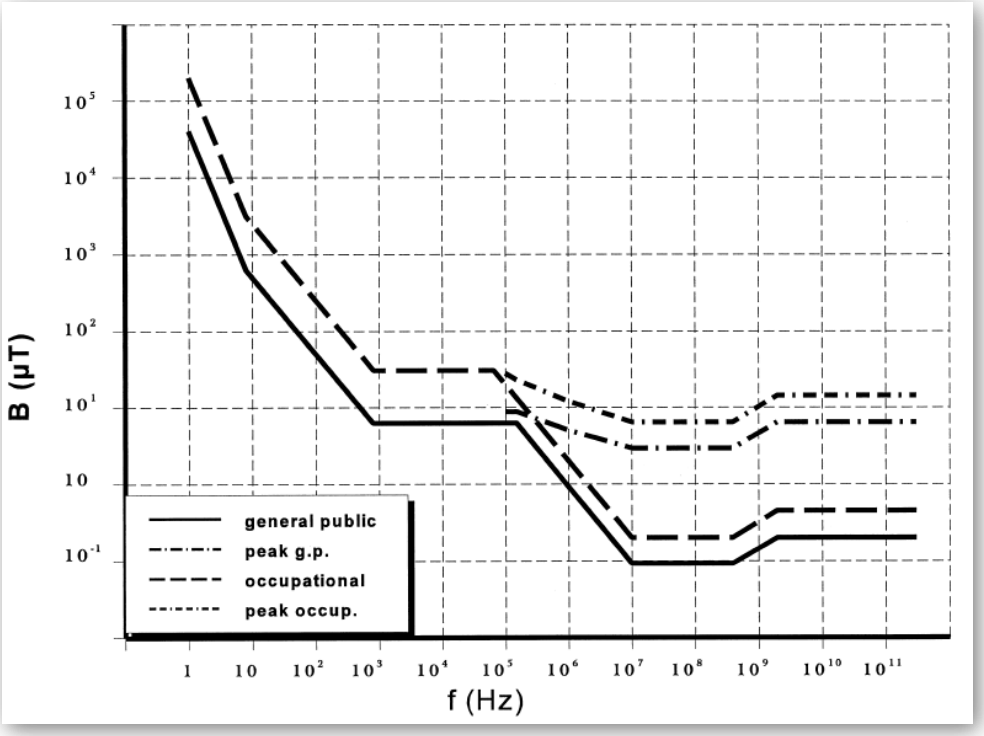

Figure 3.2 Magnetic Field restiction as function of the frequency [36]

A table is also presented with the average values for the fields E, H, B and also for the equivalent power density (S). It is important to consider that the provided basic restrictions are met and adverse indirect effects can be excluded, field strength values can be exceeded. S_{eq}, E^2, H^2, and B^2 are to be averaged over any 6-min period.

Reference levels for OCCUPATIONAL EXPOSURE to time-varying electric and magnetic fields			
E-field strength (Vm^{-1})	**H-field strength (Am^{-1})**	**B-field (μT)**	**S_{eq} (Wm^{-2})**
137	0.36	0.45	50
Reference levels for GENERAL PUBLIC EXPOSURE to time-varying electric and magnetic fields			
E-field strength (Vm^{-1})	**H-field strength (Am^{-1})**	**B-field (μT)**	**S_{eq} (Wm^{-2})**
61	0.16	0.20	10

Table 3.1 Reference levels for exposure to time-varying electric and magnetic fields

In our particular case, we have to consider the two limits:

$S_{max} = 50\ ^{W}/_{m^2}$, for the occupational exposures.

$S_{max} = 10\ ^{W}/_{m^2}$, for the general public.

We will design the whole system considering always the more restrictive values, to ensure the safety in every case. Hence we will be using the maximum value for general public.

To calculate the maximum radiated power we will need to do some assumptions. In the first place, about the transmitting antenna, we will assume that it radiates uniformly to a solid angle of π/2 sradian. Thus, the directivity of the antenna will be 9dB. From the safety point of view it is better to make this assumption, since we are concerned with the worst case. It will be also necessary to know (or estimate) the diameter of the antenna. The effective area (A_{eff}) can be expressed as a function of the wavelength in the vacuum (λ_0), the efficiency (ε) and the directivity (D) of the antenna.

$$A_{eff} = \frac{\lambda_0^{\,2}}{4\pi}\varepsilon D\left[m^2\right] \tag{3.1}$$

We can estimate the diameter or maximum extension of the antenna (D) as the square root of the value of the effective area.

$$D = \sqrt{\frac{\lambda_0^{\,2}}{4\pi}\varepsilon D}\left[m\right] \tag{3.2}$$

So, the estimated value for the diameter will be

$$D = 0.0974\ m \tag{3.3}$$

The distance (r) to calculate the maximum radiated power will be taken as the beginning of the far field. This value can be obtained by the equation:

$$r = \frac{2D^2}{\lambda_0} \tag{3.4}$$

Therefore, the considered distance will be r= 0.1548m.We can see that this is the optimal point to consider the received power, since it is the point with the maximum level of power. The free space losses are obtained from the Friis equation:

$$L_{fs} = 20\log\left(\frac{4\pi r}{\lambda_0}\right) = 20\log\left(\frac{4\pi df}{c}\right) \tag{3.5}$$

From the link budget, we can obtain the relation between the given value of the Power Density (*S*) and the transmitted power. As it is known, the received power (P_{rx}) is a function of the transmitted power (P_{tx}), the gains of the antennas, transmitter and receiver one (G_{tx} and G_{rx}), and the free space loses defined before.

$$P_{rx} = P_{tx}\cdot G_{tx}\cdot G_{tx}\cdot\left(\frac{\lambda_0}{4\pi r}\right)^2 \tag{3.6}$$

We can split this equation in such a way that it is function of the power density. As it was said before the operating frequency is 2.45GHz.

$$P_{rx} = \frac{P_{tx} \cdot G_{tx}}{4\pi r^2} \cdot \frac{\lambda_0^{\,2}}{4\pi} \cdot G_{rx} = S \cdot \frac{\lambda_0^{\,2}}{4\pi} \cdot G_{rx} \tag{3.7}$$

Since we know the desired Power Density, we can calculate the allowed transmitted power.

$$P_{tx} = \frac{S \cdot 4\pi r^2}{G_{tx}} \tag{3.8}$$

If we consider the previous 9 dB antenna it results that

$$P_{tx} = 0.3791W \tag{3.9}$$

that, in dBm, is

$$P_{tx} = 25.7876dBm \tag{3.10}$$

With this received power we can see the power levels in the room and confirm that the best distance to calculate it is the beginning of the far field, since it is the bigger power level.

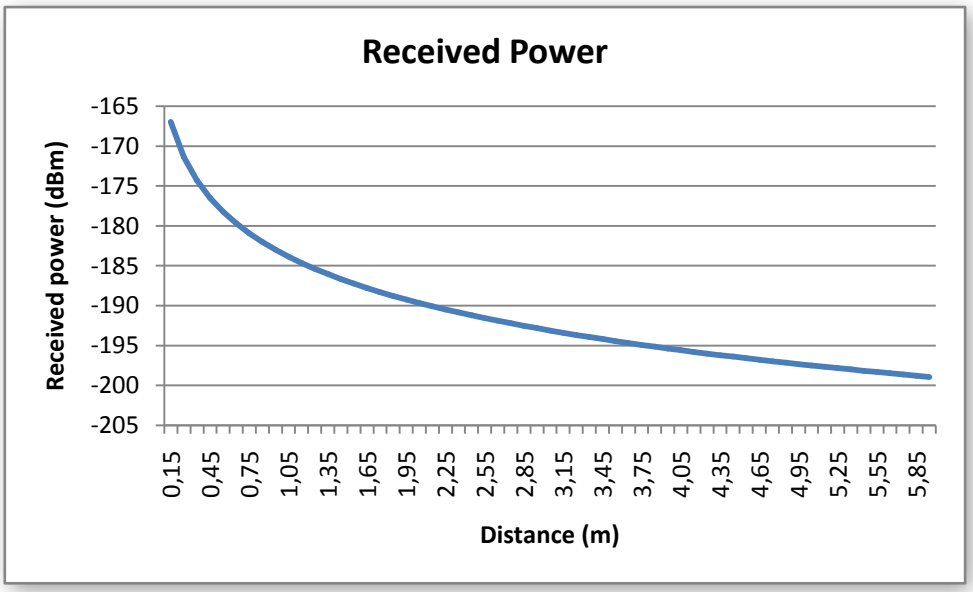

Figure 3.3 Received Power as function of the distance

Chapter 4.

Antenna

Fundamentals of radiation for patch antennas.

Patch printed antennas, also called microstrip antennas, are designed from transmission lines or resonators on dielectric substrates. The dimensions of this lines or resonators are chosen in such way that the power is dissipated in a radiation way. The first designs dates from the 50s decade, and they are used in systems from the 70s.

The structure consists of a metallic patch, of dimensions comparable to λ/2, on a dielectric substrate without any losses. The thickness takes values between 0.003 λ and 0.05 λ. The dielectric constant, , can have typical values form 2.2 to 12. In the lower part of the structure there is a perfect electric conductor (PEC) plane.

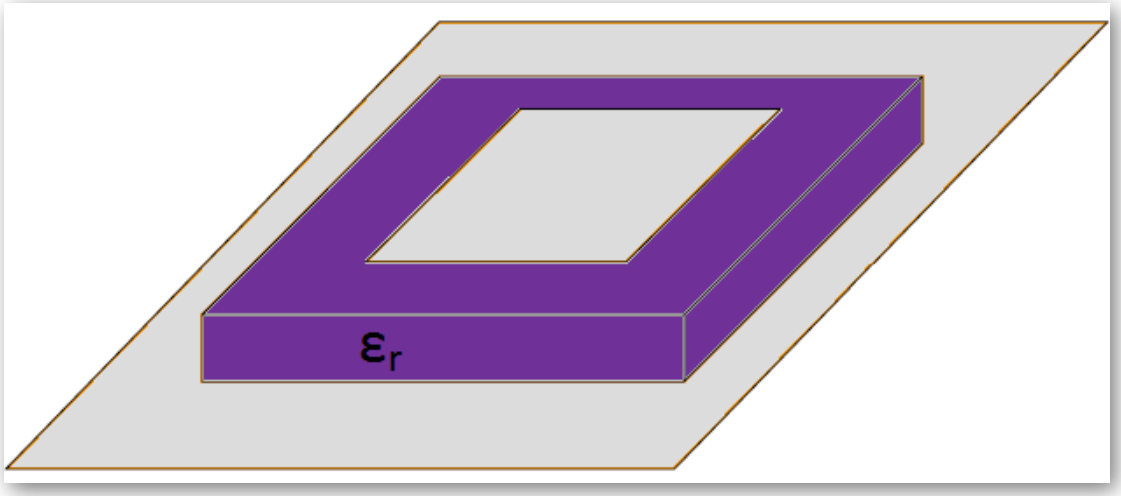

Figure 4.1 Typical rectangular patch

Its more significant advantages are its low profile and suitable shape which allows shaping and conforming the antenna to any structure (plane or curved). Its fabrication is easy and cheap. This kind of antennas is robust and it is possible to design them with integrated circuits of microwave, creating active antennas adding new features and capacities to the antenna. It is also remarkable that it is possible to achieve multifrequency performance and dual polarizations.

Their traditional drawbacks such as poor efficiencies, small bandwidth are nowadays overcome through different design strategies.

The more significant applications where patch antennas are involved are radar systems on satellites, global positioning systems, mobile antennas, hyperthermia treatment with heating systems, plane altimeters, military applications and any other microwave frequency system.

It is possible to find patch radiators with many shapes; however the most used are rectangular, circular and ring patches[**37**]

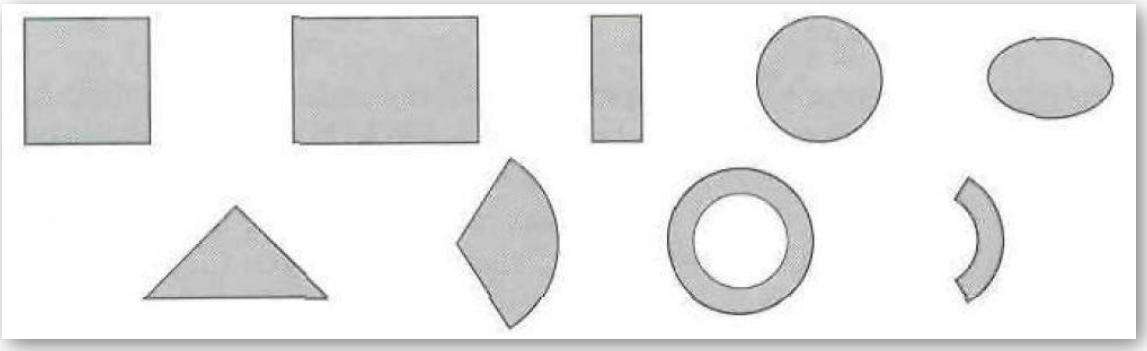

Figure 4.2 Some basic shapes of microstrip patch antennas [37]

There are multiple ways to feed patch antennas.

By conventional microstrip transmission line

It consists of a microstrip line, which has to be much narrower than the patch, arriving directly to the patch as we can see in the Figure 4.3. This is an easy fabrication process. Matching is simple to achieve by inserting the line more or less through two cuts into the patch, and modeling it is also very simple. Nevertheless, surface waves appear when the thickness of the substrate is increased and the non desiderated radiations increase too. This limits the bandwidth approximately a 2.5% [**37**].

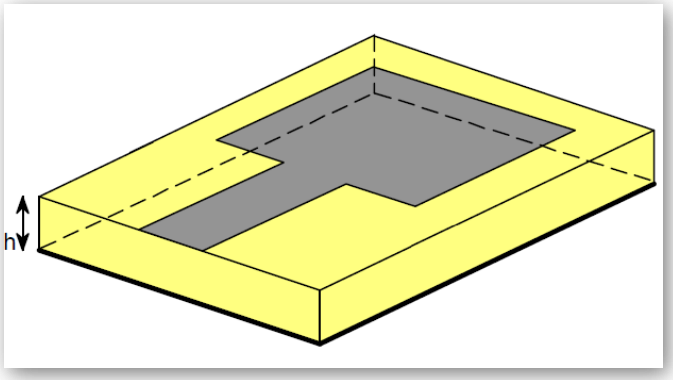

Figure 4.3 Feeding with conventional microstrip transmission line

By coaxial probe

This kind of feeding consists of coaxial transmission line where its inner conductor is connected to the patch, while the outer one is connected to the ground plane In the Figure 4.4 it is possible to see the structure of the technology. It can be easily fabricated and adapted, and the non desired radiation is low. However its bandwidth is narrow and it is difficult to model especially with thick substrates.

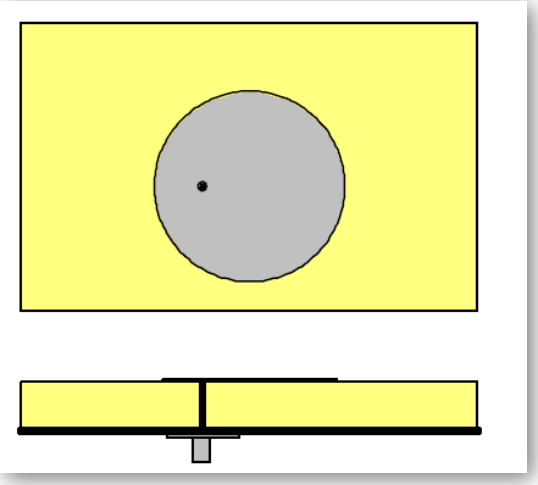

Figure 4.4 Feeding with a coaxial probe

By aperture-coupling

The asymmetries of the methods presented before generate higher order modes, and these modes produce crossed polarization radiation. The aperture-coupled patch is the one with a more difficult fabrication process. It also has a narrow bandwidth. Nevertheless it is easy to model ant has a relatively low non desired radiation. The basic structure basically consists of two substrates separated by a ground plane. In the lower part of the bottom substrate there is a microstrip line which energy is coupled to the patch by a slot in the ground plane. This configuration allows an independent optimization of the feed and the radiator. Usually, a substrate with a high permittivity is used for the feeding circuit while a thick substrate with lower permittivity will be placed as the upper substrate. The ground plane also isolates the feeding of the radiator element and it minimizes the interference with the non desired radiation. It gives very pure polarizations. Usually, the matching is achieved by changing the width of the line and the length of the slot in the ground plane.

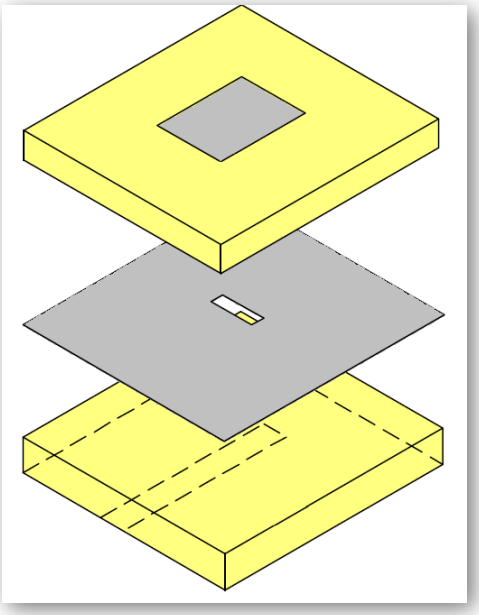

Figure 4.5 Feeding with slot

It is also possible the couple feeding but with a microstrip coupled transmission line, as we can see in the figure shown below. .

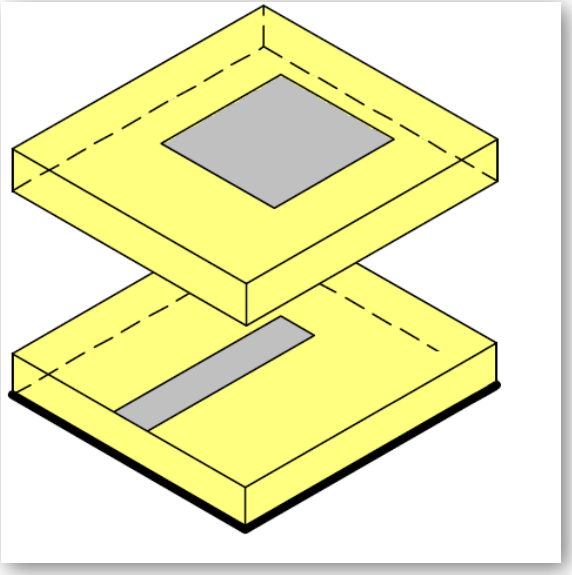

Figure 4.6 Feeding with a microstrip coupled transmission line

In the present project feeding with coaxial probe will be used due to the easiness of integrating the active of circuit with the antenna.

Microstrip antennas can be analyzed in many ways, from the simplest ones based in transmission lines or cavities to the most complex, using spectral or numerical methods.

A microstrip line consists in a conductor separated by a dielectric on a ground plane.

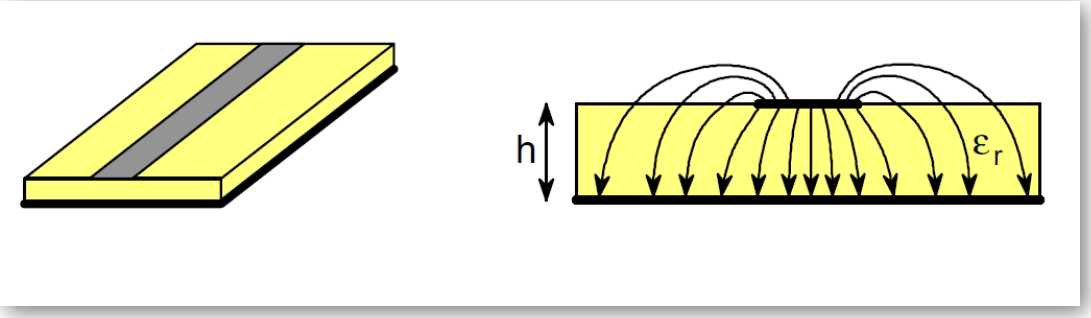

Figure 4.7 Microstrip Line

The fundamental mode is a quasi-TEM, being most of the field confined in the dielectric.

The dielectric is electrically thin (0.003 λ < h <0.05 λ) to avoid losses and superficial waves. The optimum values for the permittivity are low, i.e. in the range 2 < ε_r < 10 in order to have the field lines around the microstrip line. It is important to be careful with the high frequencies, since all the field can be confined under the line and almost eliminate the radiation.

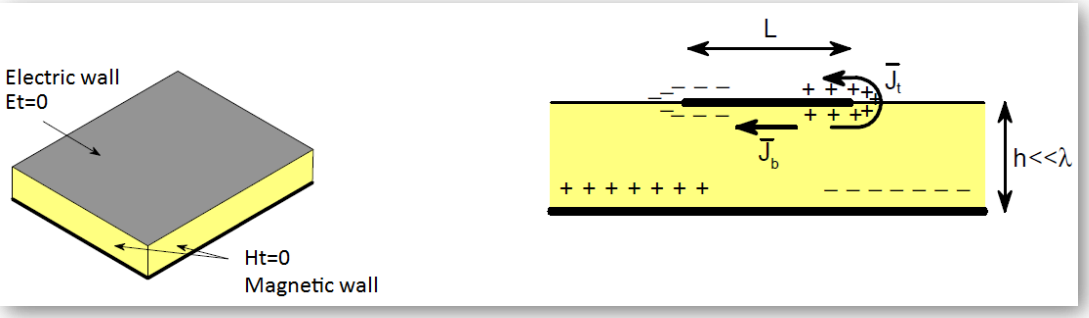

Figure 4.8 Patch antenna modeled as a cavity

The behavior of the microstrip antenna will be similar to the behavior of a cavity, because of the presence of electric and magnetic walls as we can see in the Figure 4.8. Inside the cavity, stationary waves are generated between both electric and magnetic walls. It is similar to a resonant circuit with losses.

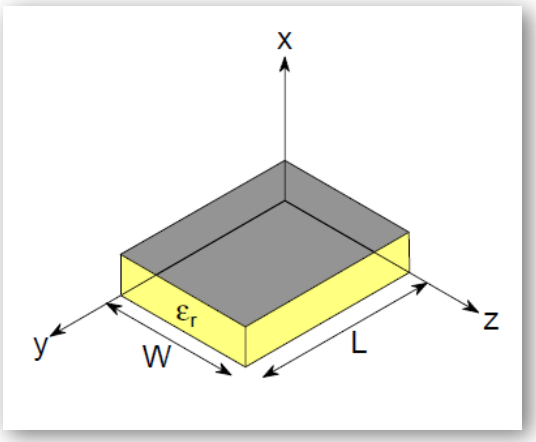

Figure 4.9 Rectangular patch parameters

If L>W, the fundamental mode will be the TEM_{010} (Figure 4.10) and if W>L or L>W>L/2, the fundamental mode will be TEM_{100} (Figure 4.11)

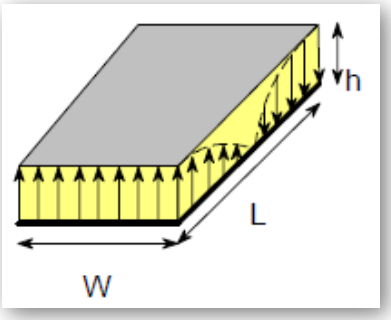

Figure 4.10 Fundamental mode TEM_{010}

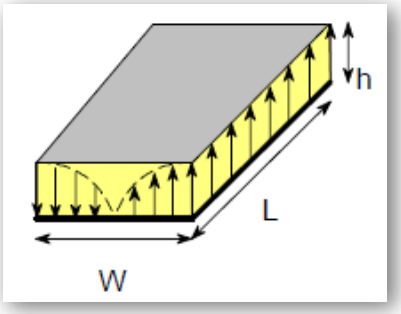

Figure 4.11 Fundamental mode TEM_{100}

The resonant frequency can be expressed as

$$(f_r)_{010} = \frac{c_0}{2L\sqrt{\varepsilon_r}} or (f_r)_{100} = \frac{c_0}{2W\sqrt{\varepsilon_r}} \quad (4.1)$$

The radiation pattern will have a shape similar to the shown in Figure 4.12.

Figure 4.12 Radiation pattern for the fundamental mode of a rectangular patch

There is an important compromise which will have to be studied in the design of the patch: how the thickness and the permittivity of the dielectric are related with the quality

factor and the bandwidth. When the permittivity of the dielectric grows, and its thickness becomes smaller, the quality factor decreases. When the quality factor decrease the bandwidth becomes greater. Hence, we will be interested in thick and with low permittivity.

The main polarization of the rectangular patch is linear polarization since it consists of a two slot array, so it will be necessary to study some variations on the typical rectangular patch to achieve the desired circular polarization.

Circular polarization in rectangular patches. Truncated Patch fundamentals.

For the current project, the best configuration for both transmitting and receiving antenna is circular polarization. This is due to the wide of the beam that will be considered in the hole experiment, because the receiver can be placed anywhere of the room. The circular polarization is better since the reflections in the walls damage the losses caused by the different polarization of the incident wave to the receiving antenna and the receiving antenna polarization less.

Antennas produce circular polarized waves when two orthogonal field components with equal amplitude and quadrature phase are radiated. This requirement is achieved by a single patch with the proper excitation and shape, or by an array of patches with an appropriate arrangement and phasing. For the current model a single antenna is chosen for simplicity reasons.

It is possible to achieve circular polarization with both rectangular and circular patches. Other shapes, as triangular, spiral or pentagonal, can also be considered. To achieve circular polarization we can choose to have double feeding in the antenna or to have special shape and feeding for a single-feed antenna. The double feeding can be achieved by the use of an external power divider and dual-orthogonal feeds modes with equal amplitude but in quadrature phase; what can be easily achieved with the use of a branch-line divider of 3dB or a Wilkinson Power divider or even with a T-junction and an additional λ/4 transmission line that achieves the quadrature phase as it is shown in Figure 4.13.

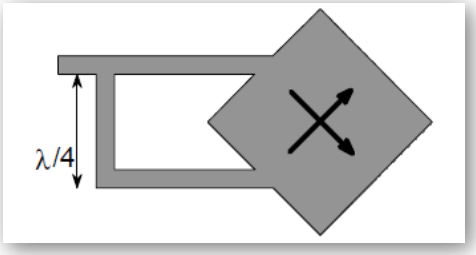

Figure 4.13 Double feeding of a rectangular patch by a Power Divider

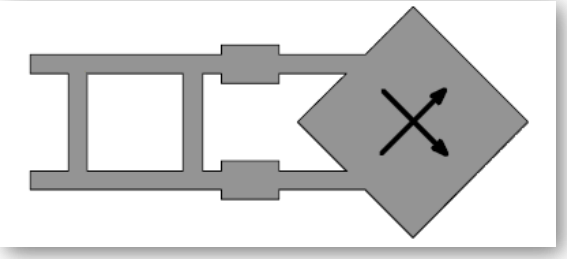

Figure 4.14 Double feeding of a rectangular patch by and Hybrid of 90°

A single-feed square patch needs no external device but special design for the feeding point of the patch or its shape, which can be perturbed from the pure rectangular or square shape. It also radiates both left-hand circular polarization (LHCP) and right-hand circular polarization (RHCP). To avoid the use of any other device besides the antenna and the rectifier, a single-feed configuration is chosen.

Circular polarization with a single-feed patch can be reached in two ways. The key is placed in the feeding position and in the existence of a perturbation segment (ΔS) which will depend on the feeding position. On one hand we can consider placing the feeding point in the *x*- or *y*-axis. When the feeding point is placed in one axis the rectangular shape of the patch needs to be changed. Several perturbations for this shape are possible as we can see in the Figure 4.15.

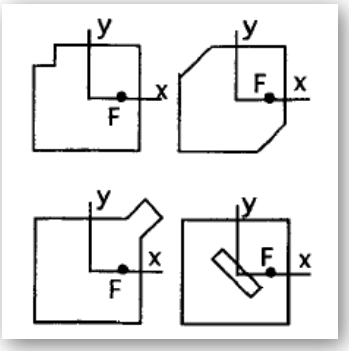

Figure 4.15 Possible variations of a rectangular patch for a feeding placed in one axis.

On the other hand, the single-feed rectangular patch feed in the diagonal needs different modifications of the rectangular shape. Some of them are shown in the Figure 4.16. In both cases, the perturbation segment ΔS is set at an appropriate sense of the direction for the circular polarized wave. The feed placed in *x*- or *y*-axis is chosen.

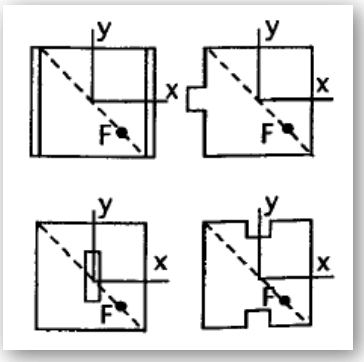

Figure 4.16 Possible variations of a rectangular patch for a feeding placed in the diagonal

It is necessary to study the effect of the perturbation segment. The square patch is considered to be an electrically thin cavity with perfect magnetic walls at the boundaries $x = \pm a/2$ and $y = \pm a/2$. In Figure 4.17 the feed point is named F and it is possible to see the perturbation segment.

The eigen functions ϕ_a and ϕ_b, which are excited in an electrically thin cavity region of the spare patch, are mathematically given by the following equations

$$\begin{cases} \phi_a = V_0 \sin kx \\ \phi_b = V_0 \sin ky \end{cases} \tag{4.2}$$

where $V_0 = \sqrt{2}/a$,$k = \pi/a$ and a is the patch size as we can see in the Figure 4.17.

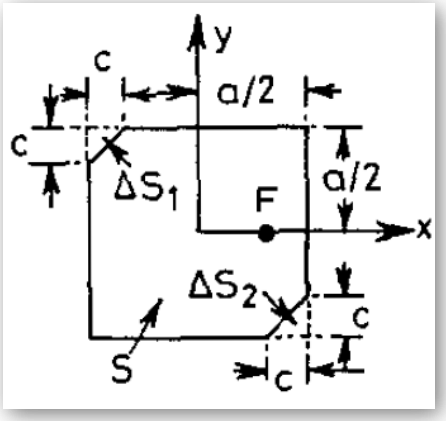

Figure 4.17 Truncated rectangular patch parameters

From the Figure 4.17, it can be seen that ΔS represents the total sum of the perturbation segments and may consist of a single or multiple segments. It can be defined as

$$\Delta S = \Delta S_1 + \Delta S_2 = c^2 \tag{4.3}$$

And

$$S = a^2 \tag{4.4}$$

With the patch of the Figure 4.17 we can achieve right circular polarization by setting the feeding point in the position $F(\pm\varrho_0, 0)$. As it was said before, left hand polarization is also possible to achieve by setting the feeding in the position $F(0, \pm\varrho_0)$.

The eigen function ϕ_a is concerned with the field distribution of TM_{100} mode and ϕ_b with that of TM_{010} mode. By setting the perturbation segment ΔS at an appropriate position of the antenna, two orthogonally polarized modes are excited in a cavity region of the antenna. The eigenvalue can be determined from a stationary formula given by:

$$k'^2 = \frac{\int_{S+\Delta S} \nabla\phi' \cdot \nabla\phi' \, dS}{\int_{S+\Delta S} \phi'^2 \, dS} \tag{4.5}$$

Where ϕ' and k' are the new modal field and the new eigenvalue. Haneishi [**38**] derivates that ϕ' can be expanded as

$$\phi' = P\phi_a + Q\phi_b \tag{4.6}$$

P and Q are unknown expansion coefficients that have to be determined to make (4.2) stationary. We can substitute (4.5) in (4.6) resulting:

$$k'^2 = \frac{\int_{S+\Delta S} (P\nabla\phi_a + Q\nabla\phi_b)\cdot(P\nabla\phi_a + Q\nabla\phi_b) dS}{\int_{S+\Delta S} \left(P\nabla\phi_a + Q\nabla\phi_b\right)^2 dS} = \frac{U(P,Q)}{V(P,Q)} \tag{4.7}$$

We can determine P and Q obtaining a set of homogeneous equations:

$$\begin{aligned} \frac{\partial U(P,Q)}{\partial P} - k'^2 \frac{\partial V(P,Q)}{\partial P} = 0 \\ \frac{\partial U(P,Q)}{\partial Q} - k'^2 \frac{\partial V(P,Q)}{\partial Q} = 0 \end{aligned} \tag{4.8}$$

Therefore, we can say that the equation in (4.7) will have nontrivial solutions only if the determinant in (4.9) is equal to zero.

$$\det \begin{vmatrix} k^2 - k'^2\left(1 - 2\frac{\Delta S}{S}\right) & k'^2 2\frac{\Delta S}{S} \\ k'^2 2\frac{\Delta S}{S} & k^2 - k'^2\left(1 - 2\frac{\Delta S}{S}\right) \end{vmatrix} = 0 \tag{4.9}$$

The new eigenvalues are found as:

$$\begin{aligned} k'_a &= k^2\left(1 + 4\frac{\Delta S}{S}\right)^{-1} \\ k'_b &= k^2 \end{aligned} \tag{4.10}$$

We obtain the new resonant frequencies ϕ_a ' and ϕ_b ' :

$$f_a = f_{0_r}^{'} + \Delta f'_a = f_{0_r}\left(1 - 2\frac{\Delta S}{S}\right)$$
$$f_b = f_{0_r}^{'} + \Delta f'_b = f_{0_r} \tag{4.11}$$

f_{0_r} is the resonant frequency of the square patch before the perturbation. $\Delta f'_a$ and $\Delta f'_b$ are the shifts in resonant frequencies for ϕ_a ' and ϕ_b ' modes after perturbation. Now P and Q are obtained ant its value is:

$$P_a = -Q_a = \frac{1}{\sqrt{2}}$$
$$P_b = Q_b = \frac{1}{\sqrt{2}} \tag{4.12}$$

And ϕ_a ' and ϕ_b ' modes after perturbation can be expressed as:

$$\phi'_a = \frac{V_0}{\sqrt{2}}\left(\sin(kx) - \sin(ky)\right)$$
$$\phi'_b = \frac{V_0}{\sqrt{2}}\left(\sin(kx) + \sin(ky)\right) \tag{4.13}$$

The energy distribution for ϕ'_a and ϕ'_b are defined as turn ratios N'_a and N'_b given by

$$N'_a = \frac{\sqrt{S}}{a}\left(\sin(kx) - \sin(ky)\right)$$
$$N'_a = \frac{\sqrt{S}}{a}\left(\sin(kx) + \sin(ky)\right) \tag{4.14}$$

Using (4.10)-(4.14) the equivalent circuit for rectangular circularly polarized patch antennas is derived, as we can see in the figure below.

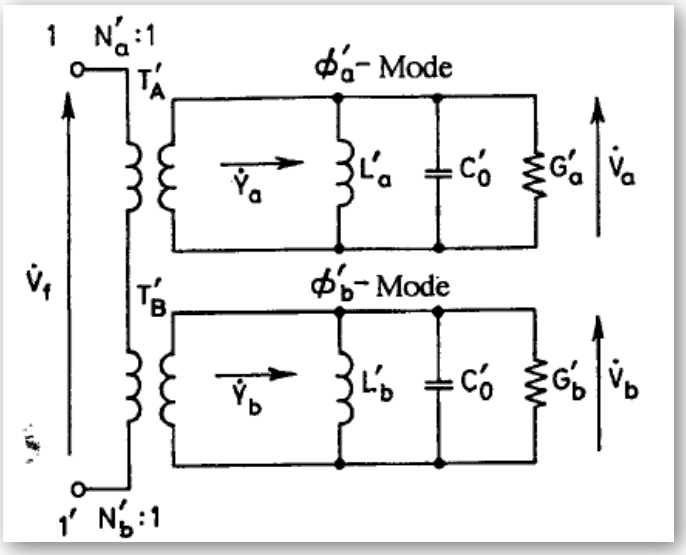

Figure 4.18 Equivalent circuit of a truncated rectangular microstrip patch antenna

T'_a and T'_b represent ideal transformers and V_f is the input voltage applied to the 1-1' terminal. Y_a and Y_b are the patch admittances corresponding to the orthogonally polarized ϕ'_a and ϕ'_b modes. G'_a and G'_b are equivalent conductances and generally include radiation, dielectric and copper losses even if the conductance losses will be dominant in front of the other losses. [**39**]

It is possible to obtain the complex axial ratio form referred to the Figure 4.18. A simplification occurs by selecting $N'_a = \pm N'_b$.

$$\left(\frac{\dot{V}_b}{\dot{V}_a}\right) = \left(\frac{N'_b}{N'_a}\right)\left(\frac{Y'_b}{Y'_a}\right) = \pm \frac{\left\{\frac{f_a}{Q_0} + j\left(f - \frac{f_a^2}{f}\right)\right\}}{\left\{\frac{f_b}{Q_0} + j\left(f - \frac{f_b^2}{f}\right)\right\}} \tag{4.15}$$

To have circular polarization it is needed that

$$\left(\frac{\dot{V}_b}{\dot{V}_a}\right) = \pm j \tag{4.16}$$

Operating, we can see that

$$\left|\frac{\Delta S}{S}\right| = \frac{1}{2Q_0} \tag{4.17}$$

Tables for the design of the parameters for X-band antennas can be found in [**39**].

Design of the patch.

A parametrical study for all the variables present in the antenna has been carried out. The main goal was to achieve circular polarization. Therefore an axial ratio as close to 1 as possible was searched. It was also important to have the resonant frequency of the patch in the desired frequency of 2.45GHz.

To achieve our goals, an initial value of the patch's length was set to half of lambda:

$$\lambda_0 = \frac{c}{f} = \frac{3 \cdot 10^8}{2.45 \cdot 10^9} = 12.24cm \tag{4.18}$$

The basic model for the antenna is a square patch with its truncated corners placed in the center of a ground plane as we can see in the Figure 4.19.

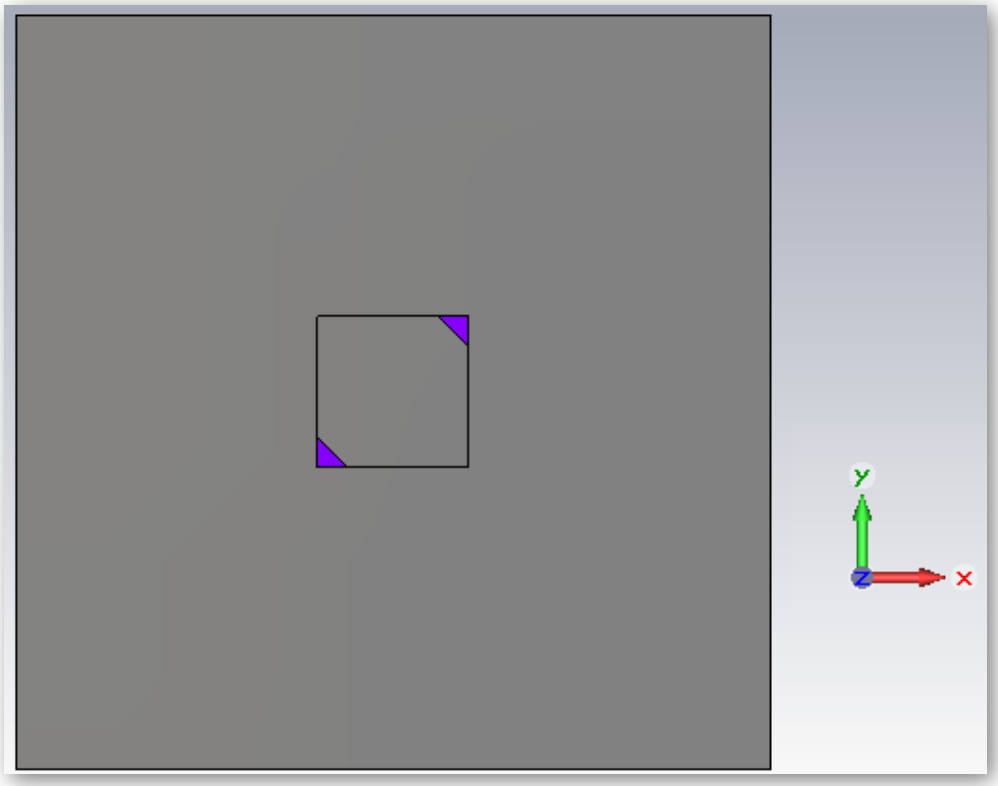

Figure 4.19 Top view of the truncated rectangular patch

Between the substrate of the patch and the ground plane we leave a gap. The side of the patch is shown in the Figure 4.20.

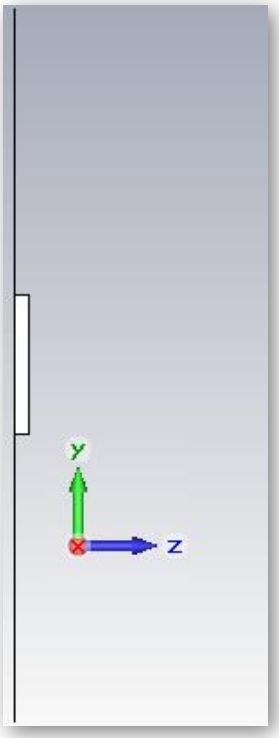

Figure 4.20 Side view of the truncated rectangular patch

With more detail, we can see how in the top of the gap we have the substrate and the patch in the Figure 4.21. In violet we can see the substrate, in grey the parts of the antenna formed by PEC (the patch on the right side, and the ground plane on the left one) and in white, the vacuum layer.

Figure 4.21 Detailed perspective view of the side of the patch

The simulation of the patch was done using the CST STUDIO SUITE™ 2009 software.

A first version with a discrete port was designed. A discrete port is a tool of the used software which considers the excitation as an impedance element that also absorbs some power and enables the S-parameter calculation. The discrete port is defined by a start point

and an end point. These two points will be connected through a perfectly conducting wire and the respective port source in the center of this wire. Therefore, in this first version the port was not modeled as a coaxial probe, but it was done just an approach to approximate the values of the parameters of the patch. Since the main goal was to obtain circular polarization, the best values for *a*, *c* and the feeding point F(*feed_x, feed_y*), according to the nomenclature of Figure 4.17, were searched.

An approximate value for the parameter *a* was given by knowing that the size of the patch should be similar to λ/2 where λ is the wavelength in the proposed substrate.

To ensure that the resonance of the patch is 2.45GHz, the behavior of the impedance of the patch should be similar to the characteristic behavior of the impedance of the rectangular patch shown in Figure 4.22.

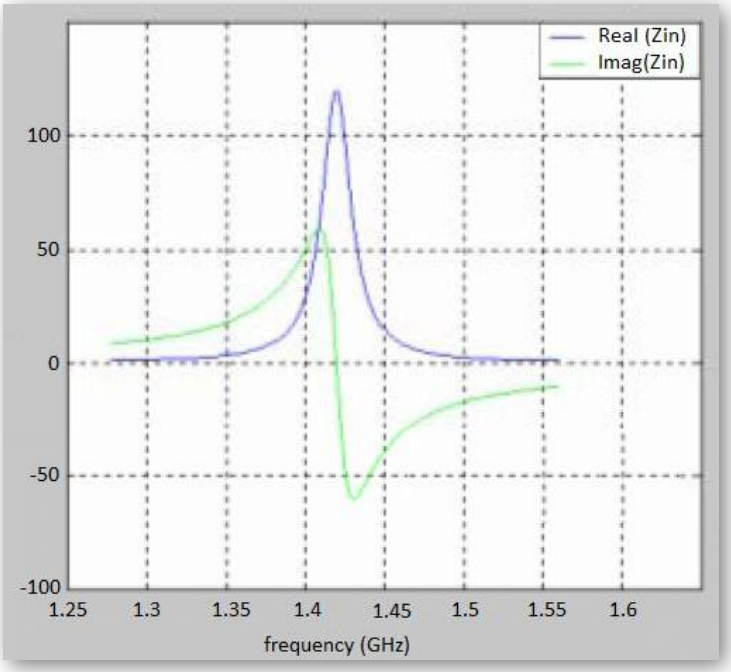

Figure 4.22 Characteristic impedance of a patch

Firstly an appropriate value for the parameter *a* (the size for the side of the patch) was searched. In second place, the c (the size of the truncation) parameter influence was studied, and in third place, the feeding point was settled. In the figures shown below we can see the influence of all this parameters to the axial ratio, and real and imaginary part of the impedance.

The initial values of the experiment were found by iterating simulations changing all of them until acceptable results to be improved were obtained. They are:

a	*c*	Feeding point (F)	
		feed_x	*feed_y*
50mm	10mm	-7mm	0mm

Table 4.1 Initial Parameters for the design of the patch

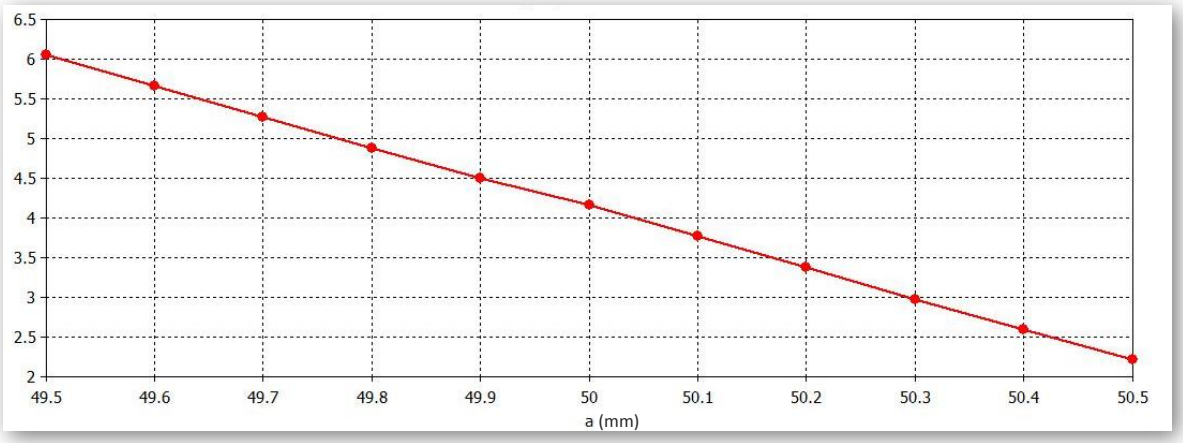

Figure 4.23 *a* parameter VS axial ratio in θ=0, ϕ=0 direction

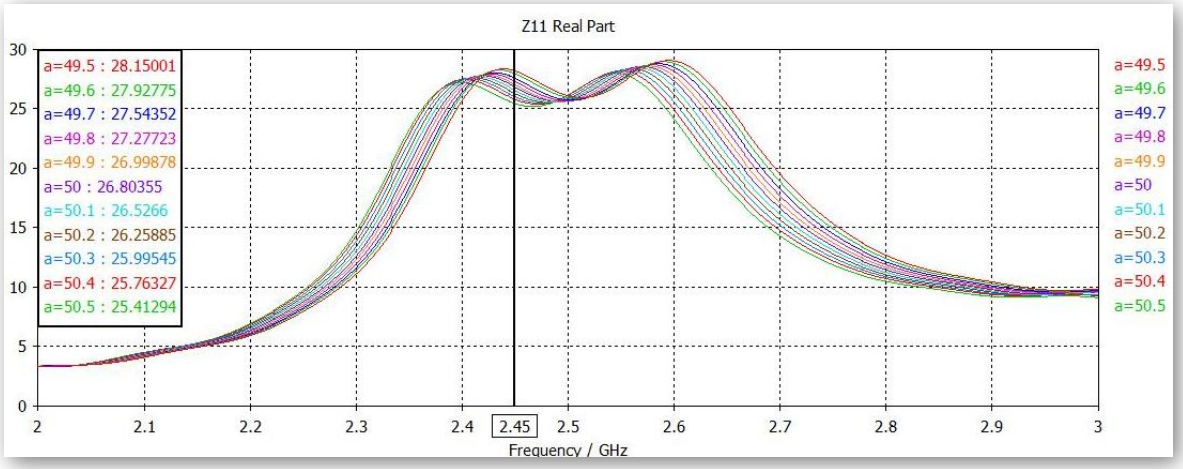

Figure 4.24 Variation of the real part of the impedance (Ω) with *a* (mm) as parameter

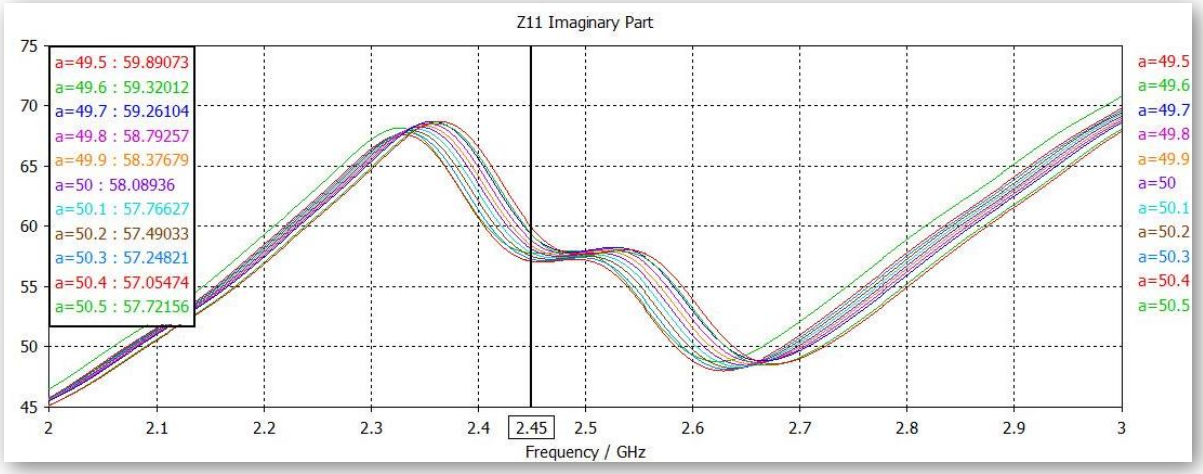

Figure 4.25 Variation of the imaginary part of the impedance (Ω) with *a* (mm) as parameter

For the *a* parameter we can see that values near 50mm are good, but when we make this value bigger, the resonance frequency is moved significantly, so a final value of 50.4mm was chosen, since this is the parameter that affects more significantly to the resonance frequency.

Once the *a* parameter was settled, the influence of the *c* parameter was studied. First a wide range from the minimum value (zero) to the maximum value (25, half of the side of the square) was considered, and then, we center the study to the best values of all the range.

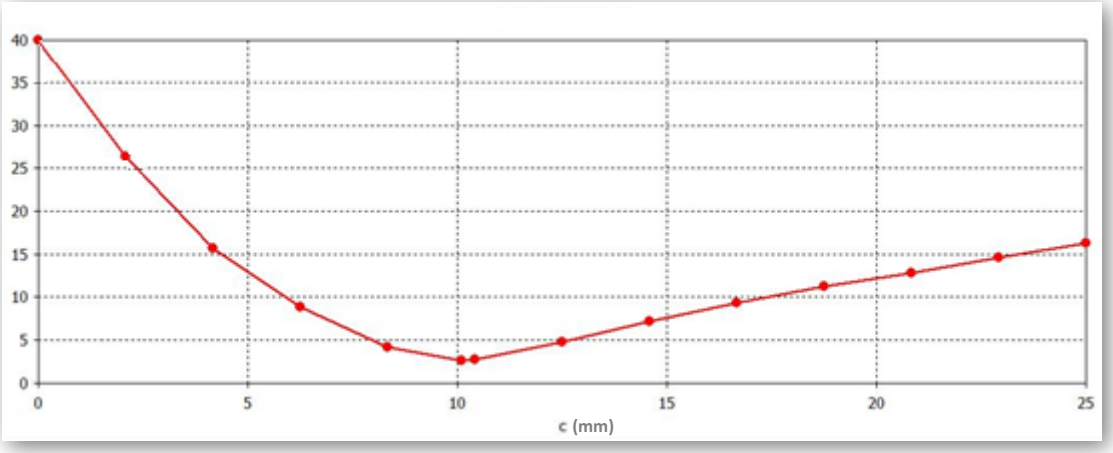

Figure 4.26 *c* parameter VS axial ratio in θ=0, ϕ=0 direction

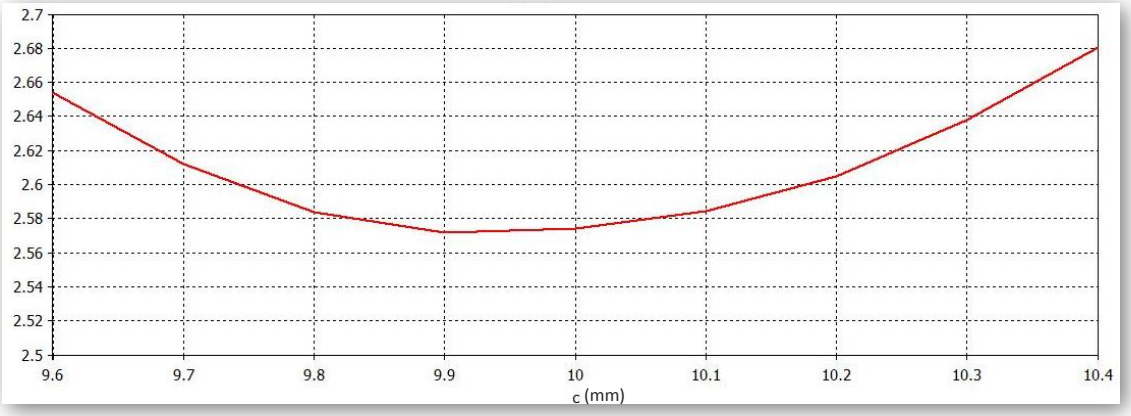

Figure 4.27 Detailed *c* parameter VS axial ratio in θ=0, ϕ=0 direction

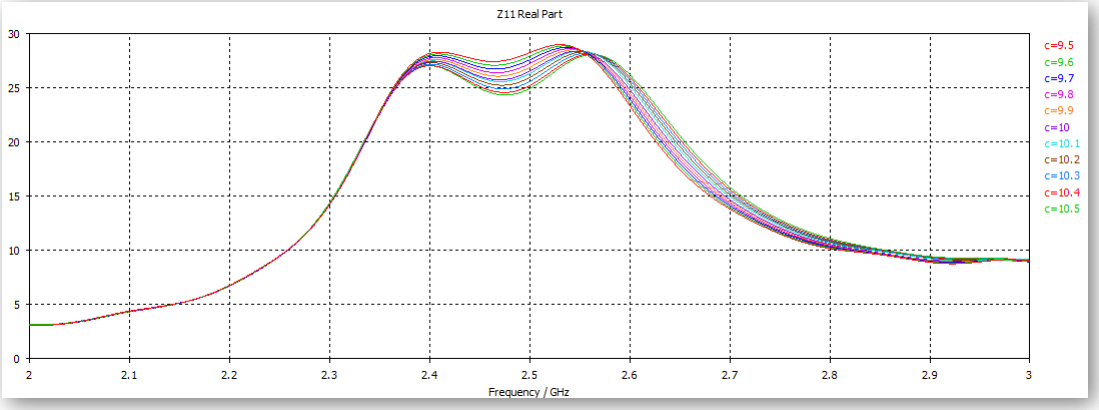

Figure 4.28 Variation of the real part of the impedance (Ω) with *c* (mm) as parameter

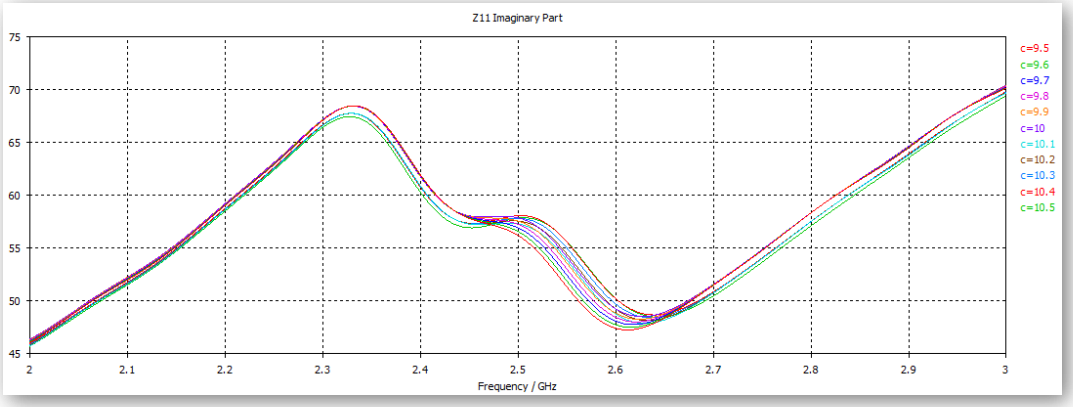

Figure 4.29 Variation of the imaginary part of the impedance (Ω) with *c* (mm) as parameter

As we can see the changes on the parameter *c* doesn't significantly change the impedance and, therefore, this parameter has no big influence on the resonant frequency of the patch. A value of 10.1mm was chosen for the c parameter. Next step was the study of the influence for the feeding point.

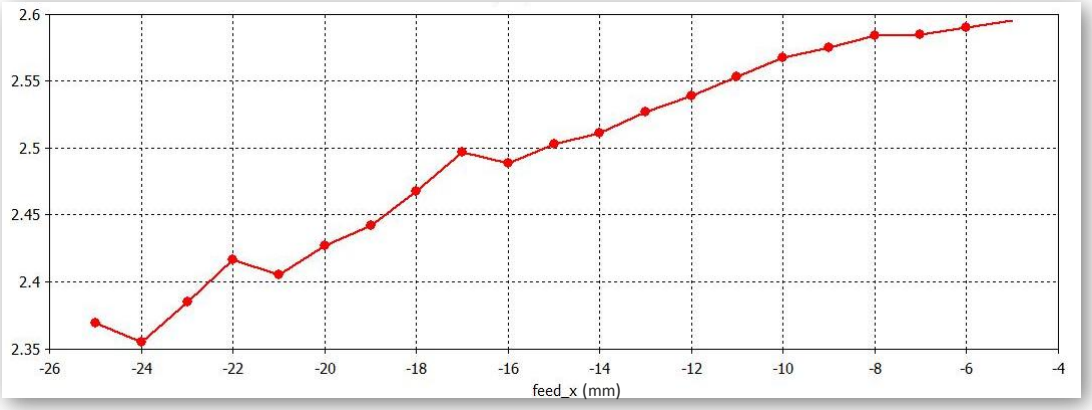

Figure 4.30 Feeding point parameter VS axial ratio in θ=0, ϕ=0 direction

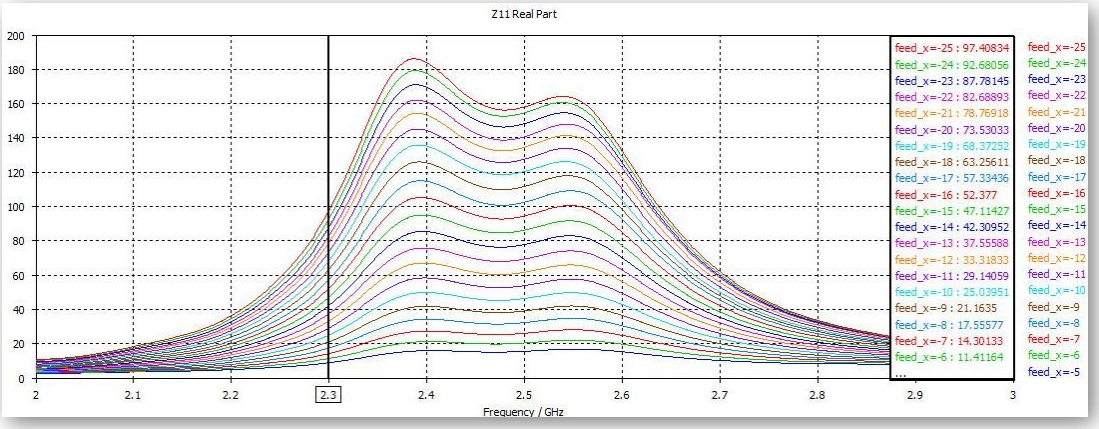

Figure 4.31 Variation of the real part of the impedance (Ω) with *feed_x* (mm) as parameter

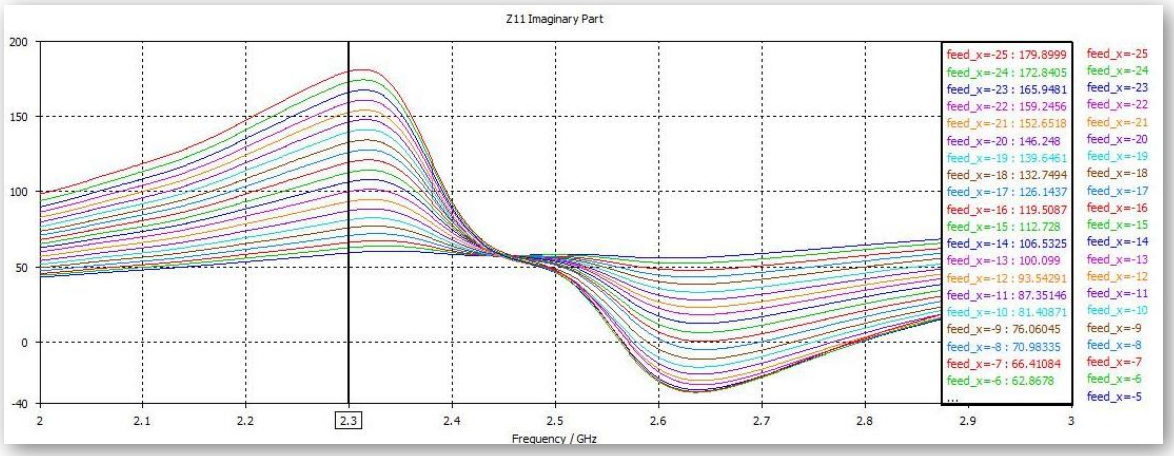

Figure 4.32 Variation of the imaginary part of the impedance (Ω) with *feed_x* (mm) as parameter

It was also probed the symmetry of the patch, verifying that the results does not change when the feeding point is moved from the positive part of the x axis to the negative part. It was also seen how the polarization change from left handed to right handed when the feeding point is changed from the x axis to the y axis.

At the end of the first step of the design, the values of the parameters are settled as:

a	*c*	Feed point (F)	
		feed_x	*feed_y*
50.4mm	10.1mm	-24mm	0mm

Table 4.2 Parameters for the first version of the patch

The features of this first final version of the patch are presented on the images below.

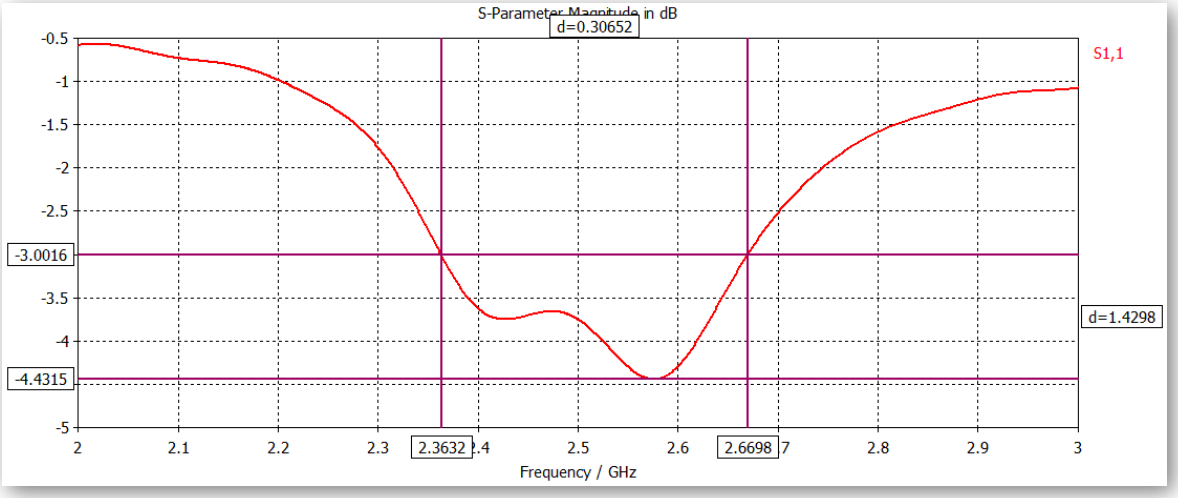

Figure 4.33 S_{11} parameter

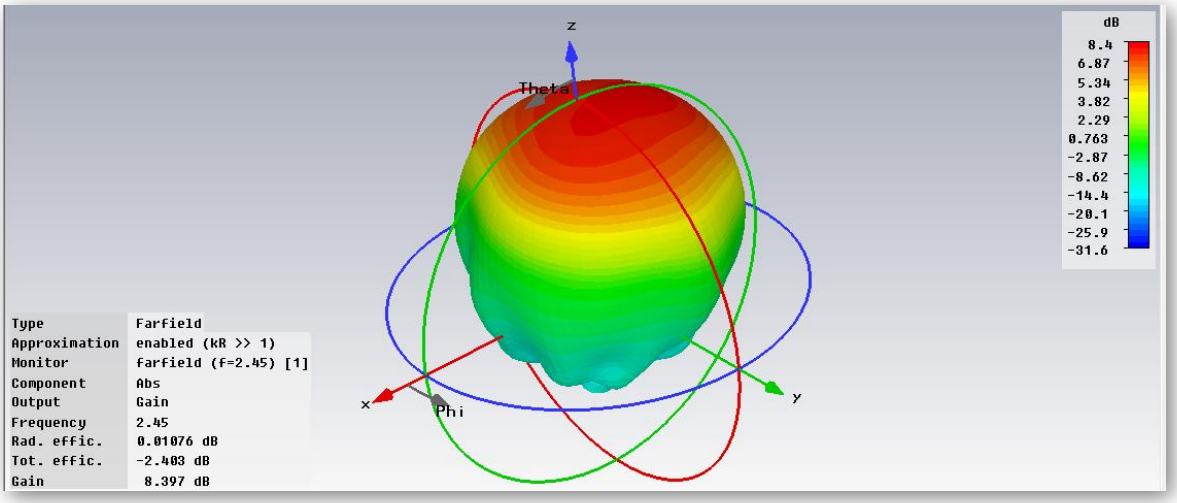

Figure 4.34 Farfield radiation pattern

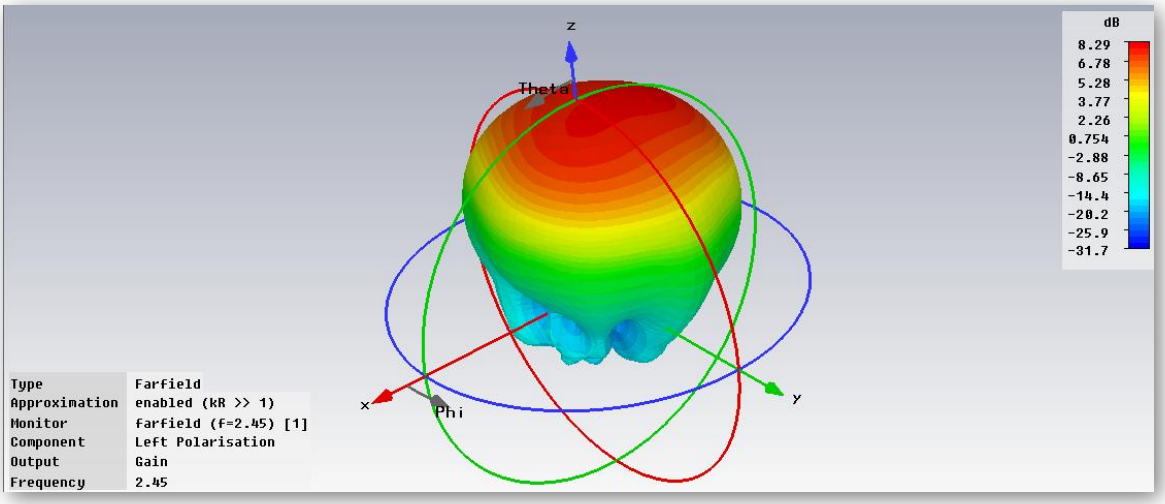

Figure 4.35 Left hand polarization

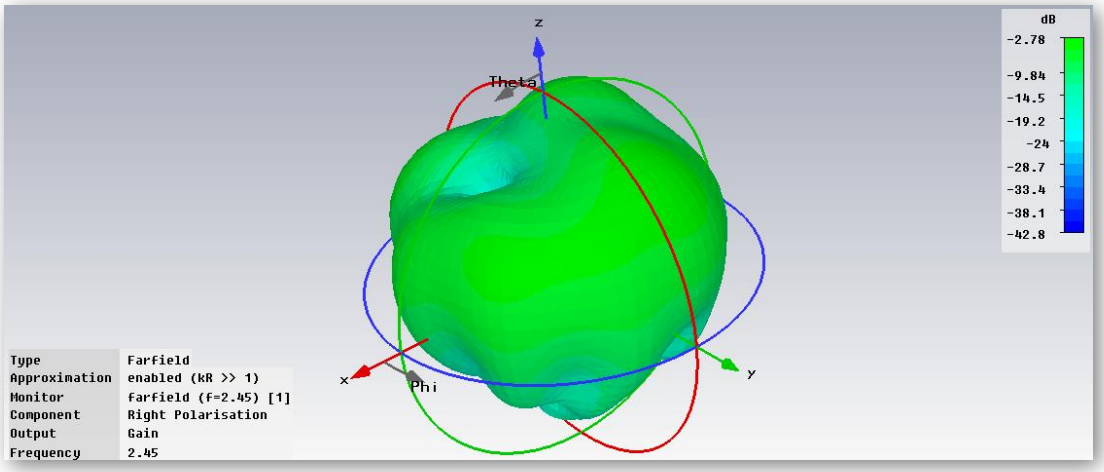

Figure 4.36 Right hand polarization

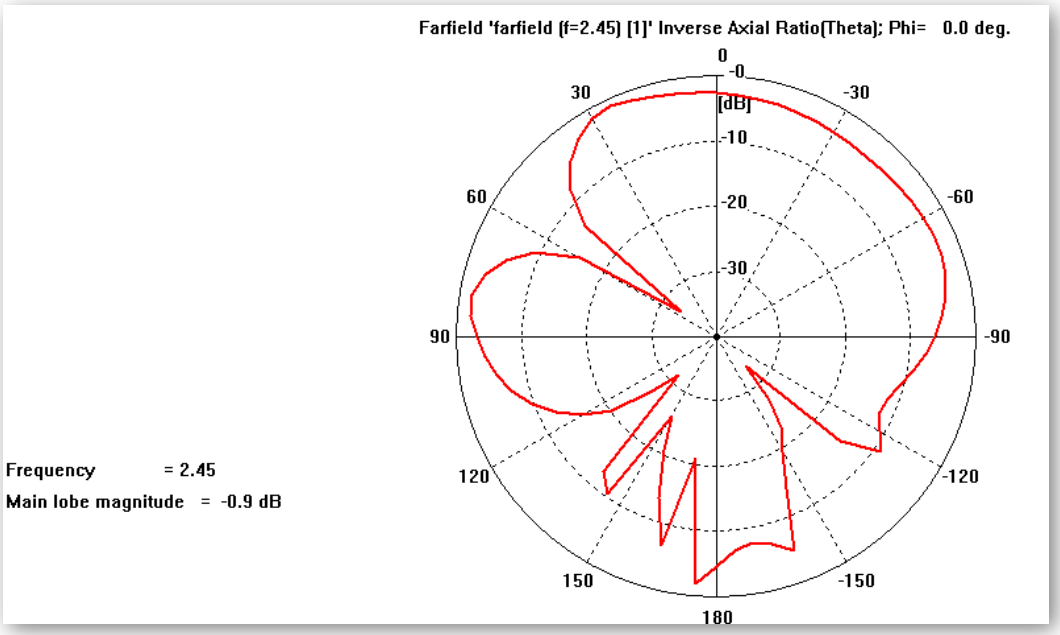

Figure 4.37 Inverse Axial Ratio in dB in ϕ=0

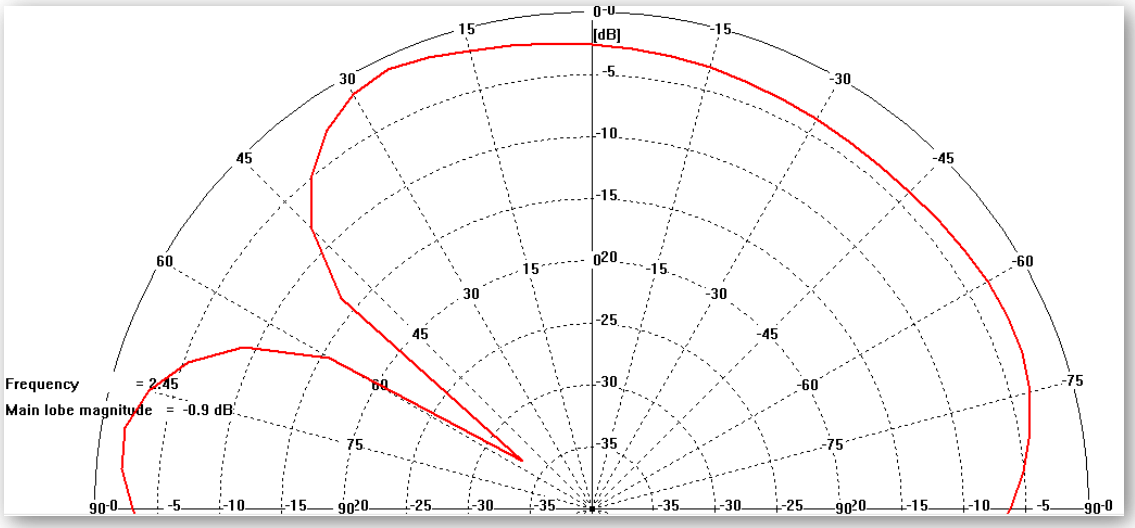

Figure 4.38 Detailed inverse Axial Ratio in dB in ϕ=0

Once the previous design was completed, the coaxial probe was included in the model of the antenna, as we can see in the Figure 4.39.

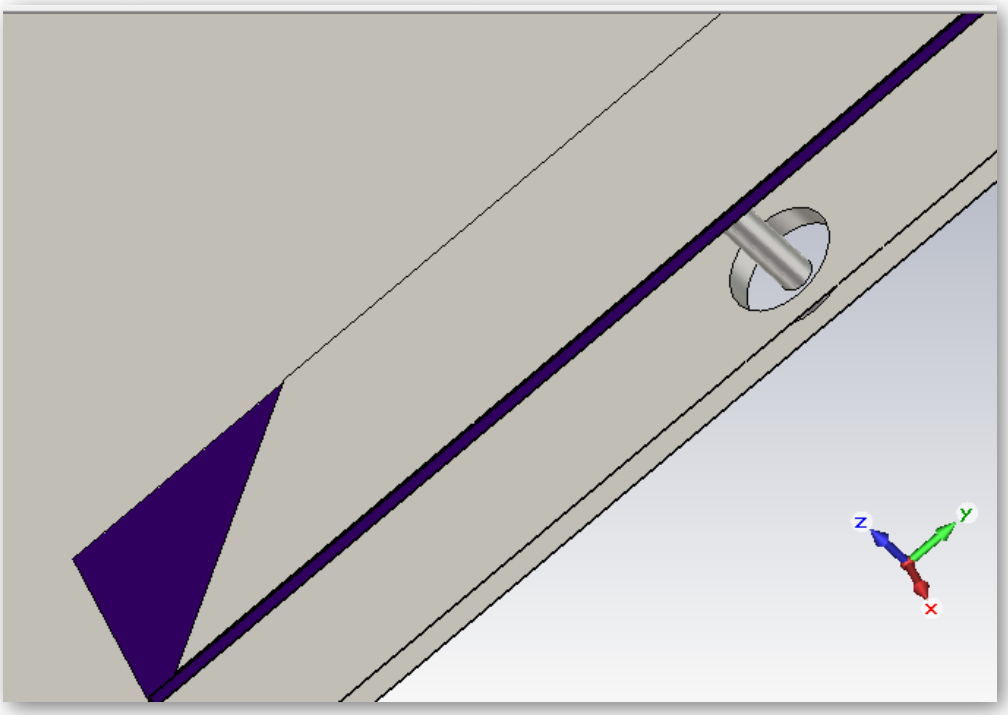

Figure 4.39 Detail of the feeding by coaxial probe

The port is modeled with a waveguide port, which is a tool of the software which represents a special kind of boundary condition of the calculation domain, enabling the stimulation as well as the absorption of energy. This kind of port simulates an infinitely long waveguide connected to the structure. The waveguide modes travel out of the structure toward the boundary planes thus leaving the computation domain with very low levels of reflections. A 2D eigenmode solver is used to calculate the waveguide port modes

The initial values of the parameters were the final values from the previous step, but the feeding point was forced to change, because it was too close to the border of the patch. With these values, a parametrical study is carried out.

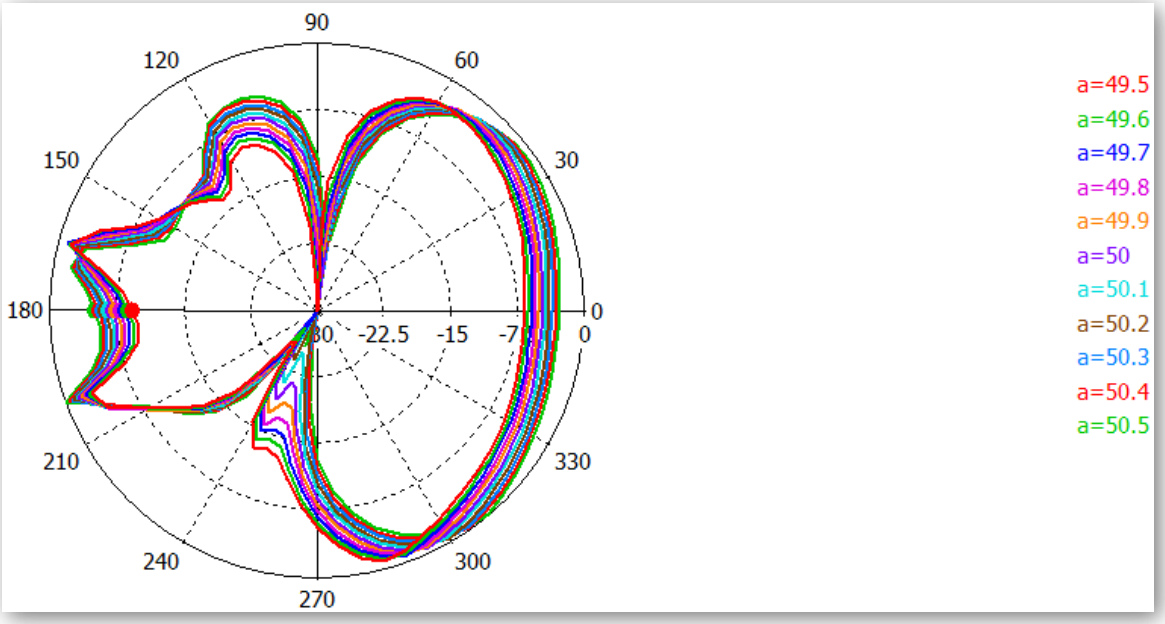

Figure 4.40 Variation of axial ratio with *a* (mm) as parameter in ϕ=0

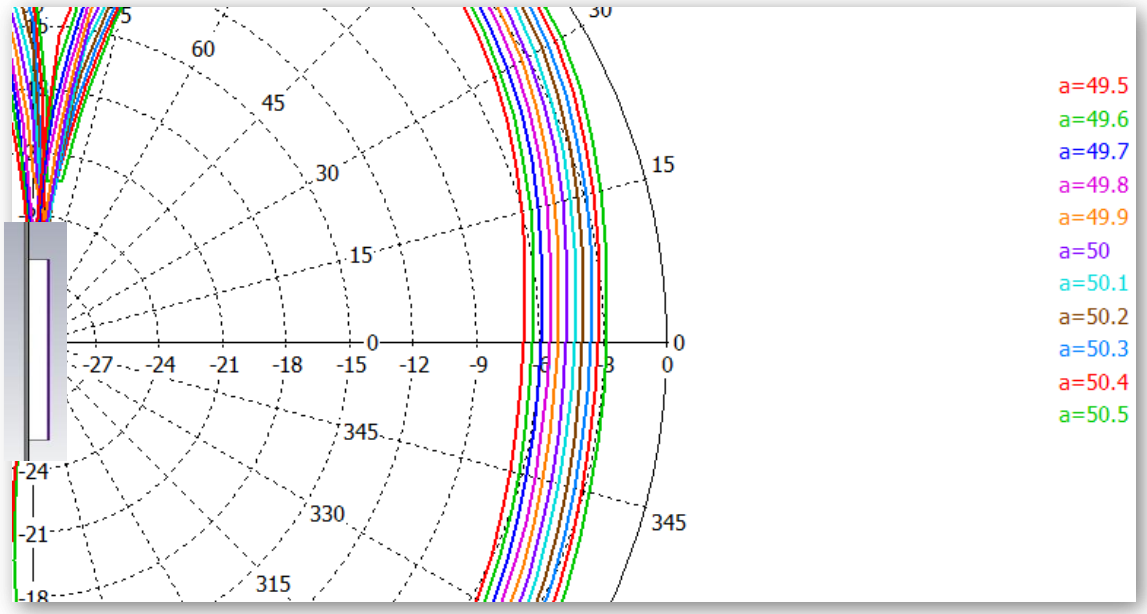

Figure 4.41 Detailed variation of axial ratio with *a* (mm) as parameter in ϕ=0

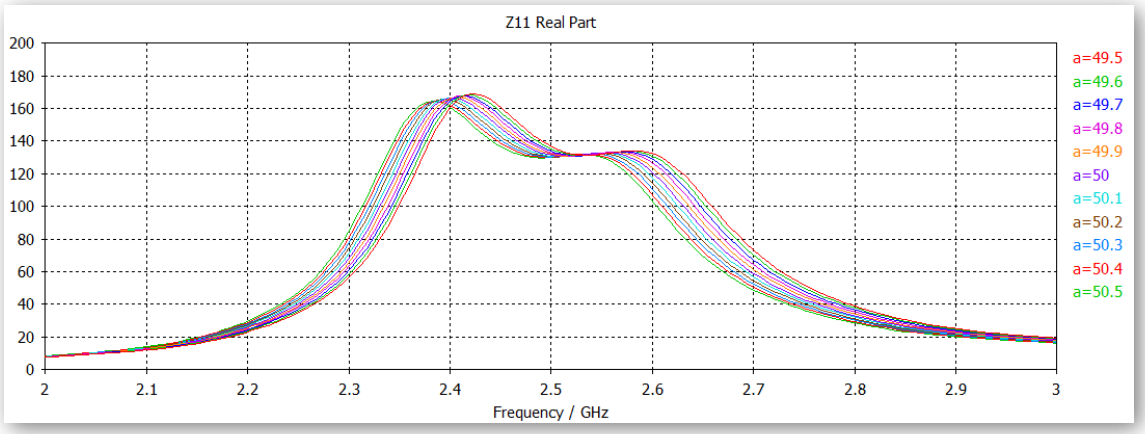

Figure 4.42 Variation of the real part of the impedance (Ω) with *a* (mm) as parameter

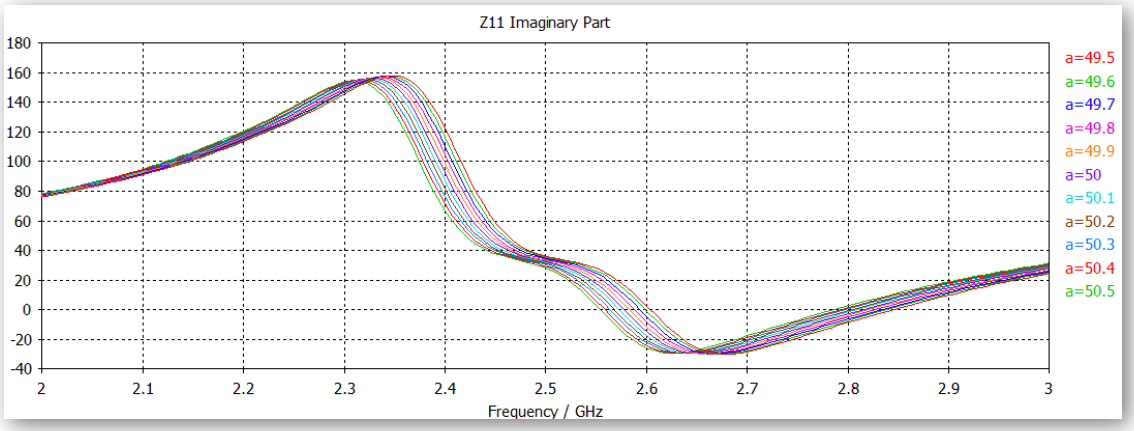

Figure 4.43 Variation of the imaginary part of the impedance (Ω) with *c* (mm) as parameter

A value of 50.4mm is chosen for the parameter *a*. Again, once selected the value for the *a* parameter, the influence of *c* is studied.

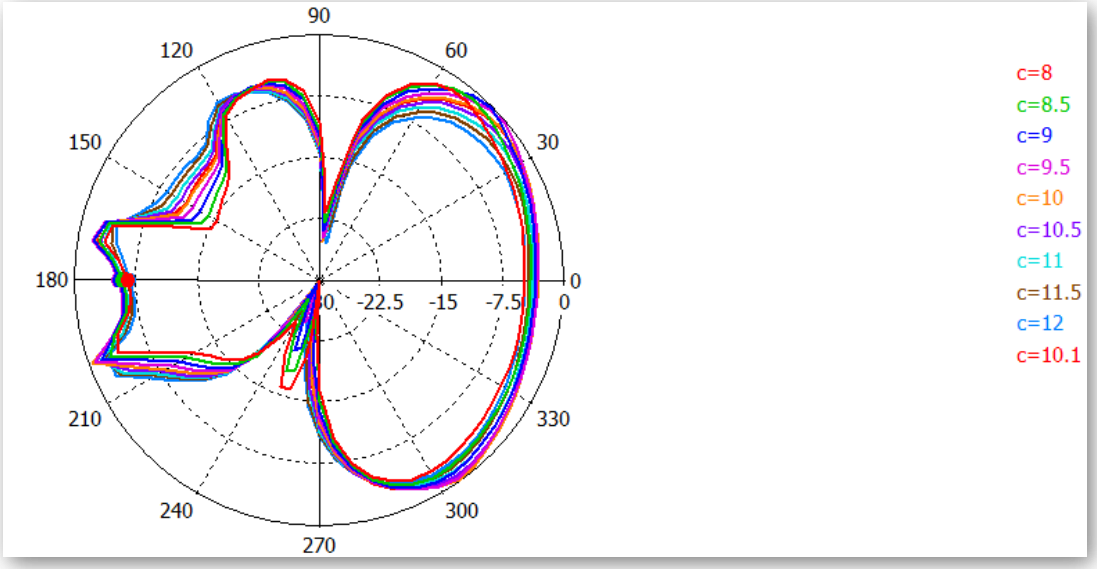

Figure 4.44 Variation of axial ratio with *c* (mm) as parameter in ϕ=0

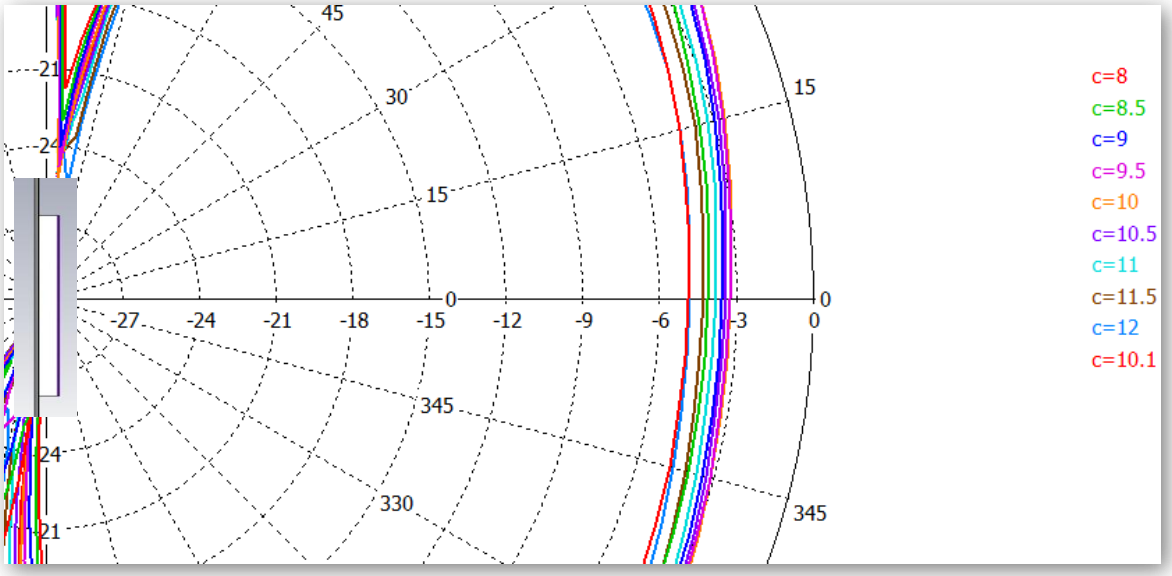

Figure 4.45 Detailed variation of axial ratio with *c* (mm) as parameter in ϕ=0

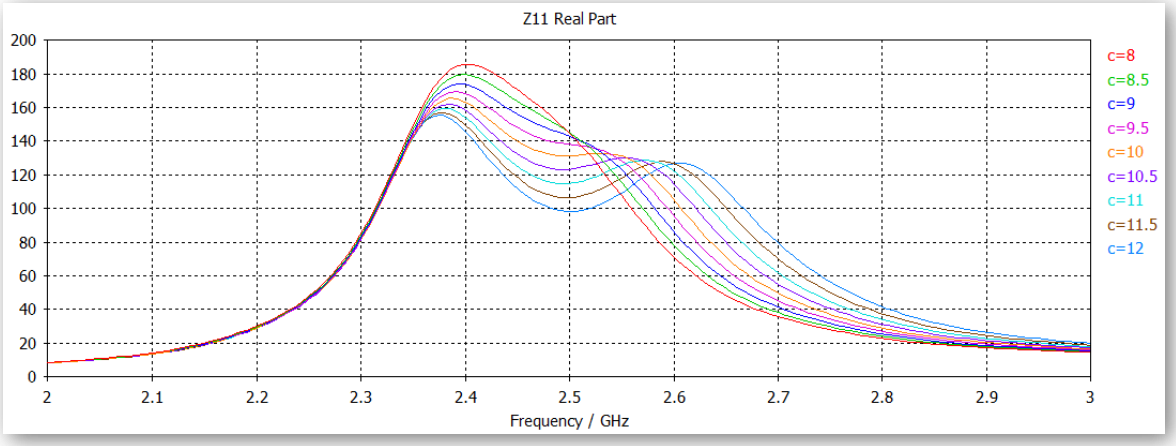

Figure 4.46 Variation of the real part of the impedance (Ω) with *c* (mm) as parameter

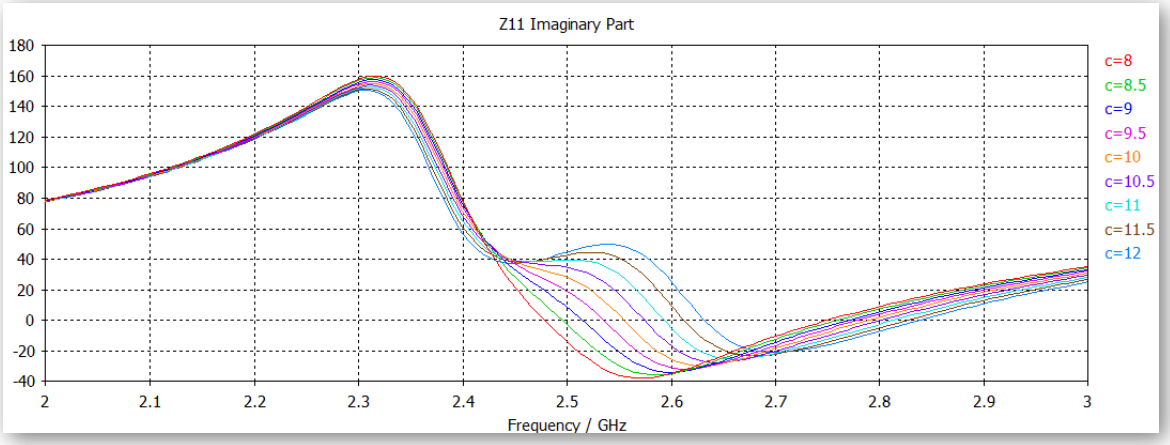

Figure 4.47 Variation of the imaginary part of the impedance (Ω) with *c (mm)* as parameter

A value of 9.5mm is chosen for the c parameter, since it is the one with best axial ratio results, as it is possible to appreciate in Figure 4.45. When this parameter is settled, the results for the variation of the feeding point are obtained:

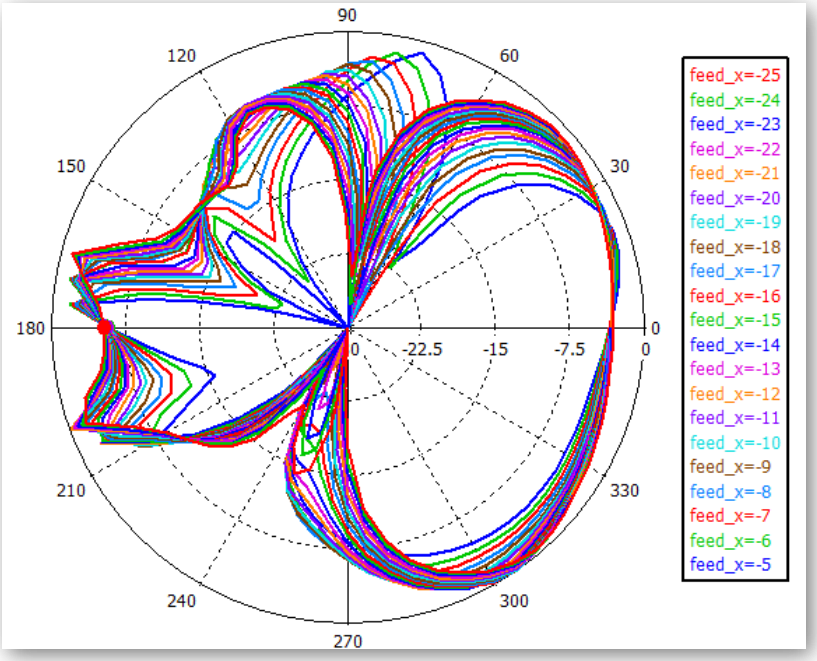

Figure 4.48 Variation of the axial ratio with *feed_x* (mm) as parameter in ϕ=0

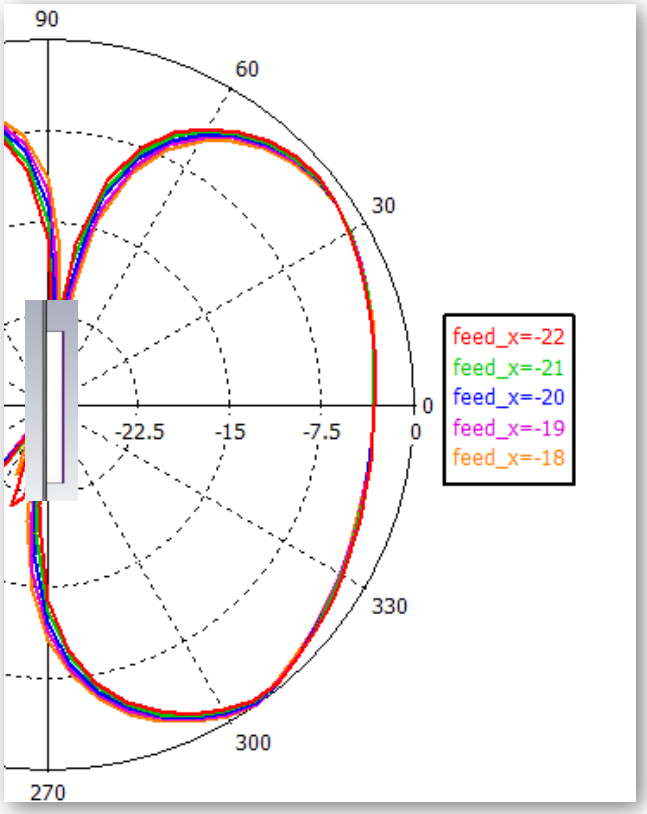

Figure 4.49 Detailed variation for selected curves of the axial ratio with *feed_x (mm)* as parameter in ϕ=0

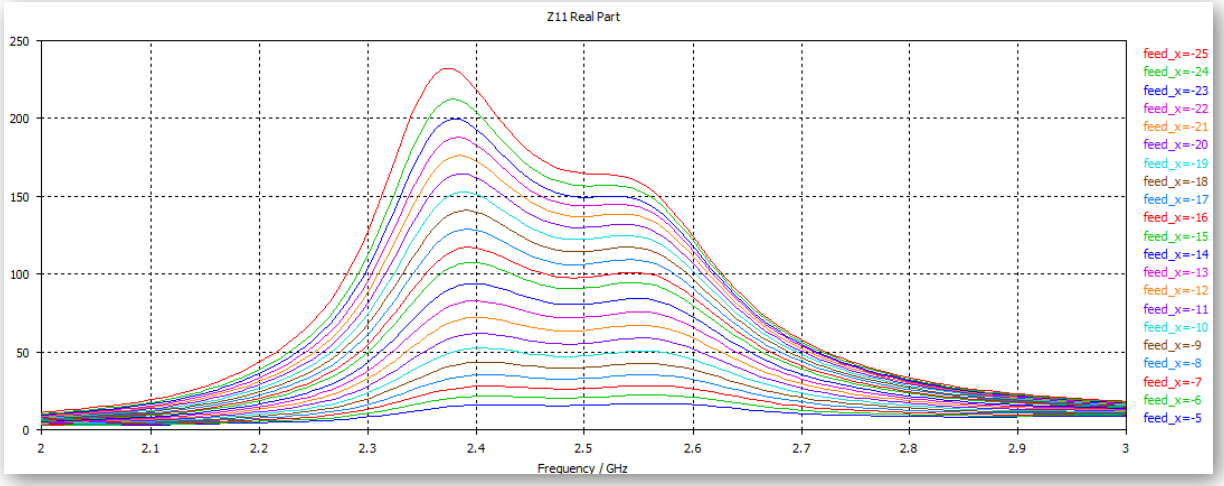

Figure 4.50 Variation of the real part of the impedance (Ω) with *feed_x* (mm) as parameter

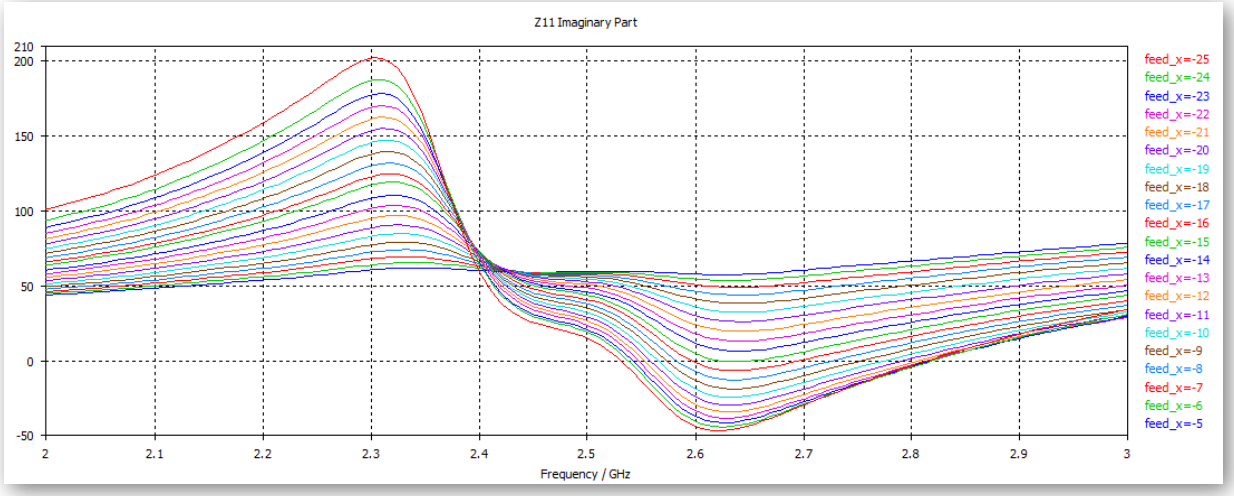

Figure 4.51 Variation of the real part of the impedance (Ω) with *feed_x* (mm) as parameter

The final value for the position of the feeding is F=(-20, 0) (mm) since the obtained results with this value are the bests ones.

The final values for all the parameters are:

a	***c***	**Feed point (F)**	
		feed_x	*feed_y*
50.4mm	9.5mm	-20mm	0mm

Table 4.3 Final parameters for the patch

This final version of the patch has features presented in the images below. The frequency range of values is wider because it is important to consider the values of all the parameters in the first and second harmonics for the correct design of the receiver.

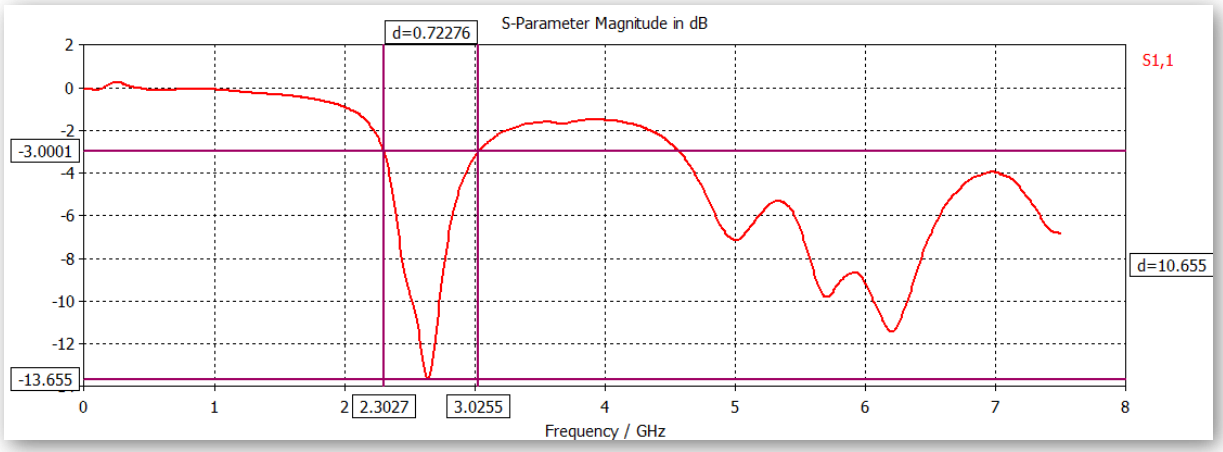

Figure 4.52 S_{11} parameter

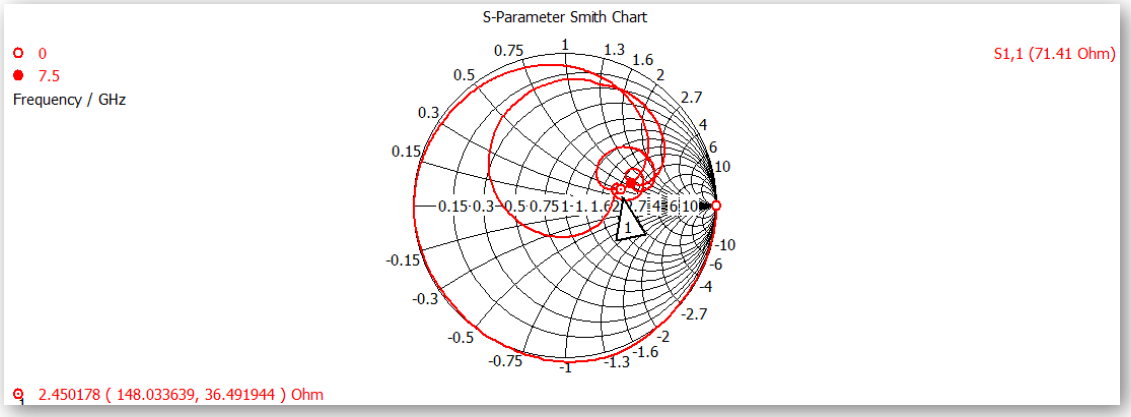

Figure 4.53 S_{11} parameter in the Smith Chart

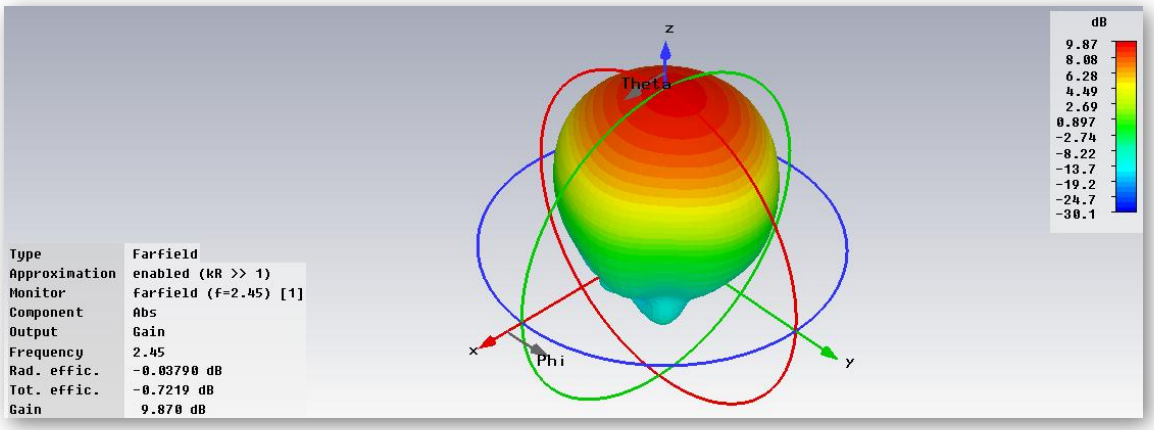

Figure 4.54 Farfield radiation pattern

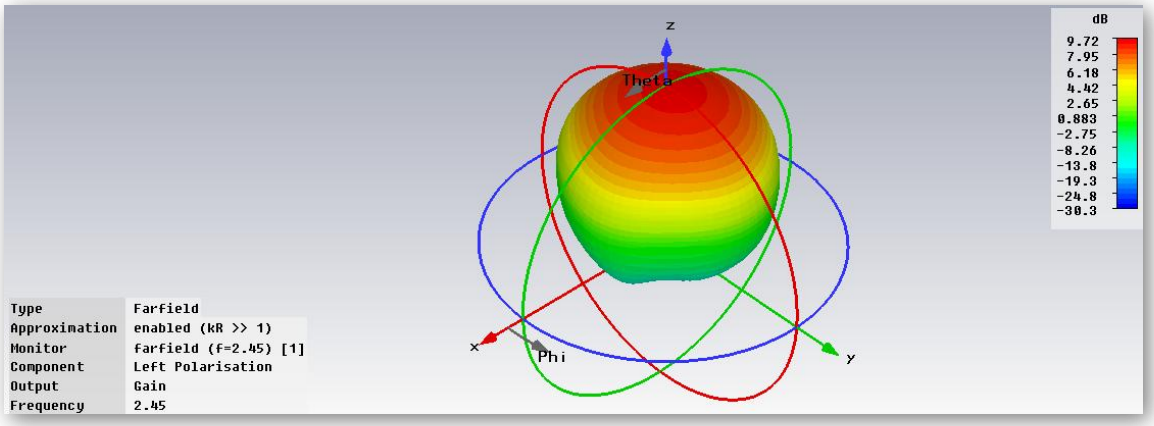

Figure 4.55 Left hand circular polarization

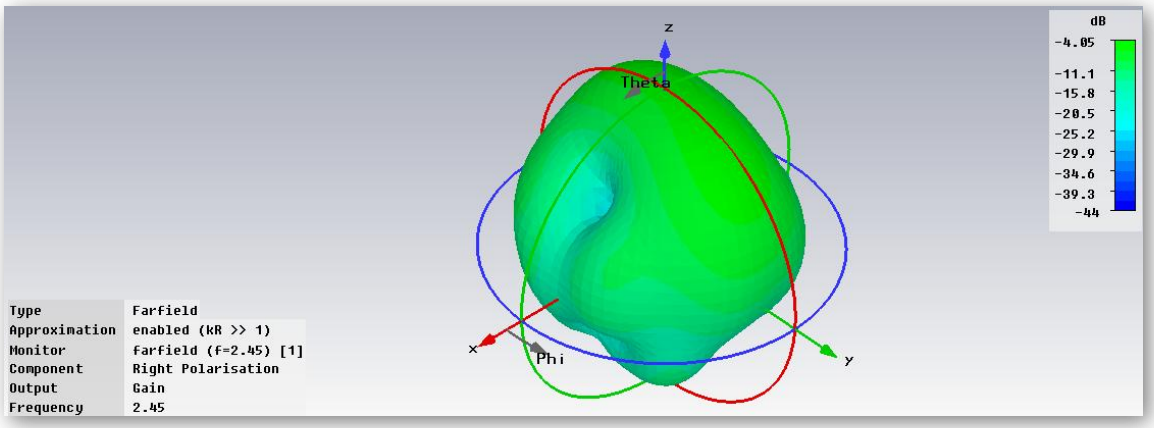

Figure 4.56 Rigth hand circular polarization

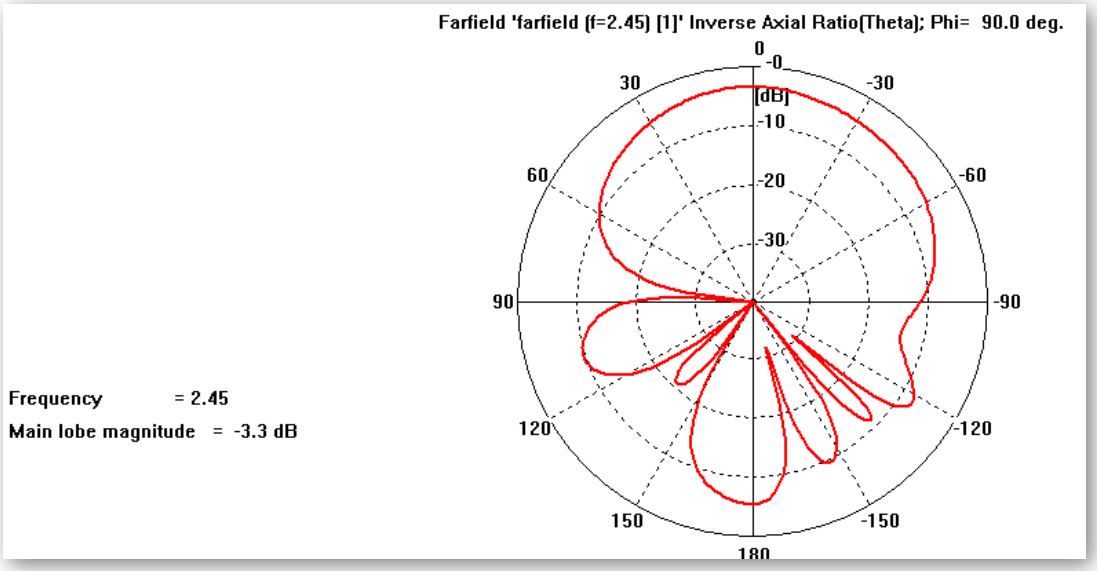

Figure 4.57 Inverse Axial Ratio in dB in ϕ=0

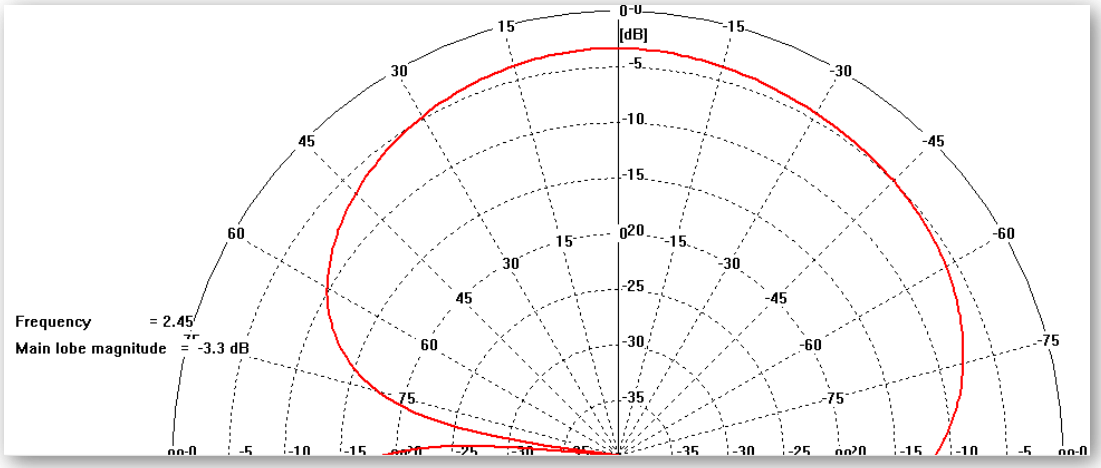

Figure 4.58 Detailed inverse Axial Ratio in dB in ϕ=0

The antenna was build and measured.

The measured S11 parameter is shown in the image below:

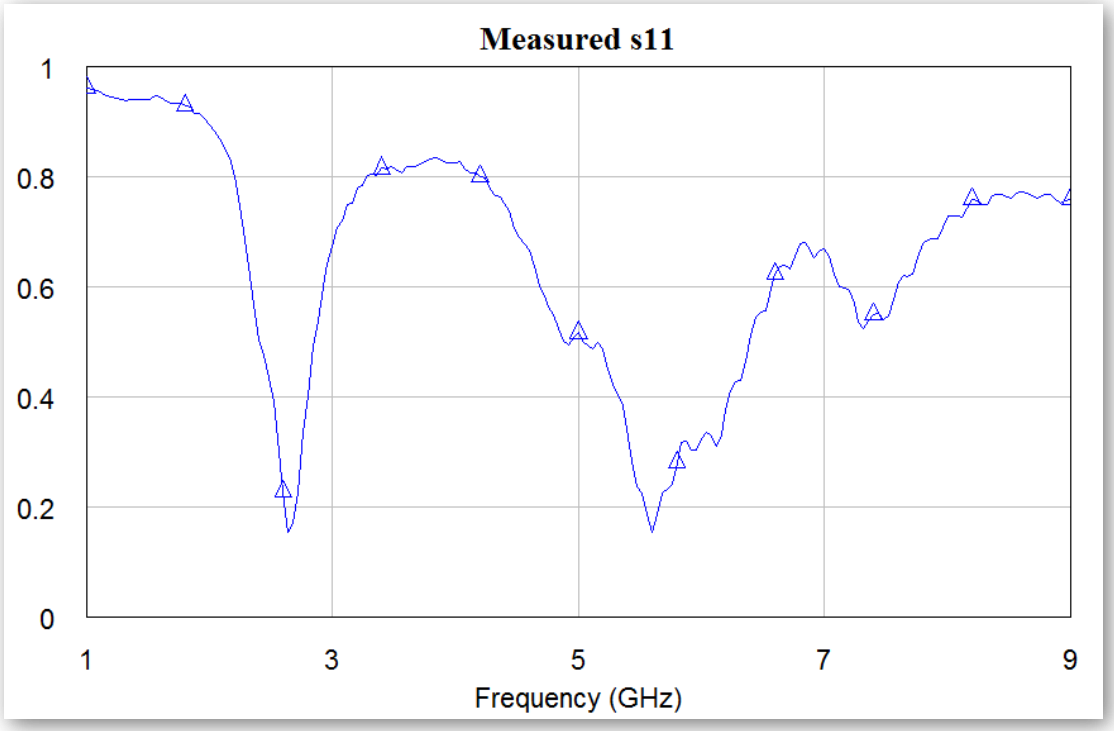

Figure 4.59 Measured s11 parameter

We can compare this value with the simulated one:

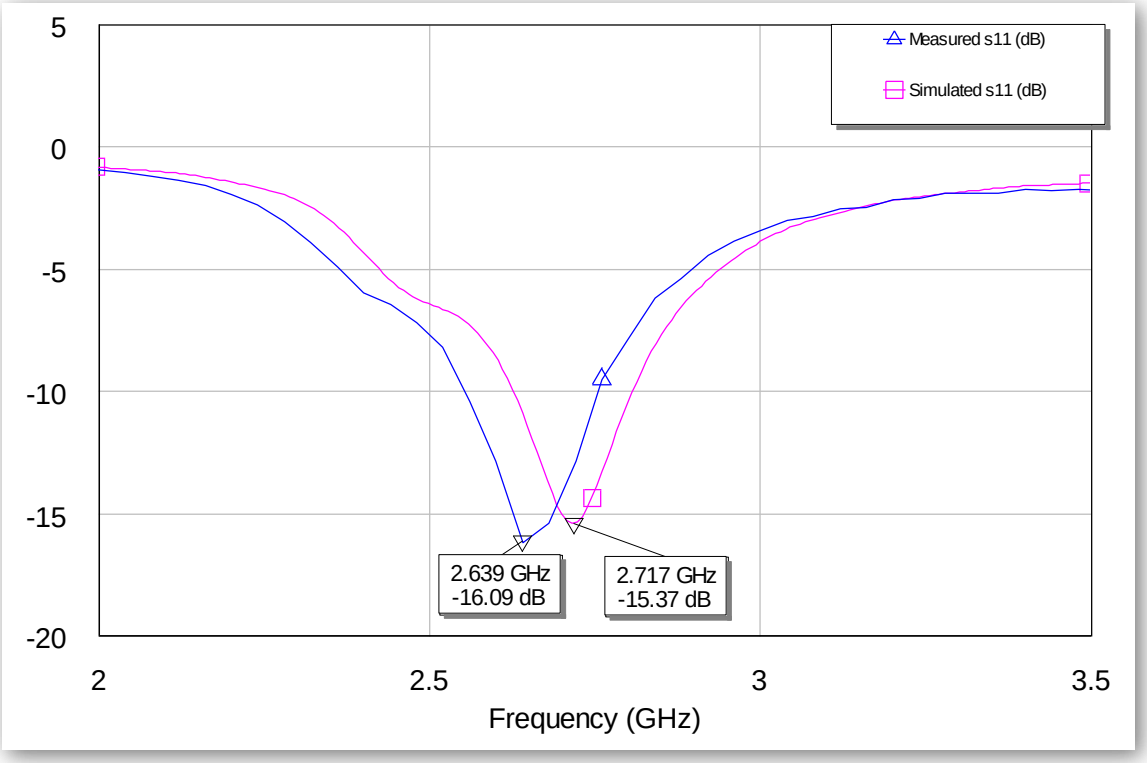

Figure 4.60 Comparison between simulated and measured s11 param

We can see as the resonant frequency has been moved towards a lower frequency and its value has decreased. Both factors benefit the design of the system.

Chapter 5.

Rectifier

Diode theory principles

As it is well known the I-V characteristic of an ideal diode is given by the Shockley equation [**40**] :

$$I_d = I_S\left(e^{V_D/nV_T} - 1\right) \tag{5.1}$$

Where I_d is the current flowing across the diode, I_S is the reverse bias saturation current, V_D is the voltage across the diode, V_T is the thermal voltage, and n is the ideality factor or quality factor. It varies from 1 to 2 depending on the fabrication process and semiconductor material, but close to 1.

It is necessary to have a model of the diode, in order to design an acceptable circuit with a simulator. Some large-signal modes are available, such as microwave diode model, the PIN diode model or the SPICE model. The diode that will be used is a Schottky diode and the SPICE model is a suitable one to model the diode. The large-signal diode model is shown in Figure 5.1. And in Table 5.1 shows a list of the diode parameters for the SPICE model.

Keyword	Description	Unit	Default
IS	Saturation current	A	0
ALFA	Slope factor of conduction current	V^{-1}	38.696
IB	Breakdown saturation current	A	0.01
VB	Breakdown voltaje	V	-∞
E	Power law parameter of breakdown current	-	10
CT0	Zero-bias depletion capacitance	F	0
VJ	Built-in barrier potential	V	0.8
GAMA	Capacitance power law parameter	-	0.5
GC1	Varactor capacitance polynomial coefficient 1	V^{-1}	0
GC2	Varactor capacitance polynomial coefficient 2	V^{-2}	0
GC3	Varactor capacitance polynomial coefficient 3	V^{-3}	0
CD0	Zero-bias diffusion capacitance (*pn* diodes)	F	0
AFAC	Slope factor of diffusion capacitance	V^{-1}	38.696
R0	Bias-dependent part of series resistance in forward-bias condition	Ω	0
T	Intrinsic time constant of depletion layer for abrupt-junction diodes	S	0
KF	Flicker noise coefficient	-	0
AF	Flicker noise exponent	-	1
FCP	Flicker noise frequency shape factor	-	1
AREA	Area multiplier	-	1

Table 5.1 Some typical parameters of the SPICE model

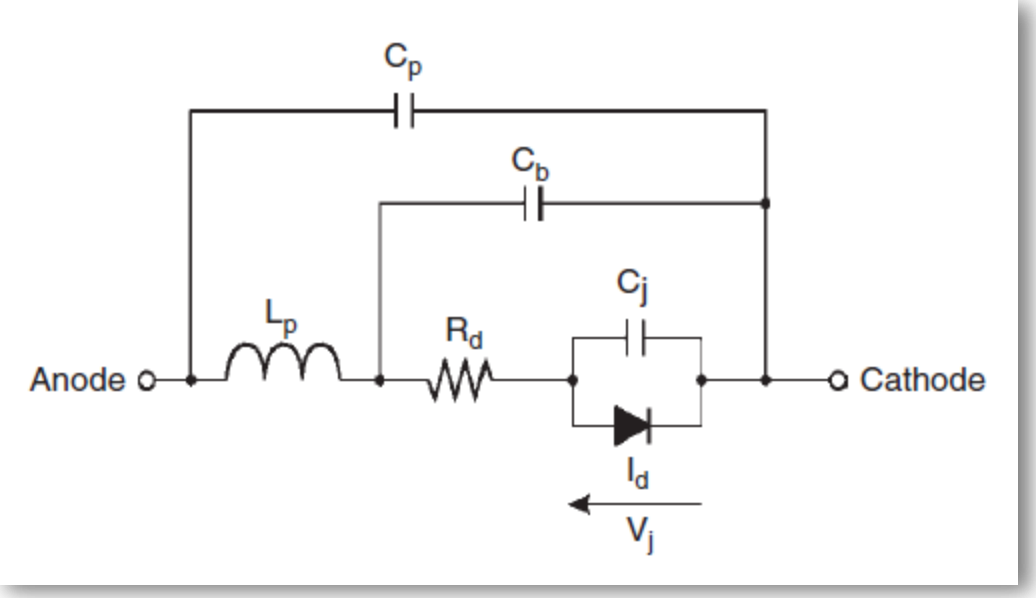

Figure 5.1 Large signal microwave diode model (temperature dependent)

For most cases, the diode capacitance is modeled as a voltage-dependent capacitor, which is connected in parallel with a nonlinear current generator, to represent the charge storage effects of the junction. There are two components which model this charge, and generate two carriers flowing through the diode. On the one hand we have the reverse-voltage capacitive effect of the depletion region. It follows the simple approximation that the depletion region (the area of the junction that is depleted of carriers) serves as the gap between the "plates" of a capacitor. On the other hand we have the forward-voltage charge represented by mobile carriers in the diode junction.

Schottky barrier diodes differ from junction diodes in that current flow involves only one type of carrier instead of both types. Diode action results from a contact potential set up between the metal and the semiconductor. When the diode is fabricated, the metal is brought into contact with an *n*-type semiconductor. It generates that electrons spread out of the semiconductor into the metal, leaving a region under that contact which has no free electrons. This is the so called depletion layer. The internal voltage difference between the metal and the semiconductor is called the contact potential.

The diode works when a positive voltage is applied to the metal. Then, the internal voltage is reduced and the electrons can flow into the *n*-type cathode material. It is important to consider that there is no flow of minority carriers from the metal to the semiconductor so no neutral plasma of holes and electrons is formed. If the forward voltage is reduced to zero the current stops and the reverse voltage is established in few picoseconds.

The voltage-current function is defined by the Richardson equation, given in many texts:

$$I = AA_{RC}T^2 \exp\left(-\frac{q\phi_B}{kT}\right)\left[\exp\left(\frac{qV_J}{kT}\right) - M\right] \tag{5.2}$$

Where A=Area (cm^2); A_{RC}=modified Richardson constant ($A/K^2/cm^2$); k=Boltzmann's constant; T=temperature (K); ϕ_B=barrier height (V); V_J=external voltage across depletion layer (positive for external voltage), =V-IR_S; R_S=series resistance; M=avalanche multiplication factor and I=diode current (A) (positive forward current).

A better equation for the design has all the parameters non-dependant from the voltage or the current and agrees reasonably with the Richardson equation.

$$I = I_S\left[\exp\left(\frac{V_J}{0.028}\right) - 1 + \frac{K}{1 - V_B/V}\right] \tag{5.3}$$

With I_S as saturation current; $0.028 = nkT/q$ at room temperature ($n = 1.08$); *n*=forward slope factor; K=reverse slope factor and V_B=breakdown voltage (the voltage when M=1). The two first parameters are strongly temperature dependant.

Even if the agreement between the two equations is no perfect, it is close enough to be possible to consider the equation (5.3) due to its simplicity. The saturation current can be obtained by a comparison between the two equations:

$$I_S = AA_{RC}T^2 \exp\left(-\frac{q\phi_0}{kT}\right) \tag{5.4}$$

The total dynamic resistance for a forward-biased diode is given by

$$R_T = \frac{dV}{dI} = R_S + \frac{nkT}{q\left(I + I_S\right)} \tag{5.5}$$

This equation is also good when it is considered at zero bias:

$$R_0 = R_S + \frac{28}{I_S} \tag{5.6}$$

The factors that determine R_S are the thickness of the epitaxial layer, the epi doping level (N_D), the barrier diameter, the substrate resistivity ("spreading resistance"), the contact resistances of the metals used for the barrier and the substrate contact, and the resistance associated with the bonding wire or whisker. Saturation current depends on the barrier height, the junction area, and temperature and the slope factors n and K depend on doping level, punchthrough voltage, and edge conditions.

It is also important to consider the junction capacitance of a Schottky diode, which mainly results from two sources: the depletion layer and the capacitance of the oxide layer under the bonding pad.

Design, construction and measurements of the rectifier

The basic block diagram purposed in a first step for the rectenna is based on the literature presented in Chapter 2 and shown in Figure 5.2.

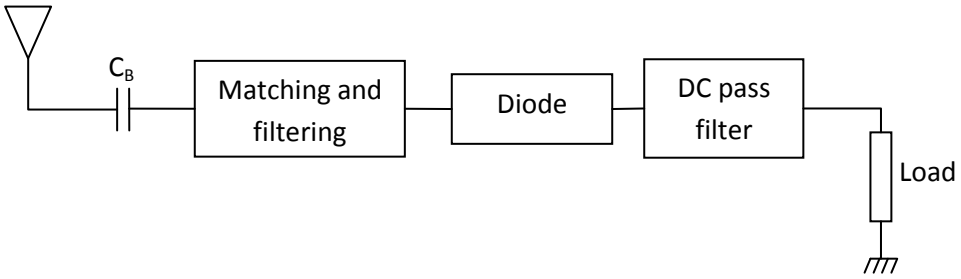

Figure 5.2 Basic block diagram for the rectenna

In a first place, between the rectifying circuit and the antenna there is a block capacitor. The rectifier is compound of four main blocks. In first place, we must build a circuit that will reject all the harmonics generated in the diode, and it will also have low injection losses for the operating frequency. In some cases, a matching circuit will be necessary because the desired impedance of the antenna cannot be reached by only changing the feeding point. Placed at a proper distance, separated by a transmission line, we have a diode connected in parallel. Then, again through a transmission line, the waves are led to a DC pass filter, which will reject all the frequencies that are not DC. Finally the load is placed at the end of the circuit.

Each block has been designed depending on the necessities of the circuit. The first block to be designed is the DC pass filter. On a second step, the matching and filtering block was planned to be designed to search the optimum value for the input impedance of the circuit.

About the diode block, the only decision to be made is if the diode is placed in series or in parallel. Since the diode is used to rectify, it works in large signal. If it is placed in parallel, it will work as a trimmer and the circuit will act as a detector. Therefore, the diode will be placed in series to build the rectifier.

The DC pass filter is designed with simplicity criteria. Therefore, it will consist of a single capacitor of a proper value.

$$|Z| = \frac{1}{\omega C} \tag{5.7}$$

$$C = \frac{1}{\omega |Z|} = \frac{1}{2\pi f |Z|} \tag{5.8}$$

If rejection is needed in the operating frequency, we can consider a high value of impedance (10MΩ) at the frequency of 1 MHz. In this way we will ensure for the central frequency to be total reflection.

$$C = \frac{1}{2\pi \cdot 10^{7} \cdot 10^{6}} = 1.6\,pF \tag{5.9}$$

So the value of the capacitor will have a value of few picofarads.

The simulations for the design and optimization of the rectifier were done using the software AWR Design Environment 2003 from Applied Wave Research, Inc.

The three models of the diodes are:

- HSCH-5312 from Hewlett Packard
- HSMS-2820 from Agilent Technologies
- MA4E-1317 from Tyco electronics, M/A COM Inc.

For the simulations, the SPICE model of the diodes was used. The parameters of the SPICE model for the three diodes are shown in Table 5.2.

Keyword	Description	MA4E-1317	HSMS-2820	HSCH-5312	Unit
IS	Saturation current	$1.5 \cdot 10^{-5}$	$1.5 \cdot 10^{-5}$	$3 \cdot 10^{-7}$	mA
JSW	Periphery reverse saturation current	0	0	0	mA
MULT	Scaling factor	1	1	1	-
AFAC	Junction area	1	1	1	-
PJFAC	Junction periphery	1	1	0	-
RS	Series resistance	4	4.942	9	Ω
N	Ideality factor	1.025	1.025	1.08	-
TT	Storage time	0	10^{-5}	0	us
CJ0	Zero-voltage bottom junction capacitance	0.045	0.7	0.13	pF
CJP	Zero-voltage periphery bottom junction capacitance	0	0	0	pF
VJ	Bottom built-in voltage	0.323	0.323	0.69	V
PHP	Periphery built-in voltage	0.8	0.8	0.8	V
M	Bottom junction grading coefficient	0.4154	0.4154	0.5	-
MJSW	Periphery junction grading coefficient	0.5	0.5	0.33	-
FC	Bottom depletion capacitance linearization param.	0.5	0.5	0.5	-
FCS	Periphery depletion capacitance linearization param	0.5	0.5	0.5	-
BV	Breakdown voltage	7	44	5	V
IBV	Current at BV	10^{-2}	$1.225 \cdot 10^{-4}$	10^{-2}	mA
IKF	Forward knee current	0	0	0	mA
IKR	Reverse knee current	0	0	0	mA
EG	Energy GAP at nominal temperature	0.69	0.69	0.69	-
XTI	Temp. Scaling coefficient	2	2	3	-
TEXT	Temp. at which diode params were determined	25	25	25	degC
T	Temperature	25	25	25	degC

Table 5.2 SPICE parameters for the selected diodes

An important decision concerns the input power considered to do the simulations. As it was introduced in Chapter 3, the power received is calculated by a simple link budget:

$$P_{rx} = P_{tx} \cdot G_{tx} \cdot G_{tx} \cdot \left(\frac{\lambda_0}{4\pi r} \right)^2 \quad (5.10)$$

Let us assume that we are emitting the maximum power. Therefore P_{tx}=25dBm. The distance that we can consider from the transmitter to the receiver is 3 meters. Using the antennas detailed in the previous chapter, the gain for both receiver and transmitter antennas will be 9.87dB.

$$P_{rx} = 25dBm + 2 \cdot 9.87dB + 20\log\left(\frac{0.1224}{4\pi 3} \right) = -5dBm \quad (5.11)$$

With this data, we can build the model in the software, and try which diode is the one with best results for the current problem.

Circuit for the HSMS-2820 diode

Following the general scheme, the circuit for this diode has been designed as follow:

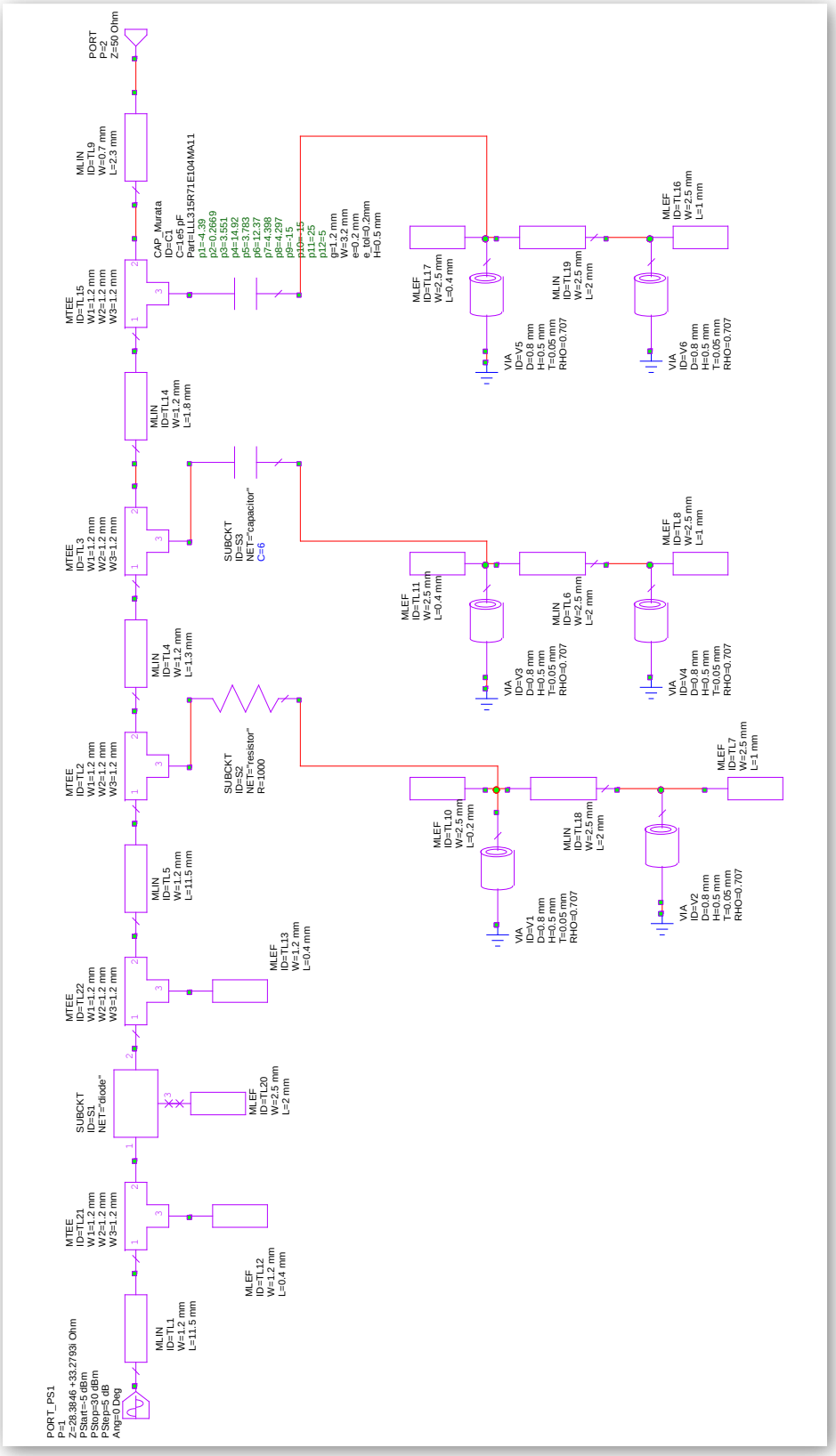

Figure 5.3 Circuit for the HSMS 2820

As it is possible to observe, transmission lines are added between the different blocks of the circuit. The lengths of the lines have been optimized (long lines has been used in the RF parts of the circuit –before the rectification- and short ones in the DC parts –after the rectification-). The effect of the cylindrical vias that connect the elements with the ground plane has been also added. It was also necessary to add another filtering stage. Without this second filter, the remaining level of the central frequency component in the load was too high. The main goal was to achieve a DC level at the output as high as possible, which means to have no residual sinus component. The impedance for input port is taken of the measured output impedance for the antenna designed in the previous chapter.

The simulation has been done at the central frequency (2.45GHz), with an input level of -5dBm, as it was shown in (5.11), and the results are presented in the figure below.

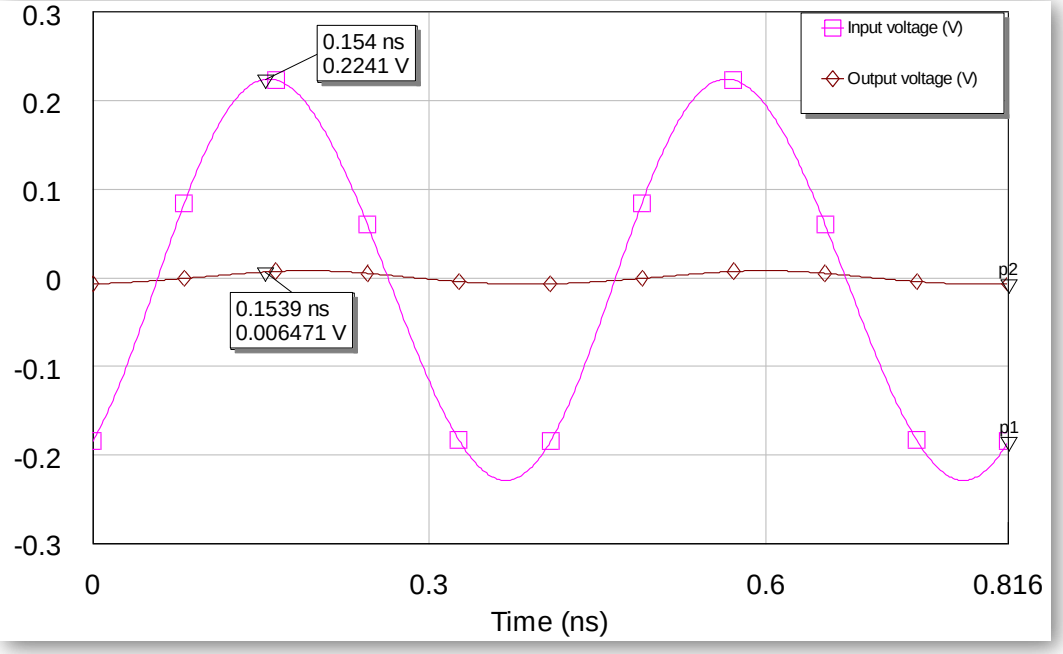

Figure 5.4 Voltage waves for the HSMS 2820 diode

In the graph we can appreciate two shapes. The pink one corresponds to the input level of voltage and the brown one the rectified wave. Both simulated results are represented in Volts. These results are not good since the output level is so low and the central frequency component can be seen easily. Some important things have to be considered to evaluate these results. On one hand, the operating frequency of the circuit is quite high, and this diode is not appropriate for such high frequencies. In fact, in the datasheet we can read that the diode is appropriate to build systems of similar characteristics up to 1.5GHz. We can try to simulate the same circuit but at lower frequencies, for example at 900MHz or 1GHz. The results obtained are better, as it is possible to appreciate in the figures below.

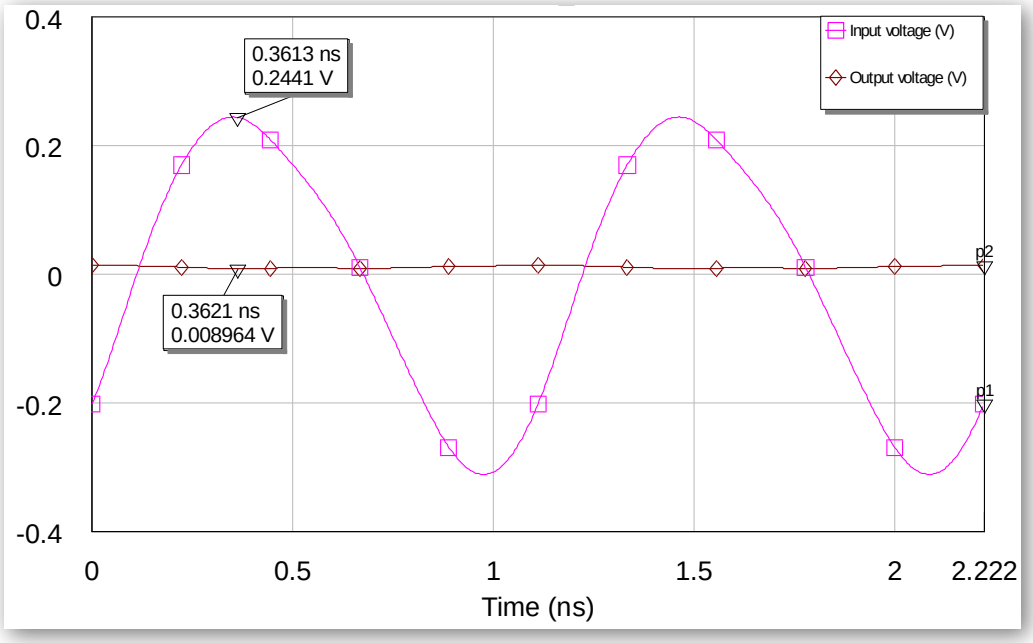

Figure 5.5 Voltage waves for the HSMS 2820 diode with a central frequency of 900MHz.

The same colors and units as explained in Figure 5.4 are applied. In this case, however, the operation frequency is 900MHz. The results are better than the previous case, as we can appreciate in the values of the output voltage. The sinusoidal component of the DC wave is lower, but still present.

To the previous frequency consideration, we can add that the received frequency is too low to have the diode completely open. This is the reason why the DC level is not good. If we simulate the same circuit by adding 10 or 15dB to the input frequency the efficiency increases, we can see how the relation between the maximum input voltage and the DC obtained voltage improves.

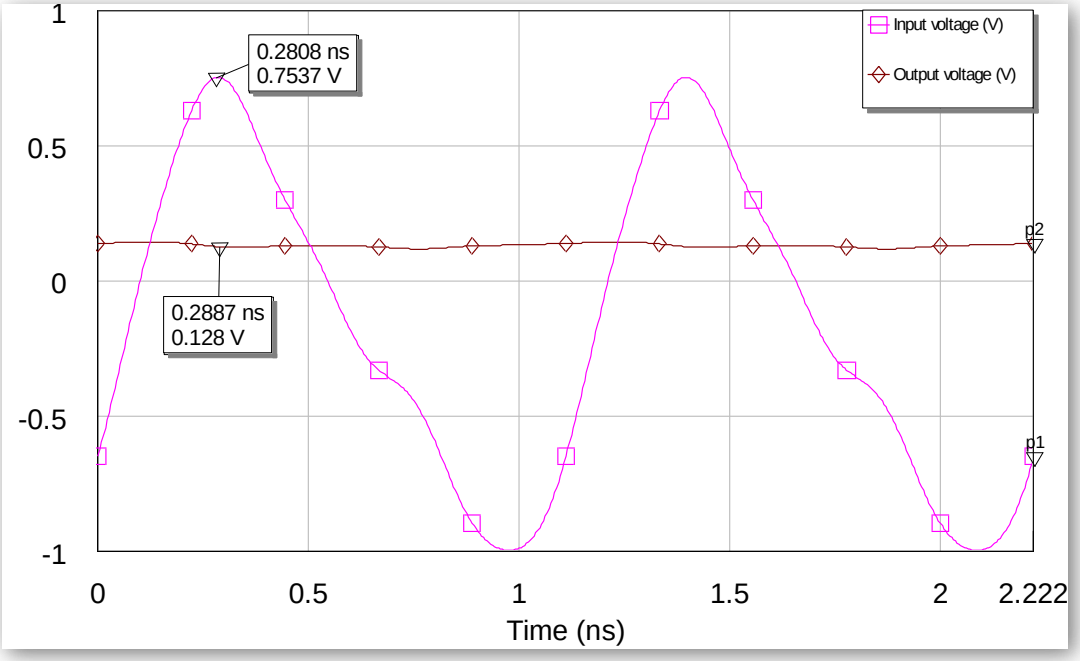

Figure 5.6 Voltage waves for the HSMS 2820 diode with a central frequency of 900MHz and input power of 5dBm.

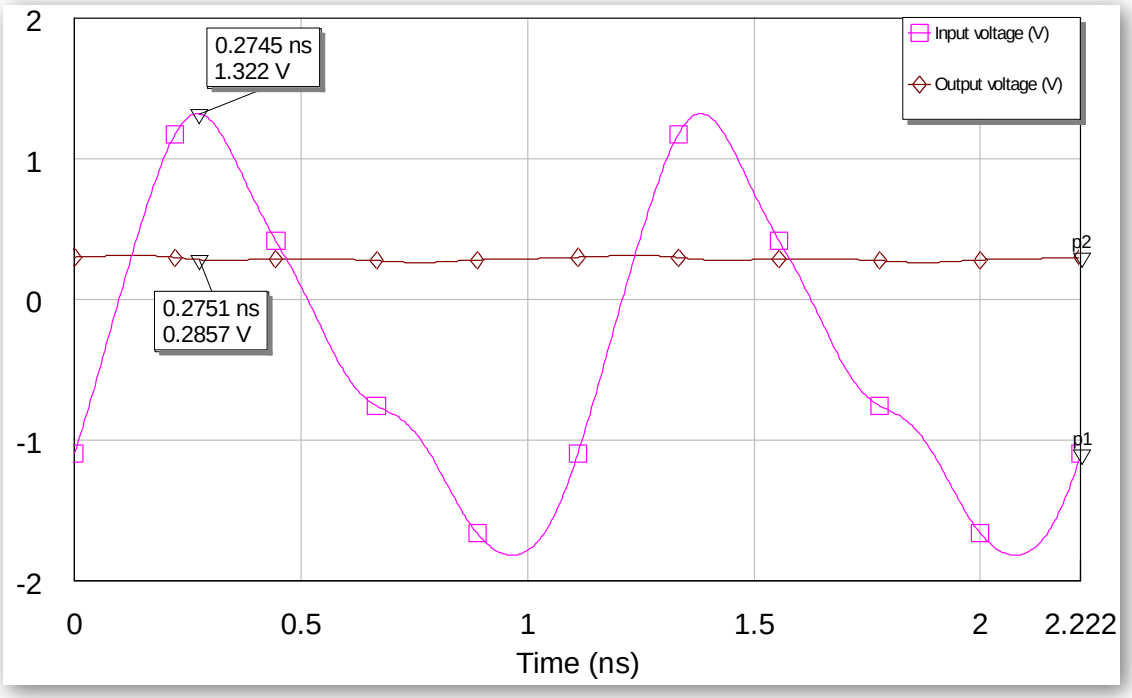

Figure 5.7 Voltage waves for the HSMS 2820 diode with a central frequency of 900MHz and input power of 10dBm.

We can estimate the percentage of voltage that is recovered at the output in each case to compare the results.

$$p = \frac{V_{DC}}{V_{RMS}} = \frac{V_{DC}}{V_{MAX}}\sqrt{2} \tag{5.12}$$

f=2.45GHz P_{in}=-5dBm	f=0.9GHz P_{in}=-5dBm	f=0.9GHz P_{in}=5dBm	f=0.9GHz P_{in}=10dBm
4.0836%	5.1934%	24.0147%	30.5628%

Table 5.3 Recovered voltage percentages for the HSMS 2820 diode

We can see how the percentage is really low when the diode input voltage is -5dBm, while it increases substantially when the input power is higher. It is important to emphasize that this is a relative measure, since the values are normalized to the maximum received power.

In the Figure 5.8 we can see the variation of the DC voltage power as a function of the input power. In the case of 2.45GHz, the diode has worst results; it takes longer to have some significant DC output value. This suggests that the diode is closed at the beginning and that it is not until really high input power when it starts to be opened. If the diode is open, then the current through should grow lineally (Figure 5.9).

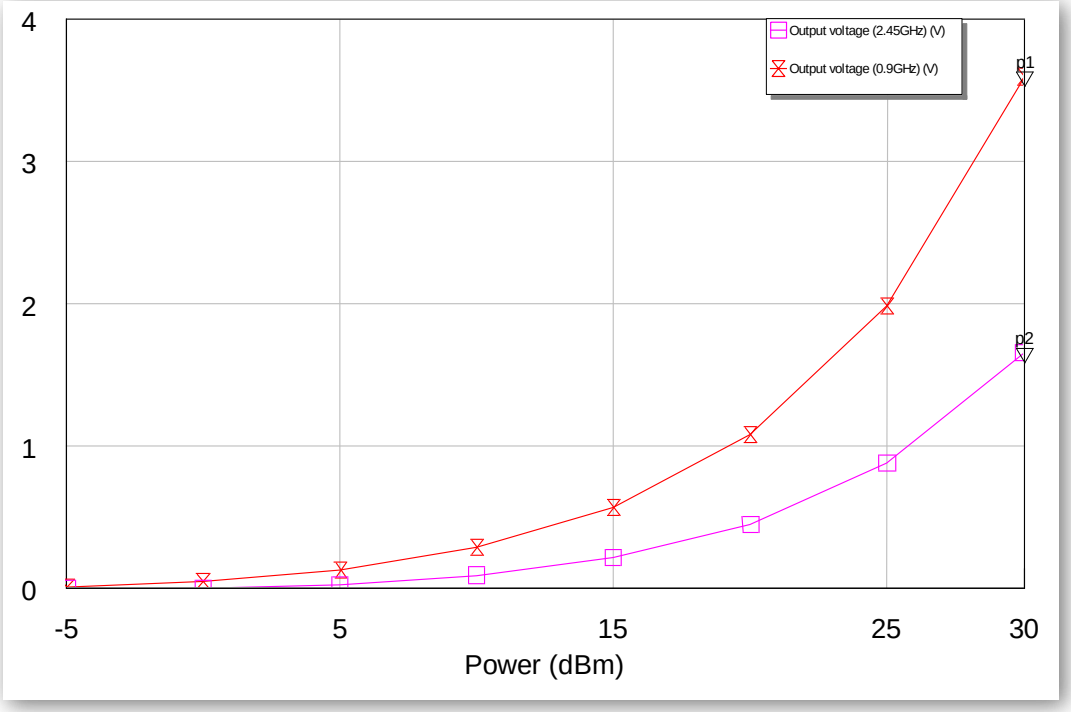

Figure 5.8 Voltage vs Input power for the HSMS 2820 diode

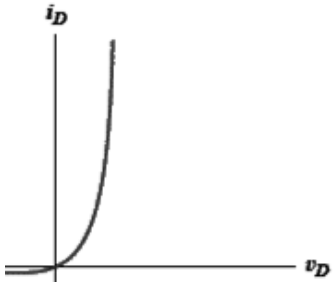

Figure 5.9 Typical diode curve

Circuit for the HSCH-5312 diode

The circuit for this diode can be seen in the image below.

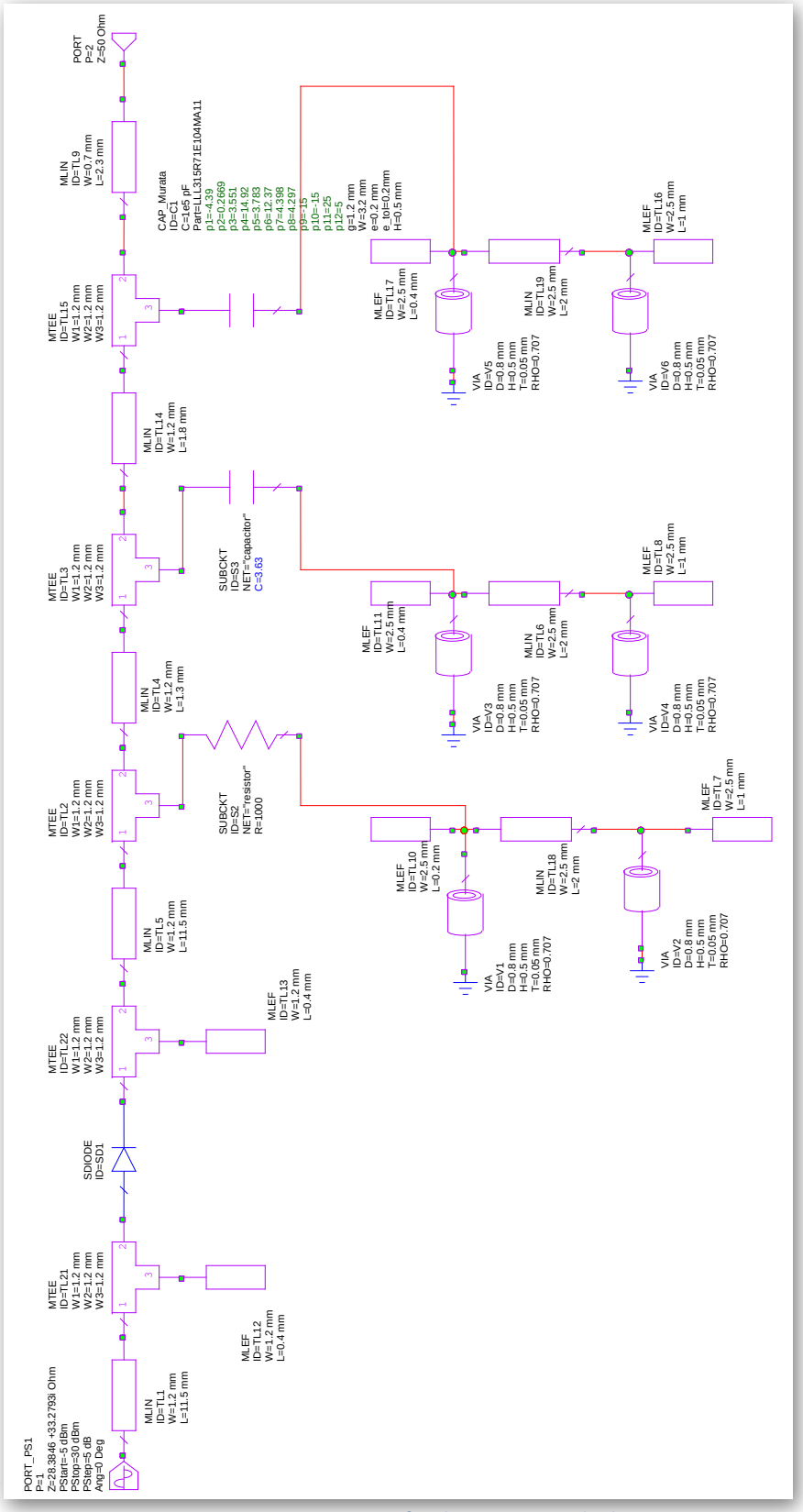

Figure 5.10 Circuit for the HSCH 5312 diode

The design and consideration are very similar to the previous circuit, designed for the HSMS 2820 diode. It has been also necessary a double DC pass filter, the effect of the vias has been also included, and the input impedance is the same for all the studied rectifiers.

The first simulation was again done with a frequency of 2.45GHz and input power -5dBm and its results are presented in the figure below.

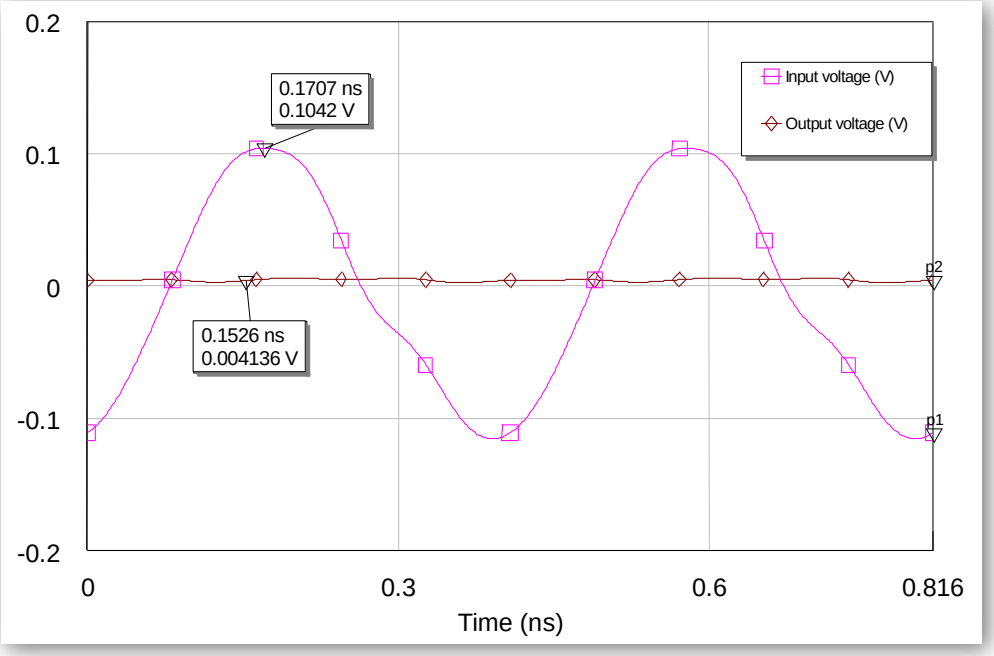

Figure 5.11 Voltage waves for the HSCH 5312 diode

Again, the recovered DC level is quite low. If we try to increase the receiver power, we can see how the results improve.

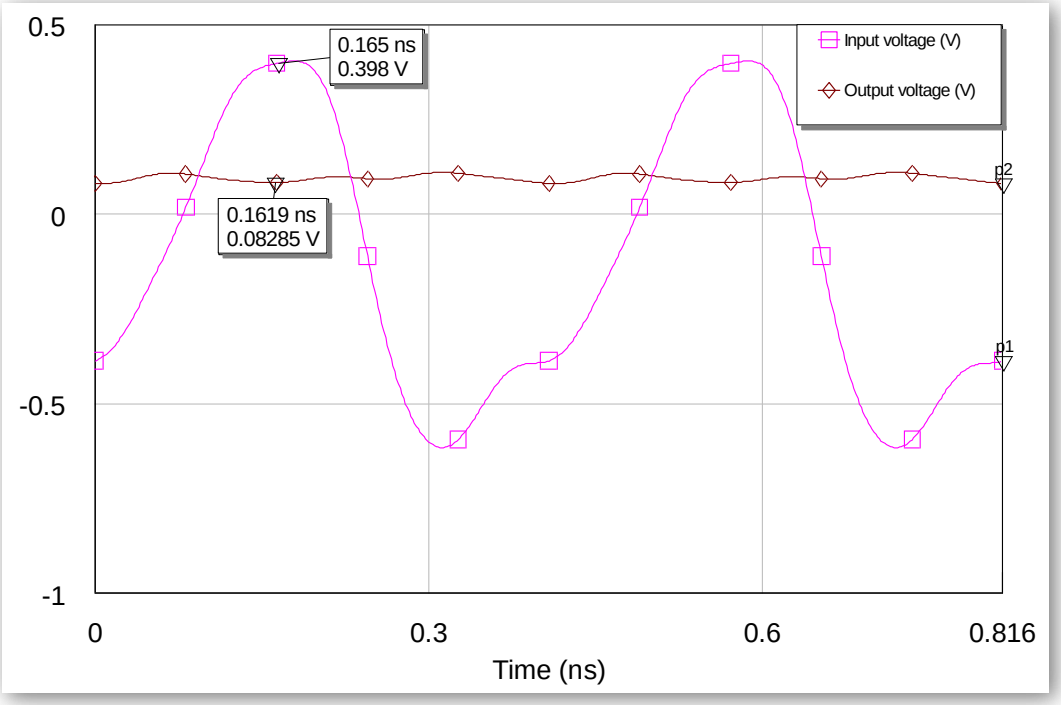

Figure 5.12 Voltage waves for the HSCH 5312 diode with 5dBm of input power

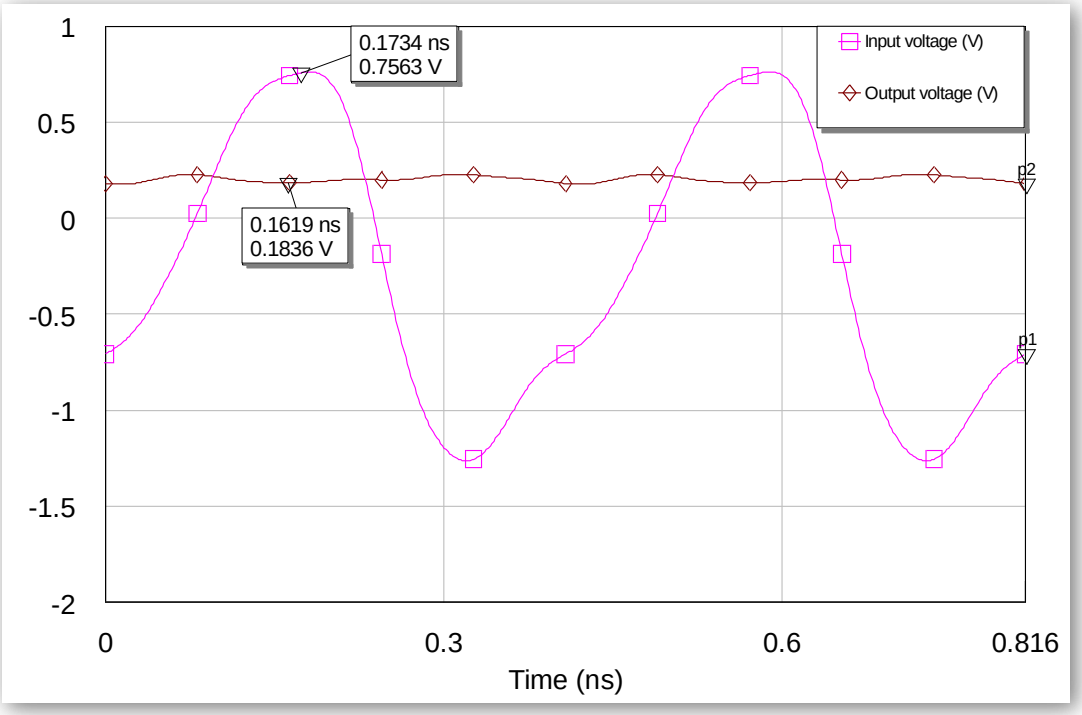

Figure 5.13 Voltage waves for the HSCH 5312 diode with input power of 10dBm

Once more, we can calculate the percentage of the voltage which is recovered using (5.12), and we obtain the following results:

f=2.45GHz P_{in}=-5dBm	f=2.45GHz P_{in}=5dBm	f=2.45GHz P_{in}=10dBm
5.6134%	29.4391%	34.3316%

Table 5.4 Recovered voltage percentages for the HSCH 5312 diode

As concluded with the previous results, when the input power is too low the recovered voltage percentage seems to indicate that the diode is closed. Again, the percentage is around five percent for the lower input power and around thirty for the high ones. Even if the values are better, it is remarkable that the better solution does not give as a DC resull as flat as the one achieved with the previous diode (the higher frequency component is more easy to recognize).

To complete the analysis of this diode, the curve of the voltage versus the input power is shown in the next figure where it is possible to appreciate that the result are quite similar to the previous ones at 900MHz.

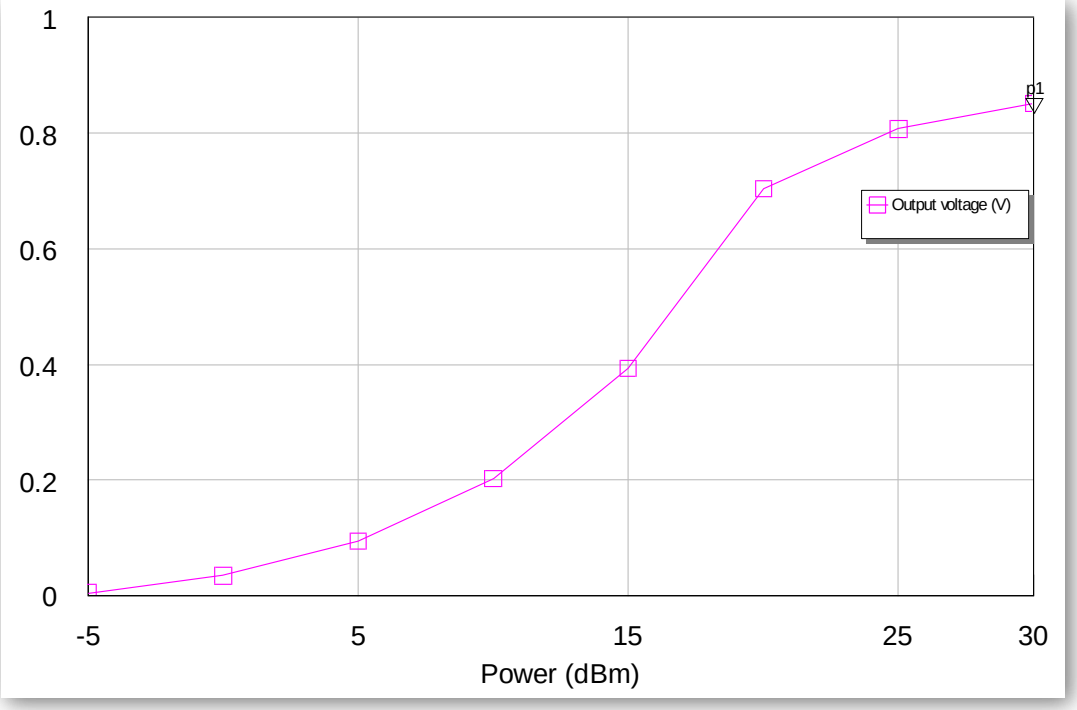

Figure 5.14 Voltage vs Input power for the HSCH 5312 diode

Circuit for the MA4E-1317 diode

The circuit is:

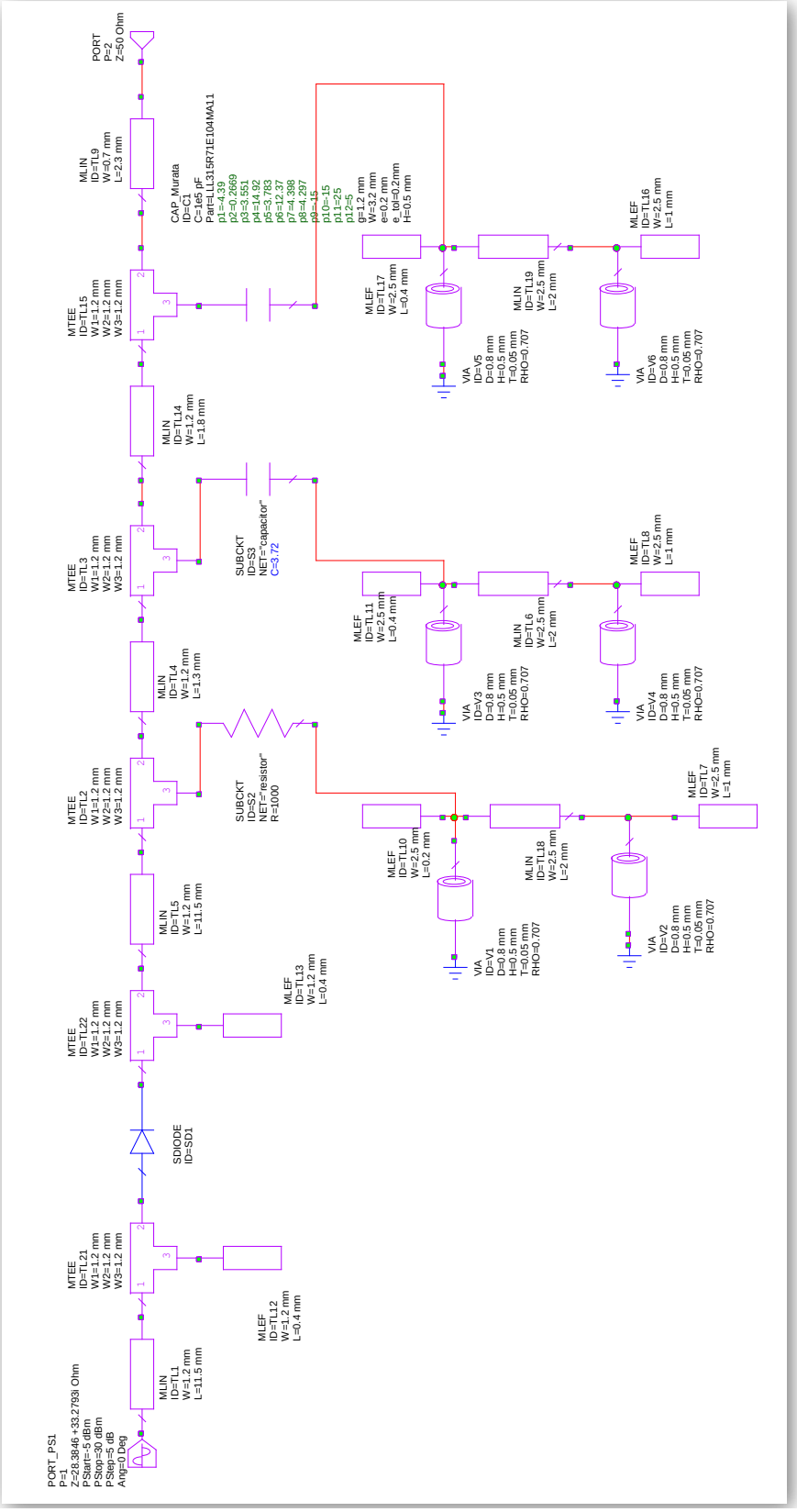

Figure 5.15 Circuit for the MA4E 1317 diode

The same explanations apply here. The first simulation is done with central frequency of 2.45GHz and input power level of -5dBm. Its results are presented below.

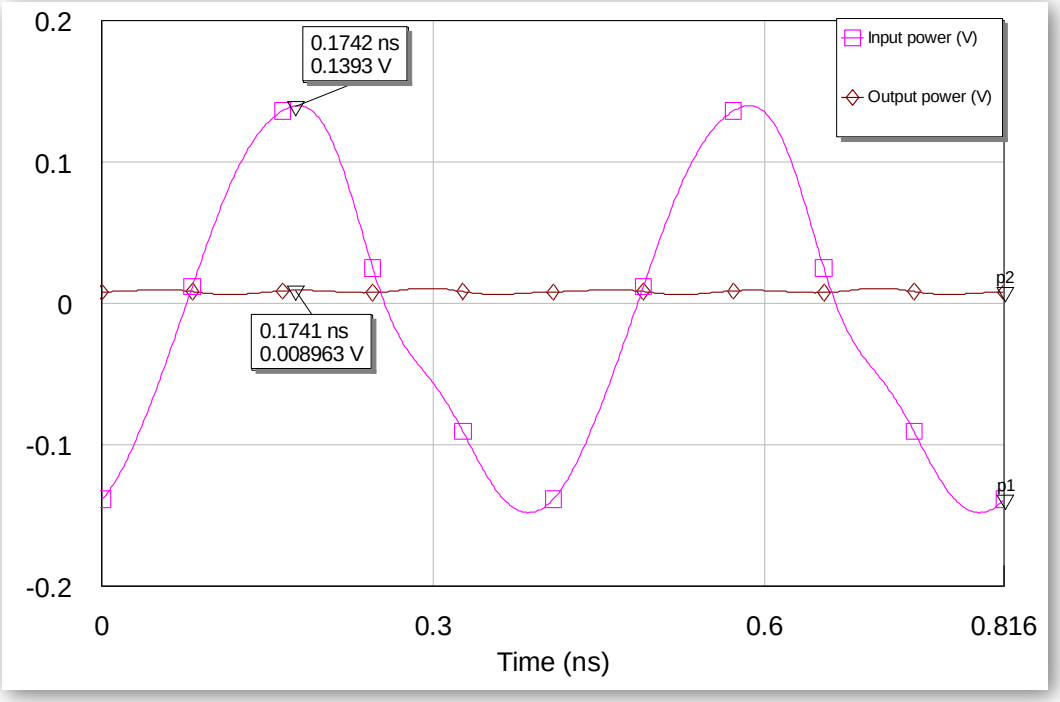

Figure 5.16 Voltage waves for the MA4E 1317 diode

If we see the response of the circuit if the input power is higher, it will be possible to compare it with the previous diodes.

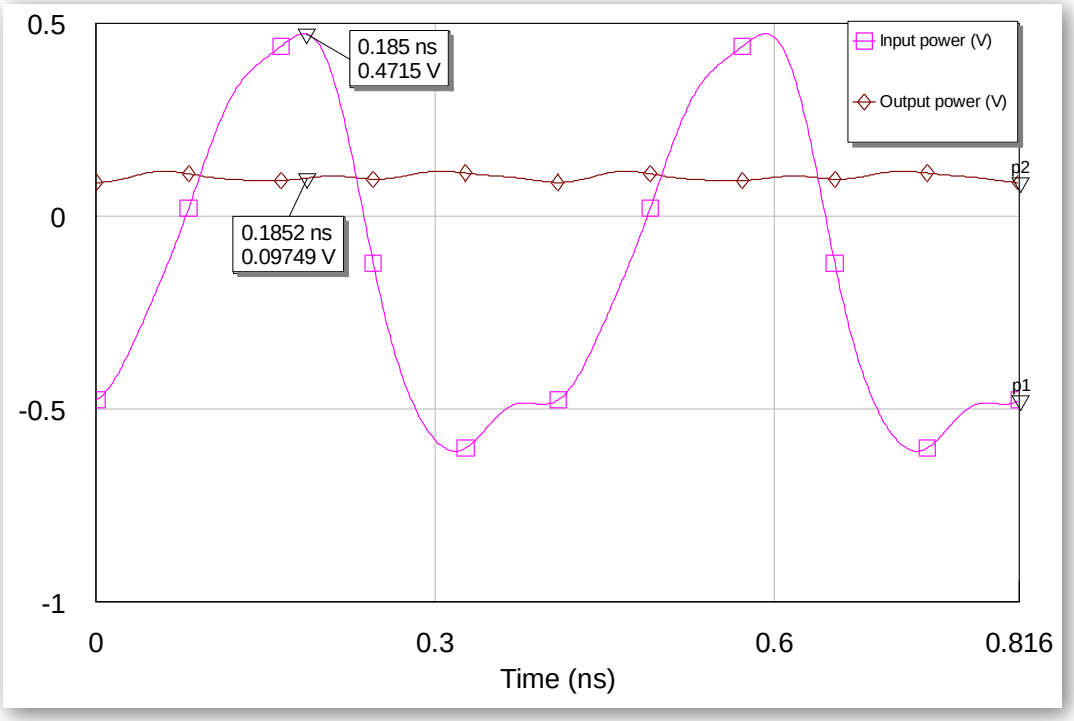

Figure 5.17 Voltage waves for the MA4E 1317 diode with 5dBm of input power

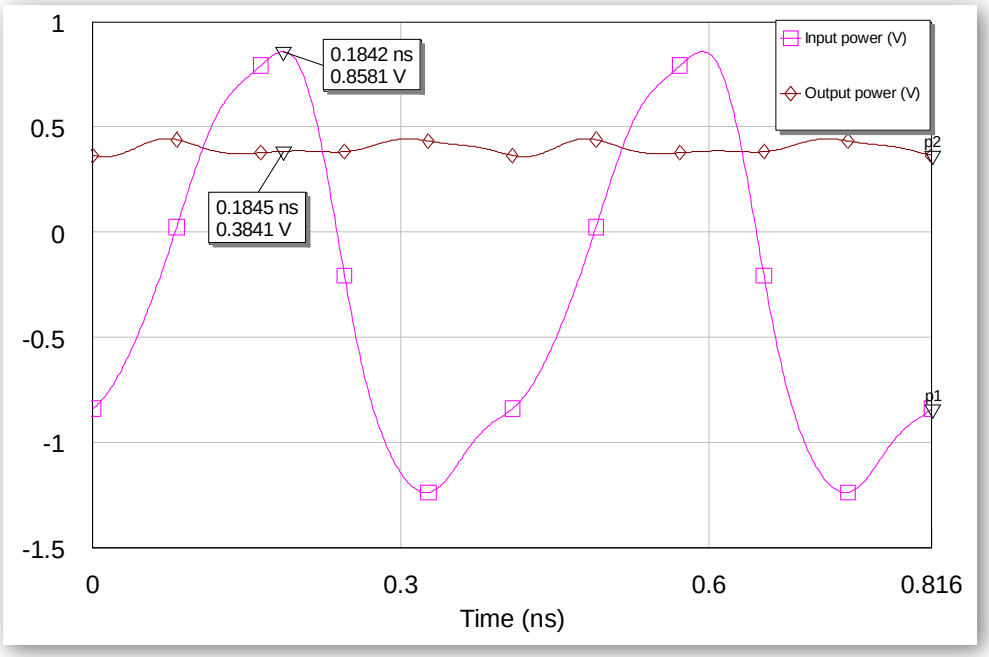

Figure 5.18 Voltage waves for the MA4E 1317 diode with 10dBm of input power

Using (5.12), we can calculate the percentage of voltage recovered as DC.

f=2.45GHz P_{in}=-5dBm	f=2.45GHz P_{in}=5dBm	f=2.45GHz P_{in}=10dBm
9.0995%	29.2411%	51.879%

Table 5.5 Recovered voltage percentages for the MA4E 1317 diode

The order of the percentages is similar for the three diodes, with the exception that in this case, the percentage obtained in the last case is much bigger than the previous ones. If we see the graph of the output voltage versus the input power we can also appreciate how rapidly the output voltage grows.

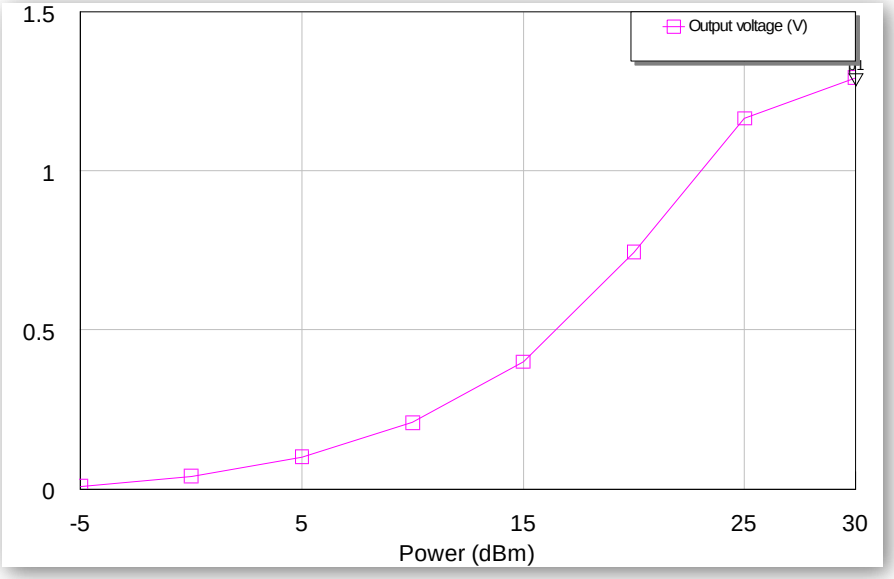

Figure 5.19 Voltage vs Input power for the MA4E 1317 diode

Diode's choice.

To chose the most appropriate diode the computed percentage will be considered. In the case of the first diode the results for the lower frequencies will be taken into account.

	f=2.45GHz P_{in}=-5dBm	f=2.45GHz P_{in}=5dBm	f=2.45GHz P_{in}=10dBm
HSMS-2820	5.1934%	24.0147%	30.5628%
HSCH-5312	5.6134%	29.4391%	34.3316%
MA4E-1317	9.0995%	29.2411%	51.879%

Table 5.6 Comparison of the obtained percentages for all the diodes

It can be easily seen that the best results are obtained with the diode from MACOM Technologies.

However, even if the obtained results with this diode are better, we can see how the DC level in the load is so low, and the diode is not completely open when the received power is -5dBm.

Chapter 6.

Conclusions

A complete study of the components for a Wireless Power Transmission system has been done. The state of the art has been studied and a technology according to the requirements has been chosen. A patch antenna with circular polarization has been designed, and three possible solutions for the rectifier have been studied.

The main conclusion is that, even if the WPT problem has been apparently widely discussed during the lasts years, it does not exist a suitable solution based on electromagnetic waves propagation when diodes are used. All the papers published until today demonstrate that when the received power is high, good efficiencies can be achieved. But the whole system is not reliable, at least not with the diode technologies known nowadays.

The limits of the system have been discussed all over this document. It is remarkable the safety consideration which limits the power that can be delivered. Considering the operating frequency and an average scenario, it results that the power that can be reached in the receiver is not enough to completely open the diode. Therefore, the losses are really high, and great amount of energy is wasted. In addition, the electromagnetic wave solution is quite limited because it is so difficult to overcome the compromise between the freedom of the receiver's location in a room and the desired (or necessary) power level achieved in this position. The first condition requires quasi-omnidirectional antennas which have low gains. The second one requires directional antennas, that will have high gains, but then we lose completely the freedom in the position of the receiver. Even if the transmitter antenna can have a narrower radiation pattern, the receiver one should be location free, eliminating the alignment obligation. In any case, we would need a really zero biased diode, which knee was exactly at 0W or really close to it. Such diode has not been found, and it seems ideal nowadays. A breakthrough in the diode technology is needed to achieve good results of the system.

With this idea, the decision made is not to build any rectifier circuit, because the system does not have the desired behavior, and it has been widely proved that is possible to build a circuit which works correctly when high power is reached in the receiver.

If an appropriate diode were founded, the next step would be to integrate the receiver antenna and the rectifier circuit, building an active antenna. It may improve the design of the rectifier not with a simple diode, but with several diode-DC pass filter stages in cascade. This configuration can rise up the efficiency to better values. Despite the cascade configuration, a diode with really low threshold voltage would be needed in that case.

Chapter 7.

References

[1] M. Cheney, *Tesla Man Out of Time*. Englewood Cliffs, NJ: Prentice-Hall, 1981.

[2] H. Matsumoto, "Microwave power transmission from space and related nonlinear plasma effects," *Radio Science Bulletin*, no. 273, pp. 11-35, Jun. 1995.

[3] W. C. Brown, "The history of power transmission by radio waves," *IEEE Trans. Microwave Theory Tech.* , vol. MTT-32, Sep. 1984.

[4] W. C. Brown, "The history of the crossed-field amplifier," *IEEE MTT-S Newslett.*, no. 141, pp. 29-40, 1995.

[5] J. C. Schuder, "Powering an Artificial Heart: Birth of the Inductively Coupled-Radio Frequency System in 1960," *Artificial Organs*, vol. 26, no. 11, pp. 909-915, Nov. 2002.

[6] J. C. Schuder and H. E. Stephenson, "Energy Transport to a Coil Which Circumscribes a Ferrite Core and Is Implanted Within the Body," *IEEE Transactions on bio-medical engineering*, vol. 12, no. 3, pp. 154-164, Jul. 1965.

[7] C. D. F. Fung, S. P. Liang, and W. H. Ko, "Design of radio-frequency powered coils for implant instruments," *Medical and Biological Engineering and Computing*, vol. 15, no. 6, pp. 634-640, 1977.

[8] E. S. Hochmair, "System Optimization for Improved Accuracy in Transcutaneous Signal and Power Transmission," *IEEE Transactions on biomedical engineering*, vol. 31, no. 2, pp. 177-187, Feb. 1984.

[9] A. Ghahary and B. H. Cho, "Design of a Transcutaneous Energy Transmission System Using a Series Resonant Converter," *IEEE Transactions on Power Electronics*, vol. 7, no. 2, pp. 261-270, Apr. 1992.

[10] M. K. Kazimierczuk and J. J. Jozwik, "Optimal Topologies of Resonant DC/DC Converters," *IEEE Transactions on Aerospace and Electronic Systems*, vol. 25, no. 3, pp. 363-373, May 1989.

[11] C. M. Zierhofer and E. S. Hochmair, "The Class-E Concept for Efficient Wide-Band Coupling-Insensitive Transdermal Power and Data Transfer," *Proceedings of the Annual International Conference of the IEEE Engineering in Medicine and Biology Society.*, vol. 14,

pp. 382-383, Oct. 1992.

[12] Koosuke, Harada, and H. Sakamoto, "A Novel Converter for Non-Contact Charging with Electromagmetic Coupling," *IEEE Transactions on Magnetics*, vol. 29, no. 6, pp. 3228-3230, Nov. 1993.

[13] T. Bieler, M. Perrottet, V. Nguyen, and Y. Perriard, "Contactless power and information transmission," *Proc. IEEE Industry Applications Conf.*, vol. 1, pp. 83-88, 2001.

[14] O. Norma, J. P. Ferrieux, M. Brunello, and R. Laouamer, "A multi-resonant converter for noncontact charging with electromagnetic," *Proc. 23rd Int. Conf. Industrial Electronics, Control and Instrumentation*, vol. 2, pp. 792-797, 1997.

[15] M. M. Jovanovic and J. Yungtaek, "A contactless electrical energy transmission system for portable-telephone battery chargers," *IEEE Transactions on Industrial Electronics*, vol. 50, no. 3, pp. 520-527, Jun. 2003.

[16] J. T. Boys, G. A. Covic, and A. W. Green, "Stability and control of inductively coupled power transfer systems," *Proc. Inst. Elect. Eng*, vol. 147, no. 1, p. 37–43, Jan. 2000.

[17] G. A. Covic, G. Elliott, O. H. Stielau, R. M. Green, and J. T. Boys, "The design of a contact-less energy transfer system for a people mover system," *Proc. 2000 Int. Conf. Power System Technology*, vol. 1, p. 79–84, Dec. 2000.

[18] W. A. Roshen, "Superconducting Inductors for Ultra-High Frequency Power Conversion," in *Power Electronics Specialists Conference*, Orlando, FL, 17-21 June 2007, pp. 2075-2081.

[19] R. Steigmann and J. Endresen, "WISA - Wireless Interface for Sensors and Actuators," Jul. 2006.

[20] H. Shinoda, et al., "Two-Dimensional Communication Technology Inspired by Robot Skin," in *Robotics and Automation, 2004. TExCRA '04. First IEEE Technical Exhibition Based Conference on* , 18-19 Nov. 2004 , pp. 99-100.

[21] Y. Makino, K. Minamizawa, and H. Sh, "Two Dimensional Communication Technology for Networked Sensing System," in *INSS2005*, San Diego, California, 2005, pp. 168-173.

[22] H. Shinoda, H. Chigusa, and Y. Makino, "Two-Dimensional Sensor Integration Using Resonant Proximity Connector - Basic Technology andApplication to Elastic Interface Device -," in *International Workshop on Networked Sensing Systems*, 2006, pp. 196-202.

[23] Y. Makino, S. Ogawa, and H. Shinoda, "EMG Sensor integration based on Two-Dimensional Communication," in *5th International Conference on Networked Sensing Systems*, Kanazawa, 2008, pp. 140-147.

[24] "Electronic and mechanical improvement of the receiving terminal of a free-space microwave power transmission system," Raytheon Company, Wayland, MA, Tech. Rep.

PT-4964, NASA Rep. CR-135194, Aug. 1977.

[25] J. Landt and B. Catlin, *Shrouds of Time: The history of RFID*. AIM inc, 2001.

[26] W. C. Brown, "RECTENNA TECHNOLOGY PROGRAM: Ultra Light 2.45 GHz Rectenna and 20 GHz Rectenna," NASA NASA CR179558, 1987.

[27] W. C. Brown and J. F. Triner, "Experimental thin-film, etched-circuit rectenna," in *IEEE MTT-S Int. Microwave Symp. Dig.*, Dallas, TX, Jun. June 1982, pp. 185-187.

[28] S. S. Bharj, R. Camisa, S. Grober, F. Wozniak, and E. Pendleton, "High efficiency C-band 1000 element rectenna array for microwave powered applications," in *IEEE MTT-S Int. Microwave Symp. Dig.*, Akbuquerque, NM, June 1992, pp. 301-303.

[29] K. Chang, L. Fan, and J. 0. McSpadden, "A high conversion efficiency 5.8GHz rectenna," *Microwave Symposium Digest, 1997., IEEE MTT-S International*, vol. 2, pp. 547-550, Jun. 1997.

[30] K. Chang and Y. H. Suh, "A circularly polarized truncated-corner square patch microstrip rectenna for wireless power transmission," *Electron. Lett*, vol. 36, no. 7, pp. 600-602, Mar. 2000.

[31] S. R. P., H. K. Smith, A. R. Khan, and L. W. Epp, "A compact dual-polarized 8.51-GHz rectenna for high-voltage (50V) actuator applications," *IEEE Trans. Microwave Theory Tech*, vol. 48, pp. 111-120, Jan. 2000.

[32] T. .-W. Yoo and K. Chang, "Theoretical and experimental development of 10 and 35 GHz rectennas," *IEEE Trans. Microwave Theory Tech.*, vol. 40, pp. 1259-1266, Jun. 1992.

[33] K. Chang and B. Strassne, "5.8-GHz circularly polarized dual-rhombic-loop traveling-wave rectifying antenna for low power-density wireless power transmission applications," *IEEE Transactions on Microwave Theory and Techniques*, vol. 51, no. 5, pp. 1548-1553, May 2003.

[34] K. Chang, Y.-J. Ren, and M. F. Farooqui, "A Compact Dual-Frequency Rectifying Antenna With High-Orders Harmonic-Rejection," *IEEE Transactions on Antennas and Propagation*, vol. 55, no. 7, pp. 2110-2113, Jul. 2007.

[35] T. Le, K. Mayaram, and T. Fiez, "Efficient Far-Field Radio Frequency Energy Harvesting for Passively Powered Sensor Networks," *IEEE Journal of Solid-State Circuits*, vol. 43, no. 5, pp. 1287-1302, May 2008.

[36] "Guidelines for limiting exposure to time-varying electric, magnetic, and electromagnetic fields (up to 300 GHz)," *Health Phys*, vol. 75, no. 4, pp. 494-523, Oct. 1998.

[37] C. A. Balanis, *Antenna Theory. Analysis and Design*, J. W. a. Sons, Ed. 1982.

[38] M. V. Schneider, "Microstrip Lines for Microwave Integrated Circuits," *Bell Syst. Tech. J.*, vol. 48, pp. 1421-1444, 1969.

[39] R. Garg, P. Bharthia, I. Bahl, and A. Ittipiboon, *Microstrip Antenna Design*. Boston London: Artech House, 2000.

[40] G. V. Vendelin, A. M. Pavio, and U. L. Rohde, *Microwave Circuit Design Using Linear and Nonlinear Techniques*, Second Edition ed. United States of America: John Wiley & Sons, Inc, 2005.

[41] "Electric light without current," *Literary Dig.*, vol. 112, no. 3, p. 30, Jan. 1932.

[42] W. C. Brown, "The history of power transmission by radio waves," *IEEE Trans. Microwave Theory Tech.*, vol. 32 , Issue:9 , pp. 1230-1242, Sep. 1984.